FUNDAMENTAL STUDY ON THE SURFACE PROPERTIES OF COMMON STEEL AND THE EFFECTS OF SALT AND RUST REMOVAL BY ABRASIVE WATER-JET TREATMENT

朴，相泓

FUNDAMENTAL STUDY ON THE SURFACE PROPERTIES OF COMMON STEEL AND THE EFFECTS OF SALT AND RUST REMOVAL BY ABRASIVE WATER-JET TREATMENT

Sanghong PARK

FUNDAMENTAL STUDY ON THE SURFACE PROPERTIES OF COMMON STEEL AND THE EFFECTS OF SALT AND RUST REMOVAL BY ABRASIVE WATER-JET TREATMENT

A Thesis Submitted

In Partial Fulfillment of the Requirements

For the Degree of

Doctor of Engineering

By

Sanghong PARK

九州大学

to the

DEPARTMENT OF CIVIL ENGINEERING

GRADUATE SCHOOL OF ENGINEERING

KYUSHU UNIVERSITY

Fukuoka, Japan

September, 2024

DEPARTMENT OF CIVIL ENGINEERING
GRADUATE SCHOOL OF ENGINEERING
KYUSHU UNIVERSITY
Fukuoka, Japan

CERTIFICATE

The undersigned hereby certify that they have read and recommended to the Graduate School of Engineering for the acceptance of this thesis entitled, "***Fundamental Study on the Surface Properties of Common Steel and the Effects of Salt and Rust Removal by Abrasive Water-Jet Treatment***" by **Sanghong PARK** in partial fulfillment of the requirements for the degree of **Doctor of Engineering**.

Dated: September, 2024

Thesis Supervisor:

Prof. Shigenobu KAINUMA, Dr. Eng.

Examining Committee:

Prof. Koji GOTOH, Dr. Eng.

Prof. Shozo NAKAMURA, Dr. Eng.

ABSTRACT

Surface treatment is an essential process in preparing steel structures for painting, playing a vital role in the lifespan and maintenance of the structure. For enhancing the durability of coatings, it is crucial to thoroughly remove rust and chlorides. The traditional surface treatment process varies depending on the extent of corrosion of the structure, typically involving manual and power tool conditioning for pre-treatment, followed by processes such as abrasive blasting or laser cleaning for post-treatment. However, in cases of severe corrosion, post-treatment may need to be repeated multiple times until the surface appears visually clean. This repetition can lead to increased labor and resources, extending construction periods and subsequently raising construction costs. Moreover, even after repeated post-treatment processes, rusts, and chlorides not visible to the naked eye may remain on the structure, leading to re-corrosion post-painting, degrading the protective performance of coatings, and ultimately resulting in premature failure. Such issues can cause significant damage to the structure, adversely affecting its stability and reliability.

In the process of surface conditioning, minimizing the need for pre-treatment and reducing the repetition of post-treatment is crucial for achieving economic efficiency and effective cleaning. This paper presents the innovative potential of Abrasive water-jet treatment (AWT) in providing suitable surface characteristics for the removal of corrosion products and the application of coatings. AWT processing, with its high energy density, enables the effective removal of thick rust and deeply embedded chlorides beneath the surface of steel plates with just a single treatment, thus eliminating the need for pre-treatment and significantly reducing the frequency of post-treatment. This leads to a reduction in construction time and costs, substantially enhancing the efficiency of the surface treatment process. However, to date, research on AWT for surface treatment has primarily focused on general steel plates or specific materials, with limited application to corroded steel or parts. Additionally, there is a lack of research on the efficiency of chloride removal and the surface characteristics suitable for coating. To address these issues, this paper applies AWT processing to both general steel samples and severely corroded bridge components, demonstrating its viability as a surface treatment method. Through experimental analysis, it proposes processing conditions for AWT that yield surface characteristics ideal for coating.

In this study, a thorough examination was conducted on the effects of AWT processing on the surface and mechanical properties of steel substrates. A focal point of our investigation was the influence of nozzle type, abrasive particle size, and processing distance on these properties. We evaluated the surface characteristics of treated specimens by analyzing the treatment area, maximum erosion depth, surface roughness, topographical changes, and distribution of residual abrasives. The mechanical properties were assessed through the analysis of surface hardness and changes in the microstructure of the surface layer. Additionally, we investigated how these alterations in surface and mechanical properties affect the corrosion behavior of the material. This study also applied selected treatment conditions to severely corroded steel samples to evaluate the conditioning effectiveness. For this purpose, we proposed a new 'Turning time test' method, analyzing the frequency and extent of re-corrosion and flash rust on the surface post-treatment. Finally, applying this technology to an actual weathered steel bridge with corrosion empirically demonstrated its engineering applicability.

Test results indicate that the usage of the developed divergent nozzle and smaller abrasive grains in the AWT processing effectively expands the treatment range while preventing significant erosion depth and surface roughness. Additionally, under the same treatment conditions, the hardness of the steel surface increased, and microstructural changes enhanced corrosion resistance compared to traditional blast processing methods. Notably, the best corrosion resistance on steel surfaces was observed with AWT processing using the convergent nozzle and larger abrasive particles. This process, free from dust generation and fire hazards, is applicable in enclosed or confined spaces without spatial constraints. It can completely treat pitting corrosion areas deeper than 500 micrometers in a single pass, entirely removing corrosion products and chlorides from the corroded steel surface, achieving a surface cleanliness level above Sa3. Consequently, surfaces treated with AWT maintain their cleanliness and are free from flash rust for up to 72 hours post-treatment. In summary, AWT creates optimal surface conditions for further coating processes under various processing conditions and ensures higher surface cleanliness in real-world engineering applications.

TABLE OF CONTENTS

LIST OF FIGURES

LIST OF TABLES

CHAPTER 1 INTRODUCTION

1.1 Background

Steel is extensively utilized in industrial and infrastructure projects due to its excellent mechanical strength, durability, and versatility. Nonetheless, its vulnerability to corrosion poses significant challenges, impacting both structural stability and financial outcomes. As per the data of the National Association of Corrosion Engineers (NACE), corrosion-related global economic damages are approximated to be around 3.4% of total GDP [1]. While it's impossible to completely eliminate corrosion-related expenses in steel structures, applying effective anti-corrosion strategies could potentially reduce these economic impacts by as much as 35% [1].

Currently, a variety of physicochemical approaches are utilized to avert the corrosion of steel constructions [2,3]. Among these, common strategies for continuous protection encompass surface conditioning and applying coatings, conducted through regularly scheduled inspections of structures prone to corrosion [4–6]. The process of surface treatment is instrumental in physically eliminating rust layers from the steel component, thereby halting further corrosion progression. Meanwhile, applying coating plays a pivotal role in extending the lifespan of the structure by creating a barrier against the ingress of oxygen, moisture, and chlorides, consequently reducing the impact of corrosion [5]. In Japan, for the maintenance of steel structures, close visual inspections are conducted every five years. Based on these inspections, the structural integrity is assessed, and necessary maintenance tasks are determined. Recently, there has been a trend toward adopting heavy-duty corrosion protection coating specifications with superior durability and corrosion resistance properties, aimed at reducing the significant portion of maintenance costs attributed to painting expenses since the main maintenance cost required for steel road bridges is the cost of repainting [7,8]. However, regardless of the high quality of the coating applied, if residual corrosion products or chloride remain on the surface prior to coating, premature detachment of the coating is inevitable due to the expansion of corrosion. Consequently, surface preparation before repainting becomes imperative, serving not only to eradicate corrosion from the surface of the steel structure but also to establish a suitably roughened texture, thereby significantly improving the adhesion of the paint [9,10]. Surface treatment is typically divided into two stages: pre-treatment and post-treatment. During pre-treatment, hand or power tools are utilized to remove rust that is easily detachable. However, this stage alone often proves insufficient for completely eliminating corrosion products deeply embedded beneath the surface or those tightly adhered to the substrate. If surface treatment is inadequate, residual chlorides or rust residues can persist on the steel surface, leading to localized corrosion beneath the coating and resulting in premature coating failure [11]. This can progress to severe corrosion and, in extreme cases, cause catastrophic damage such as material fracture or structural collapse. Thus, surface conditioning before coating is a critical process that directly affects the durability of the coating and the lifespan of the structure. After pre-treatment, additional processing steps are necessary to achieve the ideal surface condition for coating application.

A prevalent method of surface treatment or post-treatment currently applied to steel structures is abrasive blasting [12-14]. This procedure accelerates abrasive particles towards the surface, striking it with high velocities, which efficiently grinds and abrades the surface. This method is effective in eliminating contaminants from the surface while simultaneously creating a roughened texture that improves the bond strength of subsequent coatings. However, abrasive blasting generates a significant amount of dust during blasting, posing a risk to the respiratory health of workers, and its use is limited in confined spaces. Moreover, there is a disadvantage in that the abrasive can become embedded in the metal surface along with rust components, and the efficiency of the treatment diminishes in areas with thick rust layers or deep pits [15]. Such deep corrosion can accelerate corrosion by accompanying secondary corrosion. Pitting corrosion, accompanied by secondary corrosion, can act as a crack initiator in structures under dynamic loads [16], potentially reducing the fatigue life and fatigue strength of the structure. Consequently, repetitive blasting treatments are essential to maintain a certain surface condition for coating. However, even after multiple rounds of such treatments, residual corrosion remains persistent, ultimately causing subsequent corrosion beneath the coating, despite achieving the appearance of a clean surface [17].

On the other hand, Abrasive Waterjet Treatment (AWT) is emerging as an effective surface preparation method that can address existing challenges. Originally, this technology found widespread use in the manufacturing industry for cutting various materials, encompassing both metals and non-metals. However, recent research indicates that by adjusting various processing parameters associated with AWT, it can be effectively employed for abrading steel surfaces [18-20]. AWT employs a high-pressure mixture of abrasive particles suspended in water, and this mixture delivers substantial kinetic energy upon collision with the substrate, thereby facilitating material removal through erosion. The high energy density of this process contributes effectively to the removal of dense corrosion layers on steel surfaces [21]. This method can effectively eliminate thick corrosion layers and embedded impurities in a single treatment without the need for separate pre-processing procedures, eliminating the requirement for repetitive blasting treatments. Furthermore, AWT processing can impact the hardening and microstructural changes in the metal surface, thereby influencing the material's performance and corrosion resistance [22]. AWT, employing a water-based approach, poses no risk of thermal effects or thermal damage and is suitable for internal work on steel structures without generating dust. Furthermore, it is expected to be effective for surface treatment in confined spaces such as crevices within structures. However, research on the use of this technology as a surface treatment method is still inadequate, and systematic research findings have yet to be firmly settled. In particular, the author's prior research highlighted specific difficulties in implementing this technology for the treatment of corroded samples with a traditional convergent nozzle designed for material cutting. While the technology exhibits high effectiveness in corrosion product removal, it is associated with issues such as a limited processed area on steel plates, substantial thickness reduction, and a notable increase in surface roughness following treatment [22]. These issues can have a detrimental impact on the durability of the treated steel plates and the adhesion of coatings during painting processes [10][23]. Therefore, finding suitable treatment conditions to address the aforementioned challenges remains a crucial task for the effective utilization of AWT as a surface conditioning technology.

1.2 Research Objectives and Scope

This study focuses on overcoming the issues associated with the convergent nozzle during surface processing with AWT. It proposes the use of the specially developed divergent nozzle optimized for surface preparation, alongside the identification of effective AWT processing conditions that can produce optimal surface properties appropriate for applying coating. Additionally, it evaluates the various effects of abrasive grain sizes on the surface characteristics of test specimens, aiming to determine the most suitable abrasive grain size for AWT utilization in surface treatment. The dimensions and morphology of the abrasives play a critical role in the surface preparation process to ensure the achievement of highly efficient and accurate conditions on the processed surface [24-26]. The study assesses alterations in surface characteristics throughout AWT processing, considering nozzle types, abrasive particle sizes, and various processing conditions. These changes encompass treatment range, maximum erosion depth, surface roughness, surface topography alterations, and residual abrasive particle aspects. Furthermore, the study investigates the correlation between surface roughness, topographical modifications, and adhesion strength. Finally, the direct application of this technology to severely corroded structures is performed to validate the practical applicability of AWT by assessing its effectiveness in removing corrosion.

The main aims of the dissertation are as follows:

1) Identify surface characteristics suitable for coating. Propose treatment conditions that yield ideal surface characteristics for coating after AWT processing.
2) Investigate the modified structural and mechanical properties of steel, as well as their associated electrochemical characteristics, following AWT processing, in addition to surface characteristics.
3) Approach corrosion issues from an engineering perspective and validate the efficiency of corrosion and chloride removal through AWT processing.
4) To ascertain the practical applicability and feasibility of AWT processing, this technology will be applied to actual corroded bridges. A scientific analysis and validation will assess how effectively AWT removes corrosion and chloride.

1.3 Literature Review

1.3.1 Surface preparation assessment and criteria

The evaluation of surface conditions and quality is a critical stage in ensuring the reliability of surface preparation processes and coating systems. In the absence of clear assessment criteria and standards for various newly developed surface treatment methods, the integration of these technologies into the field of surface preparation can pose significant challenges. Therefore, surface treatment evaluation can be considered a fundamental prerequisite to be introduced alongside surface technology development. Currently, there are various standards for surface treatment evaluation, including ISO (International Organization for Standardization), SSPC (The Society for Protective Coatings), NACE (National Association of Corrosion Engineers), ASTM International (American Society for Testing and Materials), and JIS (Japanese Industrial Standards). The selection of standards varies depending on national and contracting entities, and a unified standard currently does not exist. The three key considerations in standard selection are as follows [9].

Firstly, the selection of parameters to be considered in the standards. Secondly, the methodologies for measuring and assessing these selected parameters. Thirdly, the establishment of criteria for defining threshold values of the measured parameters. Among various standard criteria, ISO standards are considered to excel in performing these three conditions mentioned above most effectively. Prior to coating, the evaluation of surface quality is specified in detail from various perspectives, including surface cleanliness, surface salt content, and surface characteristics. ISO standards, unlike SSPC and NACE, which are predominantly used in North America, are internationally recognized due to their comprehensive specifications for surface quality evaluation before coating applications [27]. Moreover, many countries, including Japan, and various industrial sectors often refer to ISO standards when developing suitable standards [28]. ISO 8501 provides visual assessment criteria for the cleanliness and surface preparation condition of steel surfaces, especially those treated using methods such as sandblasting or mechanical conditioning. It defines the cleaning level through the international standard Sa designation, where higher numbers indicate better cleanliness. ISO 8502 offers testing guidelines for various influencing factors on steel surface conditions, including contaminants, salt, humidity, dust, and more. This standard is particularly focused on measuring surface salt concentration using the Bresle method and establishing criteria to evaluate the extent of salt contamination. Additionally, it proposes criteria for visually evaluating the level of contamination caused by salt by assessing the occurrence of flash rust, akin to the methodology in ISO 8501. Lastly, ISO

8503 provides methodologies and criteria for measuring the surface roughness of steel before applying coatings, thereby defining the appropriate steel surface roughness for effective coating adhesion.

Therefore, ISO standards offer clear benefits that meet the three key considerations mentioned earlier for standard selection. However, there are still limitations in establishing precise threshold values for the measured parameters. Particularly, the surface roughness comparison plates (referred to as surface roughness comparators) measurements according to ISO 8501 and ISO 8503 primarily rely on qualitative methods based on visual assessment. These methods are significantly influenced by the experience and subjective judgment of the operator. This highlights the importance of establishing quantitative visual evaluation criteria for surface conditions as a crucial challenge to address. ISO 8503 should encompass a variety of surface characteristics, such as surface deformation, the quantity of residual abrasive material, and other relevant factors, as evaluation criteria for coating adhesion-related surface properties, not restricted solely to roughness.

In this study, we do not delve into the establishment of threshold values and quantitative methods for the visual assessment of steel surface conditions as specified in ISO 8501. However, we plan to explore quantitative evaluation of surface conditions in the future, utilizing color space systems such as CIE LAB to quantify color deviations and color coordinates [29]. The salt content and surface roughness were quantitatively assessed in accordance with ISO and JIS standards. Additionally, we will explore the correlation between flash rust formation caused by salt and its quantitative evaluation, as well as its impact on coating adhesion properties. Ultimately, quantitative evaluations of various surface characteristics beyond roughness will be conducted, and discussions about their influence on coating adhesion will ensue. This research will serve as valuable reference material for the selection of standards and the establishment of threshold values for surface quality assessment.

1.3.2 Surface conditioning method

Surface treatment of steel structures is an essential procedure necessary for corrosion prevention, enhancing the adhesion of subsequent coatings, and prolonging the service life in extreme environments such as marine and coastal areas. The majority of coating failures are attributed to improper surface preparation or inadequate coating application [30]. This implies that even with excellent coating materials, their effectiveness is compromised if proper surface treatment and application are not executed correctly. Surface treatment methods can vary depending on specific environmental factors and conditions of application. However, it can broadly be classified into mechanical, electrochemical, and chemical methods, grounded in the respective technological processes and operational mechanisms.

Mechanical surface treatment methods typically include hand tools, power tools, polishing, rolling, brushing, spraying, blasting, water jets, and the like. These methods involve physical contact to remove contaminants from the surface and serve the purpose of cleaning. The most basic forms, such as hand and power tool treatments, are primarily effective for coating removal and stripping loose rust. However, these methods may have difficulty completely removing strong rust layers. Therefore, additional treatments like blasting are often necessary before applying coatings. Abrasive blasting is a surface treatment method commonly employed in various steel structures and infrastructure projects, primarily utilizing various abrasives under high-pressure conditions to clean surfaces and create texture [31]. However, this method has drawbacks, such as generating a significant amount of dust during the treatment process and limitations when applied in confined spaces or on surfaces with thick rust layers. Consequently, new technologies like laser treatment are being developed; nevertheless, they still exhibit inadequate performance, especially when addressing thick rust layers or treating large structures [32]. Therefore, there is a growing demand for the development of novel mechanical surface treatment technologies that can be applied to extensive infrastructure projects without the need for separate pre-treatment or post-treatment processes.

Electrochemical surface treatment methods include cathodic protection, electrochemical chloride extraction, and re-alkalization of concrete. Cathodic protection is a method that uses galvanic sacrificial anodes or impressed current systems to protect metal structures like bridges and reinforced concrete from corrosion [33]. Electrochemical chloride extraction is used to reduce the risk of steel corrosion by extracting chloride ions from contaminated reinforced concrete. Among these, cathodic protection is a commonly used electrochemical method in the field of civil engineering. However, electrochemical treatments are more akin to maintenance approaches aimed at preventing corrosion rather than directly removing corrosion products.

Chemical surface treatment is utilized in the manufacturing process of steel and other materials and is suitable for removing light rust or mill scale from surfaces. This method primarily encompasses the application of acids or alkalis. The advantages of chemical treatment include its relatively low cost and quick rust removal capabilities. However, this method may require time to dissolve oxides and oils and can have limited effectiveness due to the difficulty of precise treatment on specific parts. Particularly, the use of hydrochloric acid can make efficient cleaning difficult if proper immersion time and concentration are not determined [34], and can lead to excessive corrosion of the material, causing mass loss [35]. Furthermore, the solution after use can cause environmental pollution, necessitating proper disposal, which requires special attention. For these reasons, the civil engineering industry, dealing with the treatment of corroded large-scale structures and infrastructure, generally does not prefer chemical surface treatment.

In addition to the surface treatment technologies discussed thus far, there are numerous methods for cleaning surfaces, including Flame Cleaning [36], Ultrasonic Cleaning [37], and Plasma Treatment [38]. However, in the civil engineering industry, the management of corrosion on-site typically involves the removal of corroded materials through blasting using hand and power tools or abrasives, followed by regular maintenance through protective coatings applied after treatment. This method is favored for its practicality and cost-effectiveness, particularly in the context of large-scale civil construction. This research aims to review a range of mechanical surface treatment processes and seeks to identify new, optimal methods to improve the effectiveness and quality of surface treatments.

1.3.3 Abrasive blasting

Abrasive blasting is one of the primary physical surface treatment methods frequently used in modern industry, and it is especially widely employed for rust removal on steel bridges. This process involves propelling solid particles onto the surface of the material under high pressure for grinding, with various methods existing depending on the purpose of use, system, and type of abrasive used [39]. Among these, sandblasting is known to be an

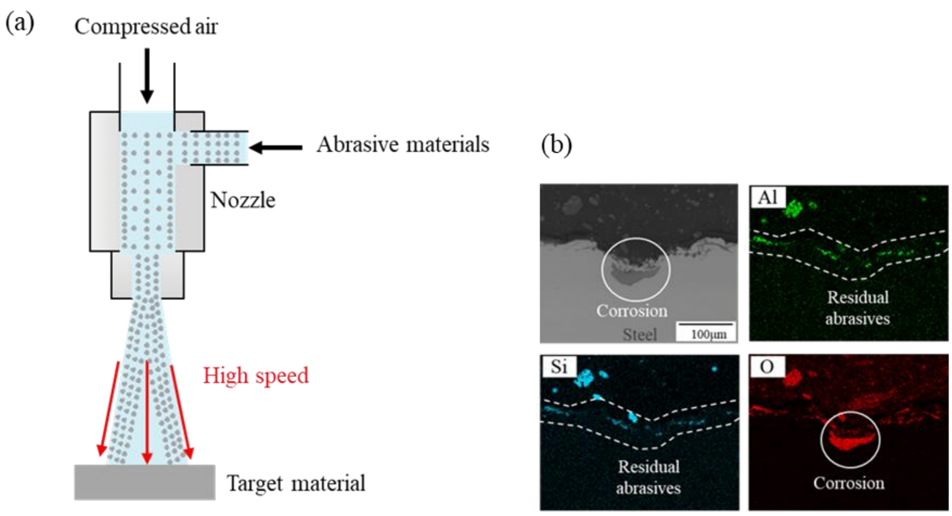

Figure 1-1 Principles of abrasive blasting: (a) Processing of abrasive blasting and (b) Residual corrosion products remaining beneath the treated surface after blast treatment on corroded steel plates.

effective method for removing rust from steel bridges [6]. This technique not only removes surface contaminants but also creates a rough surface, which enhances the adhesion of coatings. Figure 1-1 depicts the mechanisms and principles of abrasive blasting in its application to the target material. The industrial application of blasting began approximately 150 years ago with Benjamin Chew Tilghman's patented method [39], and today, various approaches like the development of eco-friendly abrasives [40] and automation of blasting [41] have been proposed and developed. However, the fundamental principles of all types of blast treatments still remain based on the age-old methodology established by Tilghman, and as an aged technique, there are several limitations in terms of the effectiveness of the blast treatment.

Firstly, in the treatment of severely corroded steel structures, the abrasive materials can deeply penetrate along with the rust layers. This can lead to reduced efficiency in areas with thick layers of rust or deep pits [15]. Such penetration may result in the formation of flash rust due to residual corrosive substances or salts after blast treatment, leading to repeated treatments that increase both the duration and cost of construction. Despite multiple iterations of blast treatments, remnants of salts and corrosive materials on the surface can persist, potentially facilitating the accelerated deterioration of corrosion beneath the coating, which may precipitate the premature disintegration of the applied coating.

Secondly, the blast treatment process generates a significant amount of dust. According to studies by the National Institute for Occupational Safety and Health (NIOSH) in the United States, blasting operations using abrasives produce a large volume of dust, which complicates its use in confined workspaces and poses a serious threat to worker health. The dust generated includes particles that can cause respiratory diseases. Additionally, this dust increases the risk of fire. Sparks created by the collision of the abrasive with the steel surface can ignite the dust when combined with heat, creating a hazardous situation that could lead to sudden explosions or fires.

Thirdly, the process of rust removal using blasting can have negative impacts on the environment. The rust separated from steel surfaces during abrasive blasting can quickly disperse into the surrounding air and, without thorough collection, can easily contaminate the environment. Notably, common abrasives often contain copper slag and coal slag, which are known to potentially contain heavy metals (such as chromium, nickel, lead) and toxic elements (like arsenic) [31]. The use of such abrasives can lead to serious environmental pollution through airborne emissions and uncollected residues. Therefore, the development of new surface treatment technologies that consider the efficiency of blast treatment, worker health, and environmental impact is essential and represents a significant challenge that must be addressed.

1.3.4 Abrasive water-jet treatment (AWT)

Abrasive water-jet treatment (AWT) is an effective surface conditioning technique that aids in resolving the aforementioned challenges. The process of abrasive water-jet machining is a distinctive, unconventional machining method. It operates on the principle of using a high-velocity water jet, with pressures often exceeding hundreds of MPa, infused with abrasive materials for the purpose of cutting or removing material [42]. Figure 1-2 illustrates the operation and treatment principles of the AWT technology when applied to the target material. During this machining process, hard abrasive particles are mixed into the high-speed water jet stream, increasing the acceleration of the particles and enhancing the kinetic energy directed at the target surface upon impact, which leads to the erosion of the workpiece [43]. This technique, based on the rapid erosion capabilities of high-speed abrasive waterjets, is effective in machining a broad range of materials. Additionally, it can accomplish rapid machining rates and produce precision-finished surfaces without any thermal deformation [20]. Moreover, the induction of compressive residual stresses, resulting from the high-pressure water jet [18], enhances the fatigue resistance of the material. Nonetheless, the issue of handling secondary waste produced by the machining process remains. However, this method has potential uses that span beyond basic cutting into multiple industries. Recent studies have revealed that this technology can also be employed in the polishing of steel

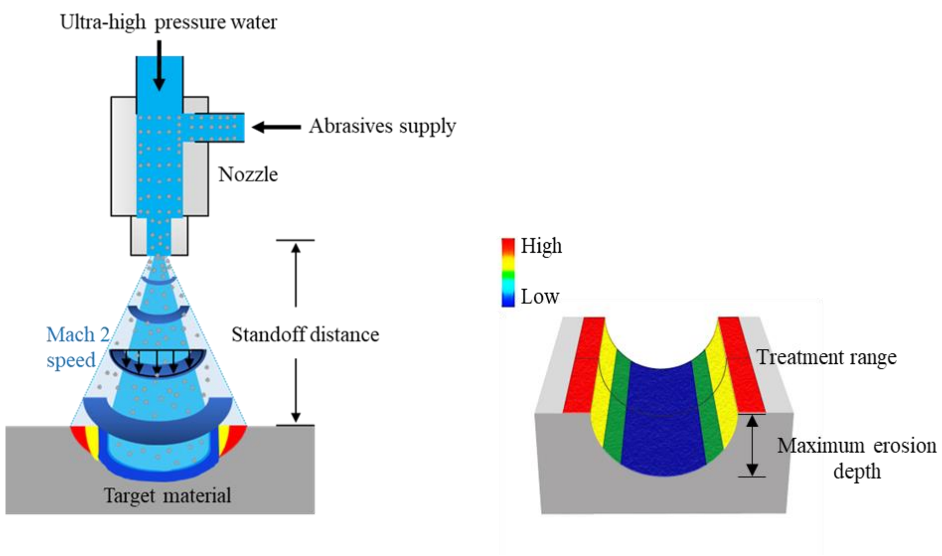

Figure 1-2 Principles of AWT processing.

surfaces [18-22]. This is attainable by managing different operational variables, including the dimension of the abrasive grains, the speed of the waterjet, the standoff distance, the angle of impact, and the pressure. Yet, research related to AWT as a surface treatment has not been systematically elucidated. Particularly, there is a dearth of foundational studies and academic validation regarding the use of this technology on corroded structures, both within domestic and international contexts.

Prior to commencing this research in earnest, a preliminary study was conducted to ascertain whether AWT can be utilized as a surface preparation technique and if it is effective in cleaning corroded surfaces. The various characteristics and potential capabilities of AWT processing are as follows. Firstly, AWT was able to achieve a surface condition of Sa 2.5 or better and a surface salt level of less than 50 mg/m^2 in just a single treatment. This implies that it can effectively remove hard rust layers and chlorides, thereby reducing the need for conventional pretreatment and repeated abrasive blasting treatments [44]. This is expected to lead to substantial reductions in both time and expenses, thereby conferring an economic benefit. Secondly, the abrasive used in the AWT process is garnet, a non-toxic natural mineral, which is less harmful to the environment compared to other abrasives [12]. Additionally, the usage of abrasives is reduced to a quarter of what is needed for blast treatment [20], greatly diminishing abrasive waste and rendering this approach considerably more environmentally friendly. Thirdly, the flexibility of AWT conditioning enables it to be tailored to specific work requirements, offering an extended range of viable treatment distances and heights. This makes it particularly suitable for special working environments, such as high altitudes or confined spaces. Finally, the high-pressure jetting process is expected to effectively remove residual substances without the risk of fire or dust generation by maintaining the water temperature above 60°C [45, 46].

Based on the results of the preliminary research, it has been shown that AWT treatment is effective in removing corrosion and presents multiple benefits in surface treatment applications. However, the effects of the various treatment conditions of AWT on the properties of steel surfaces have not yet been fully investigated. In the coating process that follows surface treatment, the adhesion between the coating and the substrate is greatly influenced by the surface characteristics of the substrate and the mechanical bonding of the coating. Moreover, AWT processing under ultra-high pressure can transform the microstructure of the substrate, which is anticipated to impact the mechanical and electrochemical properties of the material [22]. Such alterations in the properties of the material could directly affect its corrosion resistance. Consequently, this study aims to evaluate the surface and material characteristics of the substrate post-AWT processing and to determine the optimal treatment conditions that yield an ideal substrate surface suitable for coating.

1.4 Organization and outline

The substantive content of this thesis is organized into six chapters, with each chapter receiving a detailed exposition in chapters two to seven.

Chapter 2 introduces the viability of using abrasive water-jet treatment (AWT) as a surface treatment technology. This was achieved by evaluating the cleaning effect on corroded surfaces and the impact of various treatment conditions on surface characteristics. The primary characteristics and potential of AWT as a surface treatment technology are as follows: Firstly, AWT has demonstrated the ability to effectively remove most corrosion contaminants and chlorides, achieving a surface condition of Sa 3 or higher in a single treatment. This suggests the possibility of efficiently eliminating thick rust layers and chlorides, reducing the need for conventional pre-treatment processes and repeated abrasive blasting. The reduction in the number of treatments translates into significant economic benefits in terms of time and cost savings. Secondly, various conditions during AWT processing, such as standoff distance, pressure, number of treatments, and abrasive supply, have a substantial impact on the surface properties of steel plates. These characteristics enable the achievement of surface finishes suitable for a wide range of industrial sectors and conditions, indicating the extensive applicability of AWT across various industries.

Chapter 3 introduces an extensive examination of the surface characteristics exhibited by steel plates when it is subjected to AWT under a variety of conditions. This analysis covered the impact of various AWT processing parameters on surface properties, focusing on differences in nozzle model, abrasive grain size, and processing distance. The surface attributes of the steel plates treated with AWT were assessed quantitatively from several perspectives, including the extent of the treatment area, the maximum erosion depth, the level of surface roughness, topographical modifications, and the quantity of residual abrasive materials. For surface morphology, the study included not only measurements of roughness but also a quantitative evaluation of deformations, utilizing binarization analysis of cross-sectional images to assess changes in topography. The goal of the study was to determine the AWT processing conditions that are conducive to creating a surface state for coating. Results show that the application of AWT, especially when employing a newly developed divergent nozzle, selecting suitable abrasive sizes, and optimizing standoff distances, is an effective method for surface treatment in the maintenance of the actual structure. It also introduces the analysis of the tensile bonding behavior between steel surfaces treated with AWT and epoxy adhesives. It includes conducting pull-off tests to measure the surface characteristics of AWT-processed steel under various conditions and its adhesion strength with epoxy adhesives. The evaluation of adhesion strength involves analyzing surface roughness and the ratio of surface deformation, as discussed in this chapter. The findings indicate that morphological changes, such as anchor patterns, exert a more significant influence on adhesive strength than surface roughness. This study will provide valuable reference material for surface preparation in the field and painting engineering.

Chapter 4 introduces the impact of AWT processing on the mechanical and electrochemical properties of steel plates. First of all, to evaluate the mechanical characteristics of the steel plates, studies were conducted analyzing hardness tests and changes in microstructure. To understand the microstructural changes in the treated samples, micro-photography of the sample cross-sections and analysis of changes in the grain size of the materials were used to quantitatively investigate the plastic deformation of the steel surface. The results of this research shed light on the amount of energy imparted to steel by AWT processing under various conditions and its effects. This study will provide valuable reference material for structural performance and materials engineering fields. In addition, this chapter also presents the results of electrochemical experiments, including potentiodynamic polarization test and electrochemical impedance spectroscopy measurement. These experiments were designed to explore how AWT processing influences the corrosion characteristics of steel surfaces under a range of different conditions. Additionally, an analysis was performed to understand how the surface and mechanical properties of steel surface discussed in Chapters 3 and 4, influence its electrochemical properties and their interrelationships. Through these research findings, it was possible to ascertain that plastic deformation of surface particles has a greater impact on corrosion resistance than surface roughness. The results of this study are expected to provide significant reference material, especially in the fields of material science, corrosion engineering, and surface engineering.

Chapter 5 introduces an evaluation of the efficiency of corrosion removal using AWT, conducted on handhole samples from an actual bridge that had experienced severe corrosion. The bridge was composed of weathering steel, severely corroded due to the influence of airborne sea salt. Before the AWT, we measured the extent of corrosion, as well as the maximum and average depths of corrosion on the deteriorated specimens. To assess the efficiency of corrosion removal, the surfaces and cross-sections of the AWT-processed specimens were analyzed using SEM-EDX, allowing for a quantitative evaluation of the corrosion removal effectiveness. Particularly, a turning test was conducted to measure the frequency and area of corrosion occurrence on the cleaned surfaces over time after treatment. Additionally, a comparison and discussion were made regarding the time required for abrasive blasting and AWT conditioning on specimens with similar levels of corrosion. The presence or absence of flash rust after each treatment was also evaluated to quantitatively analyze the efficiency of cleaning. This study demonstrates that AWT conditioning is a more efficient method for corrosion removal compared to abrasive blasting and can serve as a valuable reference for surface conditioning operations in the field.

Chapter 6 delves into the practical applications and engineering implications of AWT conditioning technology in field settings, particularly focusing on its effectiveness in removing corrosion from severely corroded bridge members. Grounded in the foundational research presented in Chapters 2 through 5, this chapter not only documents the development and field testing of portable AWT equipment on bridges exhibiting significant corrosion but also provides a quantitative analysis of surface characteristics post-treatment. Core samples, 20mm in diameter, were extracted from the most corroded areas of bridges before and after treatment to assess AWT's corrosion removal efficiency, complemented by the turning test to evaluate the potential for flash rust development post-treatment. Remarkably, AWT processing demonstrated the capability to completely eradicate corrosion, even in instances of pitting areas several hundred micrometers deep, without the occurrence of flash rust within 24 hours, meeting the Sa 3 surface quality level required for subsequent coating or painting. By offering a detailed examination of the treatment's impact on various surface properties, including roughness, erosion depth, deformation ratio, and residual abrasive material quantity, alongside evaluations of mechanical and electrochemical material properties, this chapter proposes standardized processing conditions that cater to diverse industrial needs without dependence on operator experience. This comprehensive approach establishes AWT as a pioneering solution for maintaining structures compromised by severe corrosion, setting a new benchmark in surface treatment technology and providing improvements in the quality, efficiency, reliability, and sustainability of steel surface treatments.

Chapter 7 summarized the work presented in this dissertation and further research themes developed from this work were also proposed.

The flowchart of work in this dissertation is depicted in Figure 1-3.

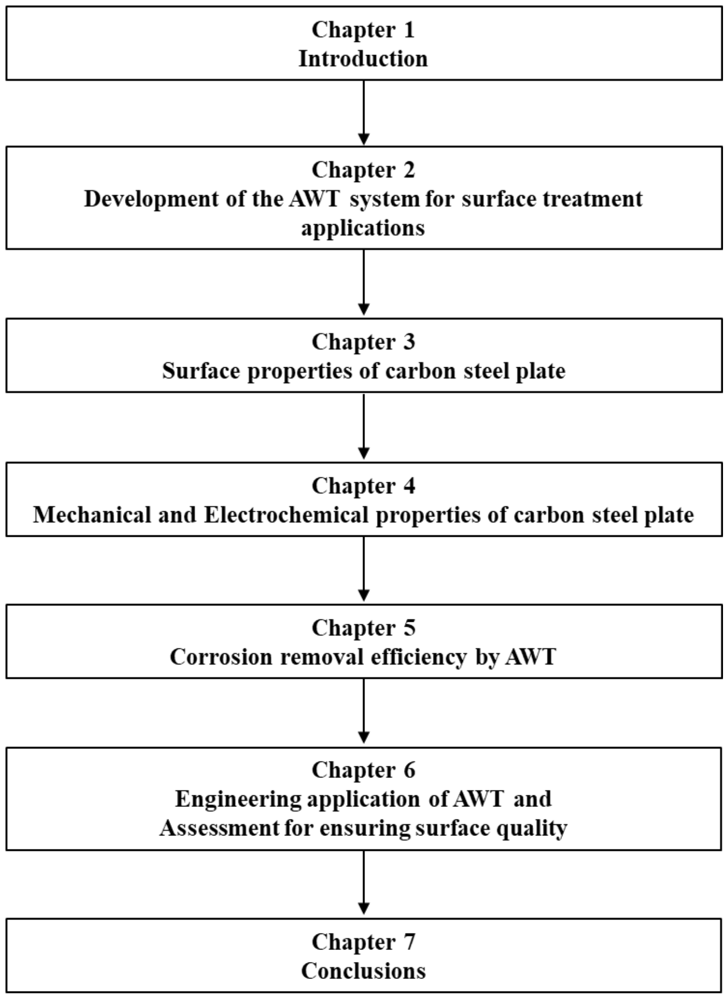

Figure 1-3 Flowchart of the dissertation.

CHAPTER 2 DEVELOPMENT OF THE AWT SYSTEM FOR SURFACE TREATMENT APPLICATIONS

2.1 Introduction

Abrasive water-jet treatment (AWT) emerges as a novel surface cleaning method, effectively addressing the limitations of traditional surface treatment techniques like blast processing, as mentioned in Chapter 1. This process employs waterjet technology, using hundreds of MPa of pressure to remove or cut materials, integrating abrasives in a non-traditional machining approach [40]. In waterjet machining, hard abrasive particles are mixed and accelerated with a high-speed waterjet stream, increasing the kinetic energy as they collide with the target surface, leading to material erosion [41]. This rapid erosive effect of the high-speed abrasive waterjet is applicable to a variety of materials, including metals and non-metals, offering fast processing speeds and clean finishes without thermal distortion [42]. Additionally, the compressive residual stress induced by the high-pressure water spray enhances the material's fatigue life [18]. Abrasive waterjet machining extends beyond simple cutting, holding potential for diverse applications, and recent studies have revealed its feasibility in polishing steel surfaces [18-22]. This is achievable by adjusting various operational parameters like standoff distance, pressure, treatment frequency, waterjet speed, and collision angle. However, research related to AWT is still not systematically conducted, and especially, foundational studies or academic evidence on its application and evaluation on corroded structures are yet to be presented both domestically and internationally.

In Chapter 2, the feasibility of using AWT processing as a surface treatment technique was explored. This was achieved by evaluating the cleaning effects on corroded surfaces and the impact of various treatment conditions on surface properties. The primary characteristics and potential of AWT are as follows. Firstly, AWT demonstrated the ability to achieve a surface condition of Sa 3 or better in a single treatment, effectively removing most corrosion contaminants and chlorides. This suggests the potential to effectively eliminate hard rust layers and chlorides, reducing the need for conventional pretreatment processes and repetitive abrasive blasting. Such a reduction implies significant economic benefits in terms of time and cost savings. Secondly, during the AWT processing, various conditions such as standoff distance, pressure, number of treatments, and abrasive supply significantly affect the surface properties of steel. These characteristics allow for the achievement of quality surface finishes suitable for various industrial fields and conditions, indicating the broad applicability of AWT over diverse industrial sectors.

The high-pressure spray process of AWT processing is expected to effectively remove salts and residual materials without the risk of fire or dust generation, by maintaining the water temperature above 60°C [44-45]. Preliminary research results indicate that AWT is efficient in corrosion removal and offers several advantages in the field of surface treatment. However, the impact of various AWT processing conditions on the characteristics of steel surfaces has not yet been sufficiently investigated. In the post-treatment coating process, the adhesion between the coating and the substrate is greatly influenced by the characteristics of the substrate surface and the mechanical bonding of the coating. The changes in surface characteristics during AWT processing, under varying conditions of standoff distance, abrasive supply, pressure, and number of treatments, were evaluated in terms of treatment range, maximum erosion depth, surface roughness, and the amount of residual abrasives. Consequently, this study aims to determine the optimal treatment conditions for AWT that can create an ideal substrate surface suitable for coating, by assessing the substrate surface characteristics after AWT processing.

2.2 Experimental method

2.2.1 Experimental process

To evaluate the corrosion removal effectiveness and surface characteristics of AWT processing, SM490A carbon steel, as specified in the Japanese Industrial Standards, was used for all experiments. The dimensions of the specimens were 150×70×6mm and 75×70×6mm, respectively. The chemical composition and mechanical properties of the specimens are listed in Tables 2-1 and 2-2. To characterize the surface properties, all samples were finished to remove all scales and contaminants. For corroded steel plates, a preliminary blast treatment was conducted before sample preparation. The parameters for the blast treatment were set to a standoff distance of 300 mm, pressure of 0.7 MPa, and angle of 90 degrees, using Fe-Ni abrasive. After blasting, the specimens were immersed in 3.5 wt%

saline solution for a day to induce corrosion on the steel plates. The AWT processing aimed primarily to (1) ascertain the efficiency of corrosion removal from the treated samples and (2) evaluate the surface characteristics of the steel plate. The specific operational conditions of AWT for evaluating the efficiency of corrosion removal are listed in Table 2-3, while the conditions for assessing surface characteristics are detailed in Table 2-4. The nozzle was positioned at a 90° angle on an uniaxial moving device and treated the samples with a traverse speed of 1m/min. A conventional convergent nozzle, used in material cutting, was employed during the AWT processing.

Table 2-1 Chemical properties of SM490A steel plate.

Elements (wt%)					
Mn	Si	C	P	S	Fe
1.31	0.31	0.17	0.019	0.003	bal

Table 2-2 Mechanical properties of SM490A steel plate.

Yield strength (MPa)	Tensile strength (MPa)	Elastic modulus (GPa)	Elongation (%)	Poisson's ratio	Density (g/cm^3)
387±5.73	482±6.01	208±4.92	23.3±2.51	0.26±0.01	7.85

Table 2-3 AWT processing parameters for corrosion removal efficiency.

Nozzle type	Abrasive material	Standoff distance (mm)	Abrasive supply (g/min)	Pressure (MPa)	Number of processing (N)	Traverse speed AWT machine (m/min)
Convergent	Garnet #30/60	100	600	230	1	1

Table 2-4 AWT processing parameters for surface characteristics.

Nozzle type	Abrasive material	Standoff distance (mm)	Abrasive supply (g/min)	Pressure (MPa)	Number of processing (N)	Traverse speed AWT machine (m/min)
Convergent	Garnet #30/60	100200/ 300	200/400/ 600	180/230	1/ reciprocating	1

2.2.2 Analysis methods for surface properties

The surface morphology of all specimens was examined and analyzed using a 3D digital optical microscope (VHX-1000, Keyence Co., Ltd.). The cross-sectional profiles of the treated specimens were measured using a laser confocal microscope (OLS4500, Olympus Optical Co., Ltd.) after undergoing AWT. Laser measurements for the cross-sectional profiles were determined by analyzing a 2.5×70 mm area centered on the treated specimen surface. Surface roughness was evaluated by measuring the arithmetic average roughness (Ra) using a portable surface roughness tester (SJ-210, Mitutoyo Corporation). The elemental chemical composition of the treated surfaces was measured using a scanning electron microscope (SEM) equipped with energy-dispersive X-ray spectroscopy (SEM-EDX, SU3500, Hitachi Ltd.) at an acceleration voltage of 15 kV and a vacuum pressure of 30 kPa.

2.3 Test results

2.3.1 Corrosion removal efficiency

Figure 2-1 displays the surface condition and the images of the corroded samples processed with AWT processing. The treated surface meets the Sa 3 level, free from residual corrosion products. Additionally, the SEM-EDX images were sequentially measured from point 1, the center of the processed area, to point 5, an untreated area, to examine the efficiency of removing corrosion products and chlorides. The treated area was approximately 20 mm, and most of the corrosion products and chlorides were removed within this treatment zone. Notably, a significant amount of Cl clusters present before AWT processing were eliminated afterwards. Furthermore, a substantial portion of corrosion products was also removed in the treated and boundary areas of point 3, demonstrating the exceptional rust removal efficiency of AWT.

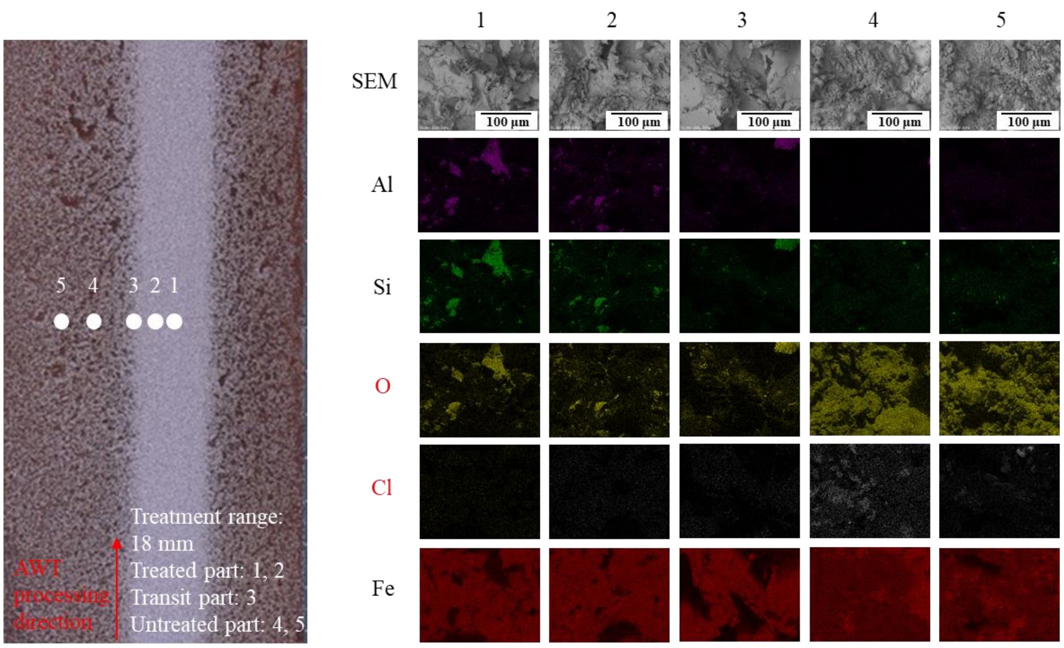

Figure 2-1 SEM-EDX examination from the unprocessed part to the central area of the AWT-processed specimen.

2.3.2 Surface profile

Figure 2-2 illustrates a schematic of the AWT processing, where the jet dynamics are divided into two distinct zones: the dynamic pressure zone and the hydraulic zone, as shown in this figure. In the dynamic pressure zone, the jet maintains its velocity, kinetic energy, and density consistent with that at the nozzle exit. Characterized by high energy, this zone is predominantly utilized for cutting applications. Conversely, in the hydraulic zone, the jet exchanges momentum and mass with the surrounding air, leading to the formation of fine droplets or a mist in the boundary region. The hydraulic zone exhibits lower energy due to energy dissipation through divergence, compared to the dynamic pressure zone. These characteristics render it more suitable for cleaning or polishing applications [54]. Even in the hydraulic zone, considerable energy is generated due to the delivery of water and abrasives at speeds exceeding Mach 2 under high-pressure conditions. This energy is sufficient to directly erode and remove material from the substrate, showcasing the efficacy of the hydraulic zone in the AWT processing.

Figure 2-3 presents the quantitative analysis of the treated area on steel surfaces following AWT processing under various conditions. Figure 2-3(a) illustrates the impact of standoff distance, pressure, and abrasive supply on the treated area of the steel plate. The experimental results revealed a linear relationship between the standoff distance and the

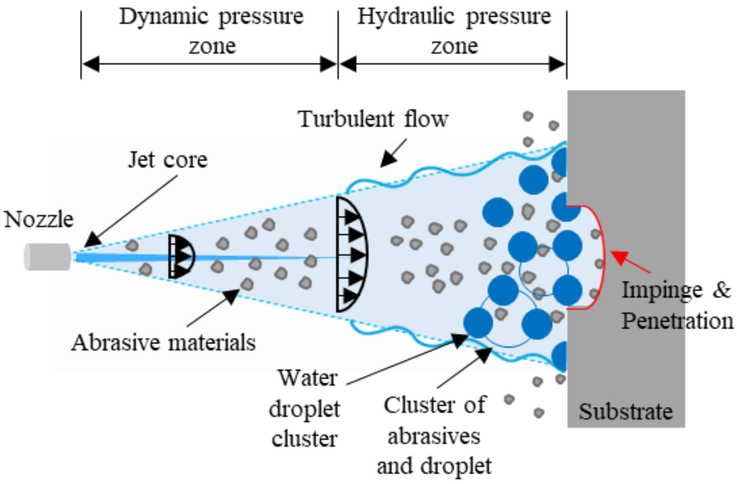

Figure 2-2 Schematic diagram of AWT polishing effects.

treatment range under constant pressure and abrasive supply conditions. Notably, with every 100 mm increase in standoff distance, the treatment range expanded by an average of 1.5 times, reaching its maximum at a standoff distance of 300 mm. In contrast, variations in pressure had minimal impact on the treated area. Conversely, an increase in abrasive supply

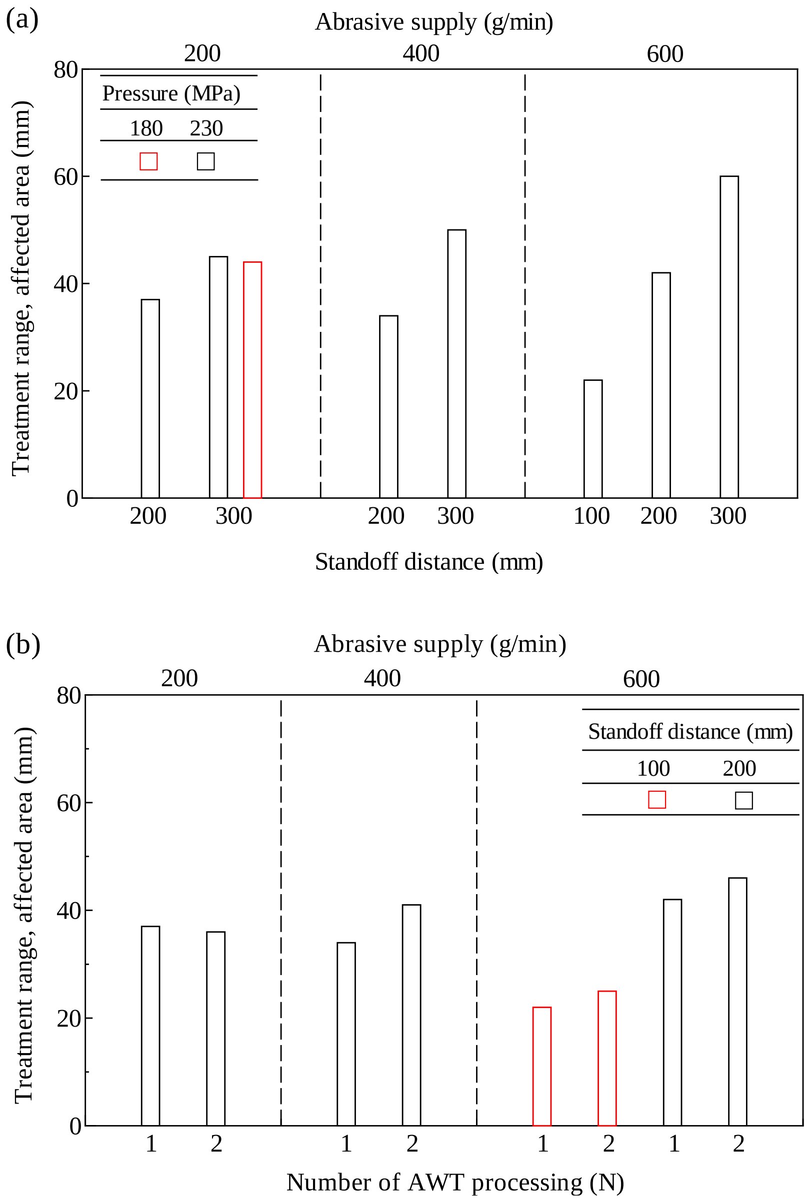

Figure 2-3 Treatment range of the treated surface according to various processing conditions: Based on (a) standoff distance, pressure, and abrasive supply and (b) AWT processing count.

led to a linear expansion of the treated area. Specifically, the treated area under a condition of 600 g/min abrasive supply was 1.2 to 3 times larger compared to the 200 g/min and 400 g/min conditions. Figure 2-3(b) shows changes in the treated area of the steel plate with increasing treatment frequency. However, except for the 400 g/min abrasive supply condition, the increase in the treated area due to repeated AWT processing was less than 10%, indicating a minor difference.

Figure 2-4 presents a quantitative analysis of the maximum erosion depth on steel surfaces resulting from various AWT processing conditions. Figure 2-4(a) displays the maximum erosion depth in steel as influenced by changes in standoff distance, pressure, and abrasive supply. The experimental data indicated a linear inverse relationship between standoff distance and maximum erosion depth under constant pressure and abrasive supply. Specifically, each 100 mm increase in standoff distance resulted in an average 1.4 times decrease in maximum erosion depth, with the smallest depth observed at a standoff distance of 300 mm. In terms of pressure, the 230 MPa condition exhibited approximately 1.3 times deeper erosion compared to the 180 MPa condition. However, increases in abrasive supply led to a linear increase in maximum erosion depth, though this difference was relatively minor, being less than 10%. Figure 2-4(b) shows the variation in the maximum erosion depth of steel with increasing treatment frequency. Depending on the experimental conditions, the maximum erosion depth increased by 1.5-2 times with more treatment. Notably, under conditions of 600 g/min abrasive supply and 100 mm standoff distance, repeated AWT processing resulted in a maximum erosion depth of up to 800 μm, highlighting the significant erosion depth achievable under these specific conditions.

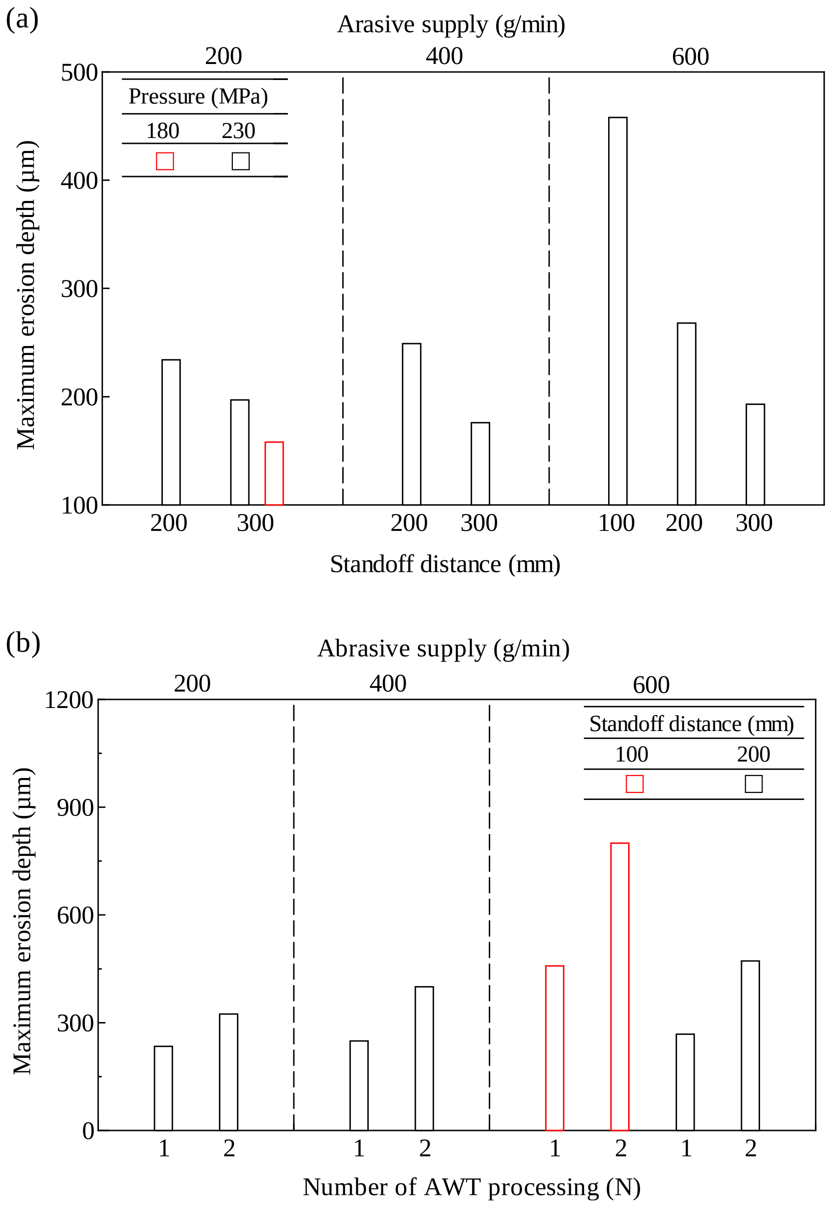

Figure 2-4 Maximum depth of the treated surface according to various processing conditions: Based on (a) standoff distance, pressure, and abrasive supply and (b) AWT processing count.

Figure 2-5 delivers a quantitative analysis of the surface roughness (Ra) values on steel plates processed under various AWT processing conditions. Figure 2-5(a) delineates the changes in surface roughness of steel in response to alterations in standoff distance, pressure,

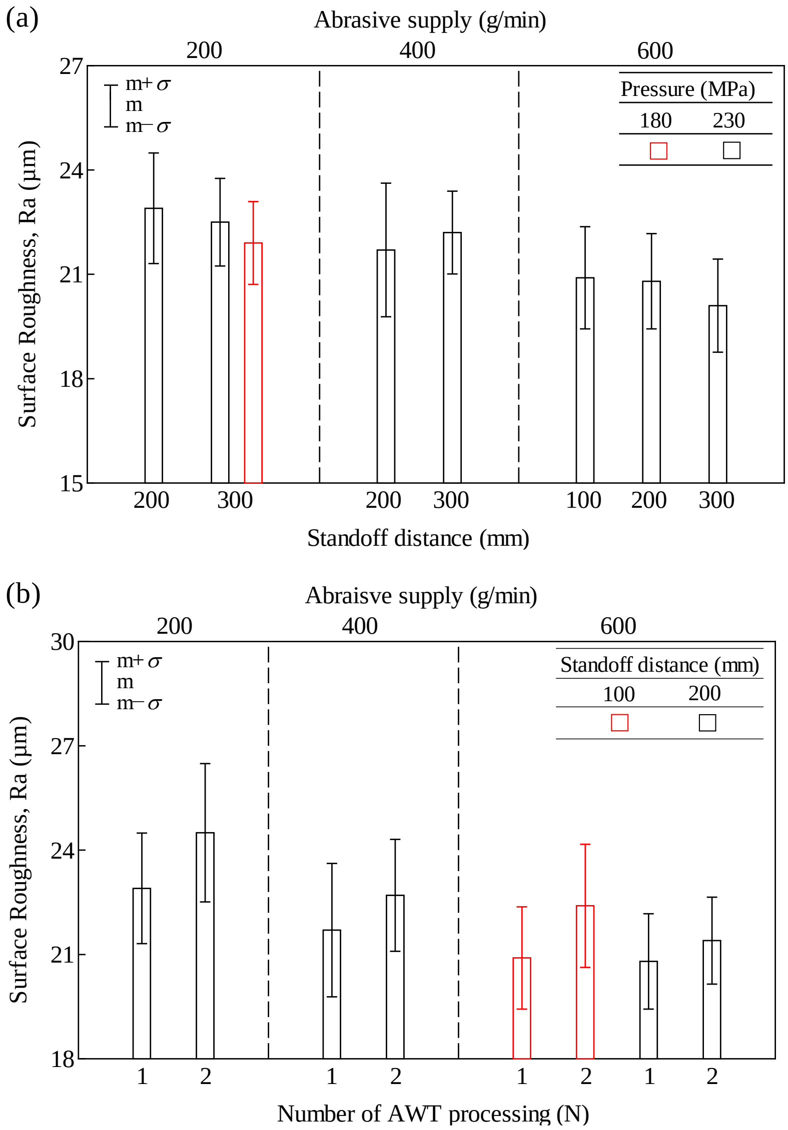

Figure 2-5 Surface roughness of the treated surface according to various processing conditions. Based on (a) standoff distance, pressure, and abrasive supply and (b) AWT processing count.

and abrasive supply. The experimental data demonstrated that, under constant pressure and abrasive supply, an increase in standoff distance correlated with a decrease in surface roughness, although this change was relatively minor, remaining below 10%. Similarly, under pressure conditions, the 230 MPa setting resulted in a higher roughness value compared to the 180 MPa setting, but again, the difference was less than 10%. Increases in abrasive supply led to reductions in surface roughness; however, these changes were also

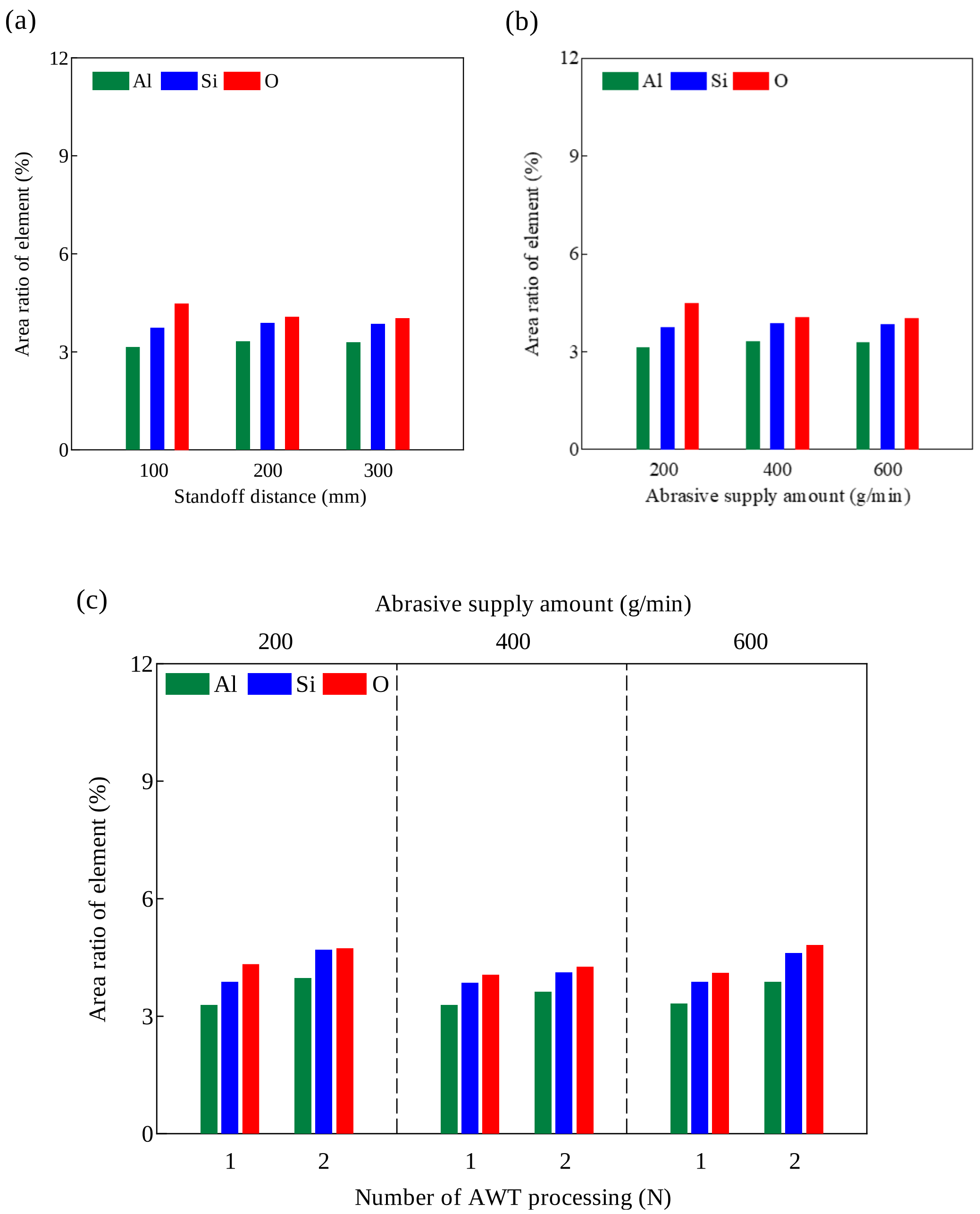

Figure 2-6 Residual abrasive materials of the treated surface according to various processing conditions. Based on (a) standoff distance, (b) abrasive supply and (c) AWT processing count.

limited, not exceeding a 10% variation. Figure 2-5(b) illustrates the variations in surface roughness of steel plate with increasing numbers of treatments. Under all treatment conditions, surface roughness tended to increase with more frequent treatments, yet the extent of this increase remained below 10%. Overall, the lowest surface roughness values were recorded under the conditions of 600 g/min abrasive supply and 300 mm standoff distance. In all tested conditions, the changes in surface roughness fell within an error range of less than 10%, a finding that, while not significantly impactful from an engineering standpoint, provides crucial insights for trend analysis.

Figure 2-6 shows the area percentage of residual abrasives present on the centrally treated surface of steel plate. In this study, SEM-EDX was utilized to obtain image results based on atomic percentages, which were measured at the micro-scale level. Based on these data, a methodology for calculating the area percentage was developed to quantitatively compare and assess the distribution of residual abrasive over a broader area. EDX mapping images of the primary chemical elements of garnet, namely aluminum (Al), silicon (Si), and oxygen (O), were combined to extract a representative image of size 3×4 mm. The area ratio from these extracted images was calculated using ImageJ software. For the comparative analysis of the amount of residual abrasive based on surface treatment conditions, the area ratio of silicon (Si), the predominant chemical component in garnet, was utilized. It was observed that the AWT-processed samples showed a consistent area ratio of 3-4%, regardless of the standoff distance and abrasive supply conditions. However, regarding treatment frequency, specimens subjected to reciprocating treatments exhibited an approximately 10-20% higher area ratio of residual abrasives compared to those that underwent a single treatment.

The primary objective of this study is to evaluate the potential applicability of AWT technology in the field of surface treatment. To achieve this, the study focuses on the quantitative analysis of the resultant treatment range, maximum erosion depth, surface roughness, and the amount of residual abrasives after treatment. These metrics serve as crucial indicators for assessing the effectiveness and efficiency of AWT processing. Chapter 2 of this paper presents a quantitative analysis of the impact of AWT processing on steel surfaces, based on these metrics, and provides an initial assessment of the results.

Subsequently, Chapter 3 delves into a detailed analysis and comprehensive examination of the causes behind these results. Through this approach, the study aims to provide an evaluation of the potential capabilities of AWT in the realm of surface treatment, thereby contributing to a better understanding of its applicability and effectiveness in this field.

2.4 Summary

In Chapter 2, the research was conducted to validate the potential of AWT as a viable surface treatment technology. For this purpose, the effectiveness of AWT in removing corrosion products and chlorides was evaluated on corroded carbon steel plates. Additionally, this study set out to meticulously investigate the impact of various AWT process parameters, including standoff distance, abrasive supply, pressure, and the number of treatments, on the surface properties of carbon steel. To achieve these objectives, a thorough quantitative comparative assessment was conducted, focusing on the treatment range, maximum erosion depth, surface roughness, and the quantity of residual abrasive material. This comprehensive approach aimed to provide an in-depth understanding of the influence of AWT processing conditions on the alteration of steel surface characteristics, thereby underscoring the efficacy and versatility of AWT in surface treatment applications.

The key findings obtained from this chapter are as follows.

1) AWT processing successfully achieved a surface condition of Sa 3 or better with just a single treatment, effectively removing the majority of corrosion contaminants and chlorides.
2) During AWT processing, the treatment range on the steel surface exhibited a linear increase with changes in standoff distance and abrasive supply. Notably, the treated area reached its maximum under conditions of a 300mm standoff distance and a 600 g/min abrasive supply. This underscores the significance of standoff distance and abrasive supply in influencing the effect of AWT on the steel surface. However, increases in treatment pressure and frequency did not have a significant impact on the variation of the treatment range.
3) The maximum erosion depth in steel during AWT processing was closely associated with the standoff distance. Experimental results indicated that an increase in standoff distance led to a decrease in maximum erosion depth, with the smallest depth

observed at a standoff distance of 300mm. Conversely, increases in pressure and treatment frequency were found to correspond with an increase in maximum erosion depth. However, the impact of increased abrasive supply on erosion depth was relatively minor.

4) During AWT processing, the roughness of the steel surface exhibited variations depending on the treatment conditions. According to the results of this study, an increase in standoff distance and abrasive supply led to a reduction in surface roughness. In contrast, increases in pressure and the number of treatments resulted in an increase in surface roughness. Notably, the lowest roughness was observed under the single treatment condition of a 300mm standoff distance, 230 MPa pressure, and 600 g/min abrasive supply in this study.
5) Regarding the residual abrasives, there was an observed tendency for their quantity to increase with the number of AWT processes. However, under other treatment conditions, the area ratio of residual abrasives maintained consistent values.

CHAPTER 3 SURFACE PROPERTIES OF AWT-PROCESSED CARBON STEEL

3.1 Introduction

Coating is commonly applied to protect steel structures from corrosion in harsh environmental conditions such as coastal and marine environments. The primary protective mechanism of coating involves blocking external oxygen, moisture, and chlorides, thereby limiting the impact of corrosion, and enhancing the performance and lifespan of the structure. However, the effectiveness of this protective mechanism is directly dependent on how the coating adheres to the substrate [47]. Therefore, the adhesion between the coating and the substrate plays a crucial role in providing superior performance and prolonged service life of the coating. The factors influencing the adhesion between the substrate surface and the coating are diverse and can vary significantly depending on the adhesion situation and the characteristics of the materials used. Generally, the adhesion between the coating and the substrate is influenced by mechanical interlocking between the coating and the substrate, the surface energy of the substrate itself, electrochemical properties, and cleanliness. Particularly, mechanical interlocking between the substrate and the coating film is of utmost importance for adhesive bonding strength and is sensitive to the surface characteristics of the substrate [15]. Surface characteristics of the substrate that affect mechanical interlocking include surface roughness, actual topographical changes, and cleanliness. To ensure excellent bonding performance, it is necessary to clean the substrate surface before painting to remove contaminants, as well as to create appropriate surface roughness and modify surface structure through surface treatment.

To evaluate the efficacy of surface treatment technologies, it is crucial to consider not only the effectiveness in removing contaminants like corrosion products and chlorides but also the surface characteristics of steel that emerge post-treatment. Among various surface properties, factors deemed significant in assessing treatment effectiveness and subsequent coating adhesion include the treated area, erosion depth, roughness, surface topography, and the amount of residual abrasive material. The reduced treatment area, substantial thickness loss, and notable increase in surface roughness of steel plates post-treatment can lead to a degradation in the durability of the steel and a decrease in the adhesion strength with the coating. Additionally, a narrow-treated area can increase the number of treatment repetitions, leading to economic inefficiency. Surface roughness and topography play a crucial role in determining the adhesion of the coating to the substrate. Generally, increased surface roughness enhances adhesion [48]. However, excessive roughness can potentially damage the coating due to sharp peaks [23], and overly deep valleys may impede paint penetration, leading to premature coating detachment [10]. This potentially compromises the durability of the steel plate and the adhesive bond between the treated surface and the paint during painting [49]. An excessive amount of residual abrasive material is undesirable as it creates a barrier between the steel surface and the coating, reducing adhesion and efficiency [50].

In Chapter 3, the impact of various conditions on the surface properties of steel plate when treated with Abrasive water-jet treatment (AWT) is examined. Specifically, this chapter aims to address issues raised by the convergent nozzle in preliminary studies using AWT. It identifies ideal AWT processing conditions capable of effectively generating surface properties suitable for coating applications and examines the effects of the newly developed divergent nozzle. Additionally, the influence of abrasive particle size on the manufactured surface properties is assessed to determine the most appropriate particle size for surface treatment using AWT. This is crucial as the size and shape of abrasive particles are key elements in the surface preparation process for achieving high efficiency and precision conditions [24-26]. Additionally, this study evaluates changes in surface properties during the AWT process in terms of treatment range, maximum erosion depth, surface roughness, surface topography, and amount of residual abrasive materials, considering various nozzle types, abrasive sizes, and standoff distances. All these characteristics are compared with those generated by conventional surface treatment techniques such as abrasive blasting. Furthermore, the study seeks to establish a basic understanding of the effect of surface properties of AWT-processed steel plate on the tensile adhesion behavior of epoxy adhesives. The surface properties of the AWT-processed steel plate are analyzed in terms of changes in surface roughness and topography. Special attention is paid to the influence of surface topography on the adhesion strength of coatings and the mechanical interlocking effect. This is because morphological changes, such as the anchor pattern of the surface, can have a more direct impact on adhesion strength than microscopic parts of surface roughness [51]. Therefore, this chapter investigates the impact of surface roughness, resulting from AWT treatment under various conditions, on the tensile adhesion strength of epoxy adhesives. Additionally, this study evaluates and compares the adhesion behavior of steel surfaces and epoxy adhesives by calculating the surface contact area ratio through SEM images of the cross-sections of AWT-processed steel.

3.2 Experimental method

3.2.1 Experimental AWT process in laboratory

For the evaluation of surface characteristics of steel treated with AWT and blast treatments, SM490A steel plate, as defined by the Japanese Industrial Standards, was utilized. The dimensions of the test specimens were 150×70×6mm. The chemical composition and mechanical properties of the specimens are listed in Tables 2-1 and 2-2, respectively in Chapter 2. To characterize the surface properties, all samples were finished to remove scales and contaminants. The AWT process was conducted primarily to (1) assess the surface properties of carbon steel plate and (2) evaluate the efficiency of corrosion removal in severely corroded bridge samples. The specific operational conditions of AWT for surface property evaluation are detailed in Table 3-1. The nozzle was positioned at a 90° angle on a uniaxial moving device and treated at a transverse speed of 1m/min. Both conventional convergent nozzle and newly developed divergent nozzle were used to investigate the impact of nozzle type on surface property changes during the AWT processing. The convergent and divergent nozzles are referred to as AWJ and AWT nozzles, respectively. The AWJ nozzle was designed with a linear structure from inner to outer diameter, resulting in a narrow,

Table 3-1 AWT processing parameters.

Specimen	Nozzle type	Nozzle diameter (mm)	Abrasive materials	Standoff distance (mm)	Abrasive supply (g/min)	Pressure (MPa)
AWJ#30/60	Convergent	2	Garnet #30/60	100/200/300	600	230
AWT#30/60	Divergent	5				
AWT#80			Garnet #80			

Table 3-2 Specifications of abrasive materials.

Abrasive materials	Particle size (μm) (Sieve analysis)	Bulk density (t/m^3)	Specific gravity	Hardness (Mohs)
Garnet #30/60	150–425 (99%)	2.3	4.1	7.5
Garnet #80	106–300 (99.8%)	2.5		

Table 3-3 Chemical composition of abrasive materials.

Composition (wt%)						
Abrasive materials	Al_2O_3	SiO_2	Fe_2O_3	MgO	CaO	TiO_2
Garnet #30/60	20.4	34.7	33.8	5.89	2.62	1.64
Garnet #80	20	33.4	33.8	5.64	2.3	3.43

straight-directional water flow. In contrast, the AWT nozzle widens from the inner to outer diameter, designed to expand the flow direction of water, from the flow rectifier end to the inlet, along the nozzle's longitudinal axis. This design feature allows ultrahigh-pressure water containing abrasive particles discharged from the AWT nozzle to disperse over a wider area, thereby extending the contact area with the target material. Compared to the AWJ nozzle, this characteristic promotes more effective rust removal within the expanded treatment area while effectively mitigating significant thickness reduction within the permissible limits of steel plate thickness. Garnet was selected as the abrasive material [24]. To assess the impact of abrasive particle size on surface properties, two types of garnet with different particle sizes, namely mesh sizes 30/60 and 80, were used for comparative evaluation. The specific composition of the garnet is presented in Table 3-2. Table 3-3 provides information about the chemical composition. The appearance and particle size distribution of the garnet are shown in Figure 2-1. Samples treated with various nozzle types and abrasive particle sizes are designated as AWJ#30/60, AWT#30/60, and AWT#80 specimens. For a comparative analysis of surface treatment characteristics and the effectiveness of rust and chloride removal by AWT, abrasive blasting was used as a control group. The abrasive blasting was conducted using garnet with a mesh size of 30/60. Specific

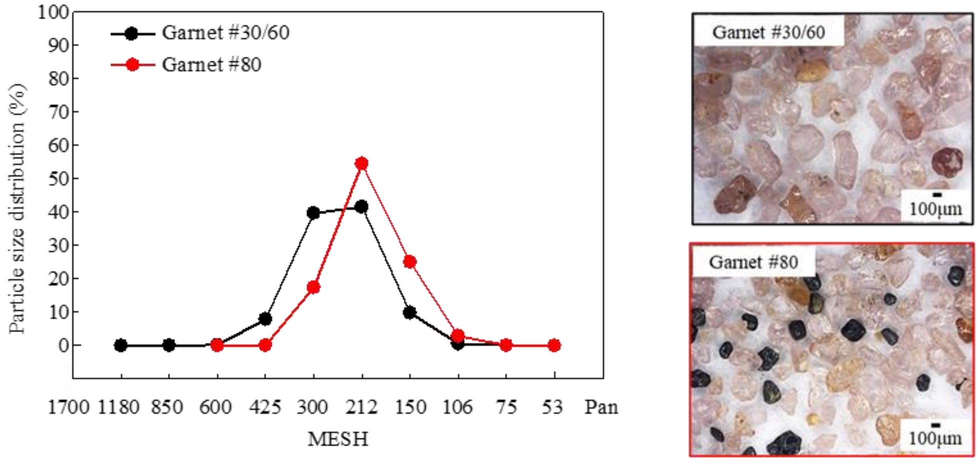

Figure 3-1 Particle size and distribution of abrasive materials.

Table 3-4 Abrasive blasting parameters.

Specimen	Nozzle diameter (mm)	Abrasive materials	Standoff distance (mm)	Pressure (MPa)	Abrasive supply (g/min)	Blasting Time (sec)	Blasting Angle (º)
Abrasive blasting	8	Garnet #30/60	100/200 /300	0.7	1,740	5	90

blasting conditions used for surface property evaluation are listed in Table 3-4. The nozzle was positioned at a fixed 90° angle and treated for 5 seconds. The duration of the blast treatment was measured considering the machining time, based on the maximum treatment area of the AWT #30/60 specimen.

3.2.2 Analysis methods for surface properties

The surface morphology of all specimens was inspected and analyzed using a three-dimensional digital optical microscope (VHX-1000, Keyence Co., Ltd.). The cross-sectional profiles and surface roughness of the treated specimens were measured with a laser confocal microscope (OLS4500, Olympus Optical Co., Ltd.). Laser measurements of the cross-sectional profiles covered a 2.5×70 mm area centered on the treated specimen surface, while surface roughness analysis involved a 0.6×10 mm area centered on the treated surface. Roughness was evaluated by measuring the arithmetic mean roughness (Ra) and Rzjis.

According to the Japan Society of Civil Engineers (JSCE), Rzjis represents the ten-point average roughness, used to assess appropriate surface roughness values for steel bridges before repainting. For changes in surface topography, selected cross-sectional images measured by scanning electron microscopy (SEM) were chosen. The selected images were binarized using Image J software, after which the x,y coordinates of the binary surface deformation area were extracted to calculate the length of the altered area, thereby determining the surface deformation ratio (DR). To provide statistically reliable data and estimate high-confidence values, five rounds of image analysis were performed on samples treated under each condition. The elemental chemical composition of the treated surfaces was measured using the SEM-EDX method introduced in Section 2.2.2 of this paper.

3.2.3 Pull-off test

Pull-off tests were performed to evaluate the impact of surface characteristics of steel treated with AWT and blasting on the tensile adhesion behavior of an epoxy adhesive. The epoxy adhesive chosen was a two-component, room-temperature curing epoxy system (Three Bond 2087), widely used in structural adhesives. For pull-off tests, a dolly made of aluminum alloy A2017 (JIS H 4000) was employed. The diameter of the dolly was determined to be 20 mm in accordance with JIS K 5600[52] (General testing methods for paints) and JIS H 8300[7] (Metal spraying of zinc, aluminum, and their alloys), to ensure uniform coverage over the entire surface. Additionally, the adhesion face of the dolly was uniformly abraded using sandpaper (#120) to standardize its roughness.

To minimize bending stress between the adhesive and the dolly during testing, the clamping section was machined with an R10 radius to facilitate a two-point contact structure between the jig and the dolly [53]. The appearance of the press device used for attaching the dolly to the substrate is illustrated in Figure 3-2. After applying the two-component, room-temperature curing epoxy adhesive (Three Bond 2087) to the adhesion face of the dolly, a custom-made press was utilized to exert a consistent vertical force of 0.9 MPa for 30 minutes in an indoor environment (approximately 25°C, 60%RH), as depicted in Figure 3-2. Subsequently, the adhesive was cured for approximately 48 hours in a small high-temperature chamber (ST-120) at 35°C and 10%RH.For the adhesive cured outside the dolly's adhesion area, a hole saw was used to trim the periphery until the adhesive area

Figure 3-2 Pressurization device and dolly compression process.

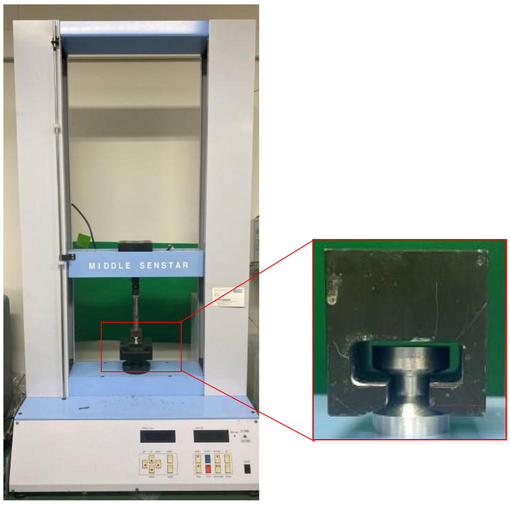

Figure 3-3 Desktop pull-off adhesion tester.

reached 314mm². The tensile adhesion tests were conducted on the central projection area of the AWT and blast-treated specimens, based on the pull-off method (JIS K5600-5-7). Figure 3-3 shows the benchtop tensile adhesion tester (MSC-10/500-2) used in this study. A universal joint was installed in the jig of the test specimen holder to reduce the effect of bending during the test. The tensile speed was set at 0.5 mm/min, and an autograph (load capacity: 10 kN, crosshead speed range: 0.5~500 mm/min) was used to evaluate the relationship between load and displacement and the effect of bending during the tensile adhesion test. Following the completion of the pull-off test, the steel surface and the dolly's surface were examined using a digital microscope (HRX-01, Hirox Co., Ltd.).

3.3 Surface properties according to AWT conditions

3.3.1 Surface profile

Under high-pressure conditions, water and abrasives are delivered to the target surface at speeds exceeding Mach 2, resulting in significant energy generation in the hydraulic zone, which can directly erode and remove material from the substrate. Figure 3-4 displays

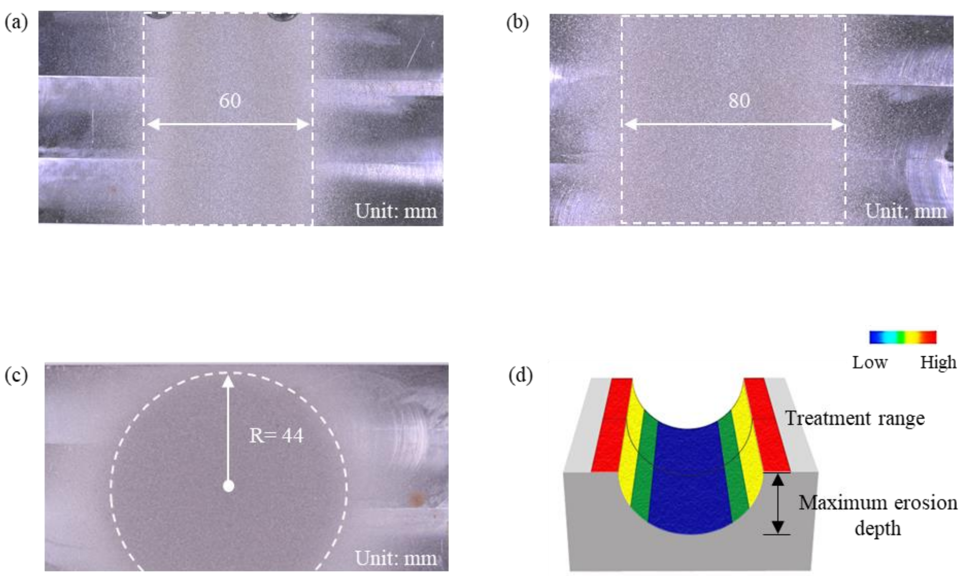

Figure 3-4 Surface states of the treated carbon steel plates: (a) AWJ#30/60, (b) AWT#30/60, (c) Blasted samples, and (d) 3D visualization of the processed surface.

photographs and 3D images of specimens treated with various surface treatments. Figures 3-4 (a-c) provide an overview of the treated range of steel subjected to AWT and blast treatment. The maximum erosion depth refers to the depth measured from the trench profile as shown in Figure 3-4 (d). All treated surface areas demonstrated various treatment ranges, maximum erosion depths, and surface roughness.

Table 3-5 shows the numerical representation of the treated area on steel surfaces after AWT and blast treatments. It is observed that the specimens treated with blasting exhibit a wider affected area due to the larger diameter of the blasting nozzle compared to that used in AWT processing. The treatment efficiency of the AWT nozzle was emphasized by the fact that the AWT#30/60 specimen showed more than twice the treatment range at the same standoff distance as the AWJ#30/60 specimen. This difference can be attributed to the divergent spray of the AWT nozzle, a phenomenon enhanced by the larger nozzle diameter. Consequently, these findings indicate an improved treatment efficiency of the AWT nozzle compared to the AWJ nozzle. Upon comparing the treatment range according to the size of abrasive particles, it was observed that a decrease in particle size led to a gradual improvement in the treatment range. This trend was further amplified with an increase in standoff distance. Particularly at a distance of 300 mm, the AWT#80 specimen exhibited about 10% higher treatment range than the AWT#30/60 specimen. Additionally, the observations indicated a significant correlation between the size of abrasive particles and the treatment range, especially when the standoff distance exceeded 300mm. In this study, the particle size accounted for an error margin of approximately 10%, which, while not significant in practical engineering implications, is important in the context of trend analysis. This discrepancy arises due to the smaller ratio of inertia to drag in smaller particles in the water-abrasive mixture, leading to a wider external spray [26]. Furthermore, it was noted that as the distance from the nozzle increases, the spray diverges more, resulting in an expanded treatment range with longer standoff distances.

Table 3-5 Treatment range of the of the processed surface.

Specimens	Standoff distance (mm)	Treatment range (mm)
AWJ #30/60	100	22
	200	42
	300	60
AWT #30/60	100	45
	200	67
	300	79
AWT #80	100	46
	200	70
	300	87
Blast treatment	100	51
	200	77
	300	87

Figure 3-5 displays the overall cross-sections and maximum erosion depths of specimens treated with AWT and blasting. Under all conditions, AWT-processed specimens exhibited greater treatment depths compared to those blasted, with the depth decreasing as the standoff distance increased, a phenomenon that was visually evident. Notably, at a standoff distance of 100mm, all AWT-processed specimens showed of plastic flow, such as the formation of raised lips at the edges of the trench profiles, indicative of the substrate curling upwards. In contrast, no plastic flow was observed in the blasted specimens. This difference is attributed to the AWT mechanism, where abrasives reaching the substrate surface is higher in the AWT compared to the blast treatment.

Figure 3-6 provides quantitative values for the maximum erosion depths achieved through AWT and blast treatment. In all conditions, specimens treated with AWT exhibited greater maximum erosion depths compared to those subjected to blasting. During AWT processing, at the same standoff distances, the maximum erosion depth of the AWT#30/60

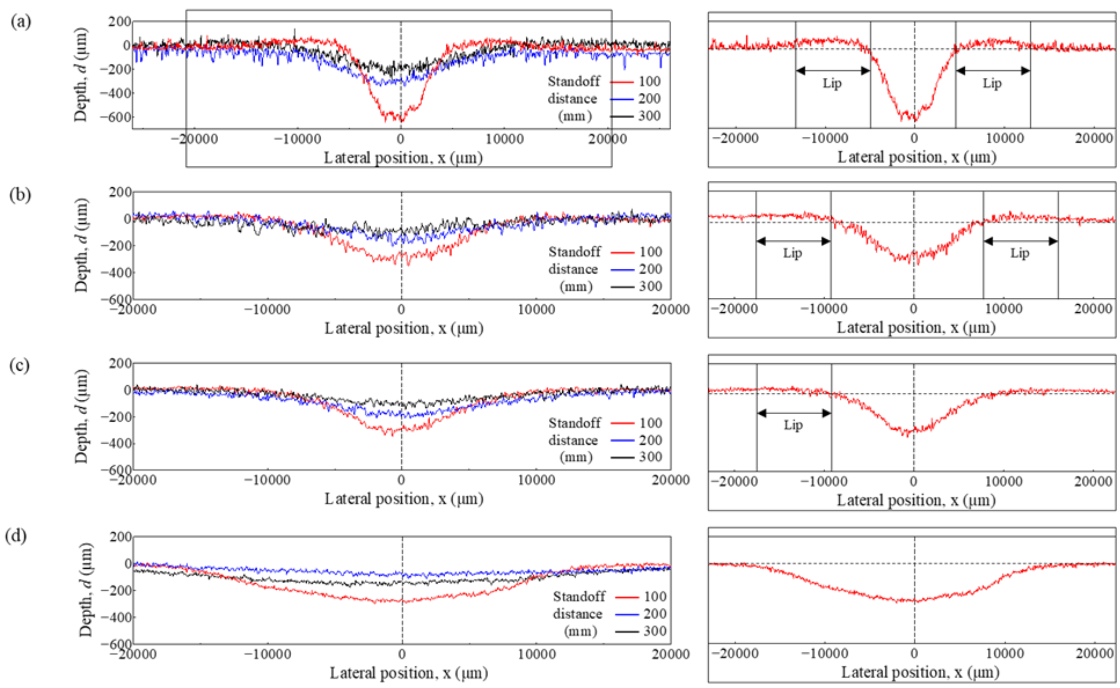

Figure 3-5 Assessment of the trench profile on a processed surface: (a) AWJ#30/60, (b) AWT#30/60, (c) AWT#80, and (d) Blasted specimens.

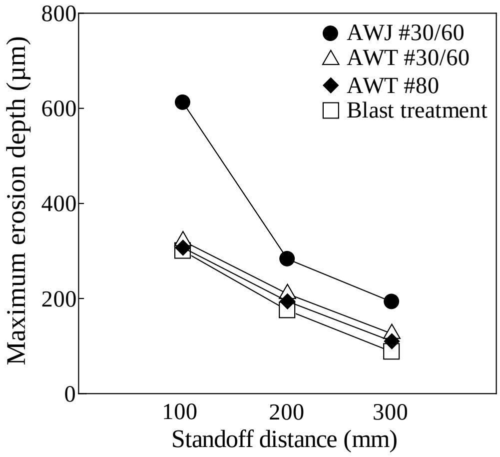

Figure 3-6 Maximum erosion depth of the processed specimens.

specimen was approximately half that of the AWJ#30/60 specimen and 1.4 times greater than that of the blasted specimens. This indicates that the AWT process using the AWT nozzle results in reduced maximum erosion depths compared to treatments using the AWJ nozzle, which assists in preventing significant reductions in the steel surfaces. Meanwhile, the maximum erosion depth was up to 15% greater in AWT#30/60 specimens compared to AWT#80 specimens, suggesting that larger abrasive particles lead to greater erosion depths. Larger particles, under the same pressure, disperse less along the nozzle axis, increasing the frequency of repetitive impacts on the substrate [26]. Additionally, larger particles retain more kinetic energy due to their greater mass, resulting in deeper erosion. Under all treatments, the maximum erosion depth decreased with increasing standoff distances. This reduction can be attributed to the expansion of the spray angle due to jet divergence at higher standoff distances. Consequently, as abrasive particles collide with the nozzle inlet and move towards the outlet, they gradually lose kinetic energy, ultimately leading to reduced erosion depths.

Figure 3-7 presents the microscopic images of specimens after AWT and blast treatment at a standoff distance of 200mm. Visual inspection revealed that regardless of the nozzle and abrasive particle size, specimens treated with AWT exhibited rougher surfaces compared to those treated with blasting. Specifically, the AWJ#30/60 specimen exhibited the highest peak roughness, measuring 245μm, whereas the AWT#30/60, AWT#80, and blasted specimens

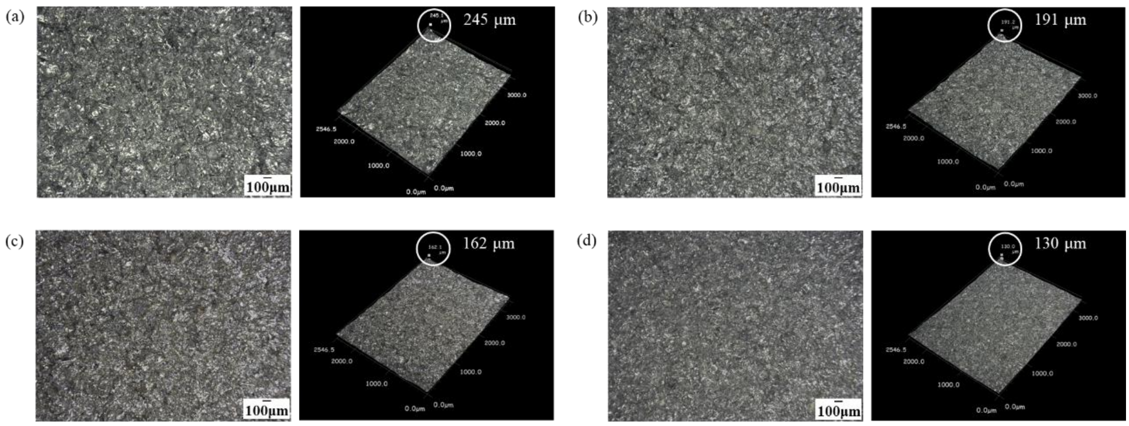

Figure 3-7 Surface appearances of the processed samples: (a) AWJ#30/60, (b) AWT#30/60, (c) AWT#80, and (d) Blasted samples.

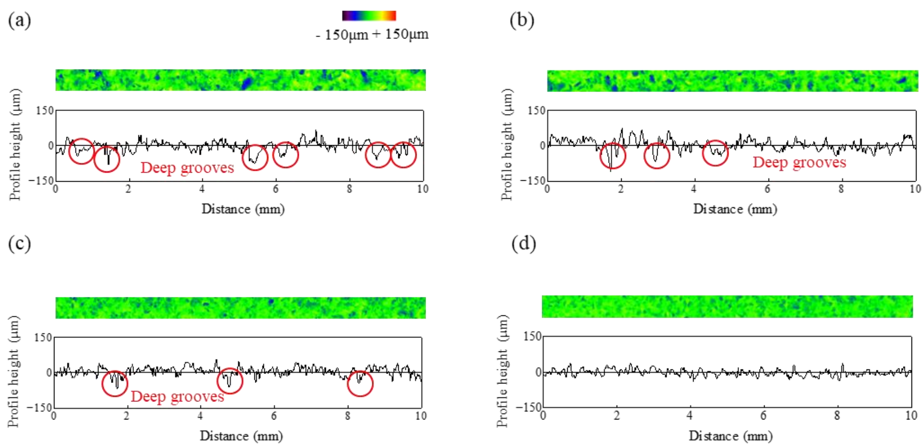

Figure 3-8 Cross-sectional view of the processed samples: (a) AWJ#30/60, (b) AWT#30/60, (c) AWT#80, and (d) Blasted samples.

showed peak values of 191, 162, and 130µm, respectively. This indicates that the use of the AWJ nozzle with larger abrasive particles during AWT processing results in increased surface peak values.

Figure 3-8 shows the detailed cross-sectional profiles and contour plots of surface roughness for specimens after AWT and blast treatment. Under all conditions, AWT-processed specimens showed a broader range of peak-to-valley and roughness features compared to the blasted specimen. The use of high-impact energy in AWT allows the abrasive particles to penetrate deeper into the substrate surface, forming more pronounced grooves, whereas blasting leads to shallower indentations due to lesser penetration, which is consistent with the respective treatment mechanisms. Furthermore, it becomes clear that the application of the AWJ nozzle with larger abrasives in AWT processing contributes to the creation of deeper grooves and more distinct variations in the surface roughness profiles, as observed in the contour plots.

Figure 3-9 shows quantitative values for surface roughness following AWT and blast treatment. All the roughness parameters of AWT processed specimens were found to be 1.5 to 3 times greater than those of blasted specimens, indicating that the impact force of AWT surpassing blasting contributed to the increased surface roughness. During AWT processing, the surface roughness of AWJ#30/60 specimens was up to 1.3 times higher than that of AWT#30/60 specimens at the same standoff distance, demonstrating that the use of AWT nozzles results in smoother surfaces. Additionally, the surface roughness relative to the size of abrasive particles revealed that AWT#30/60 specimens exhibited up to 1.3 times greater roughness compared to AWT#80 specimens. This could be attributed to the higher collision energy produced by larger particles upon contact with the substrate, leading to the formation of cracks or a rougher surface.

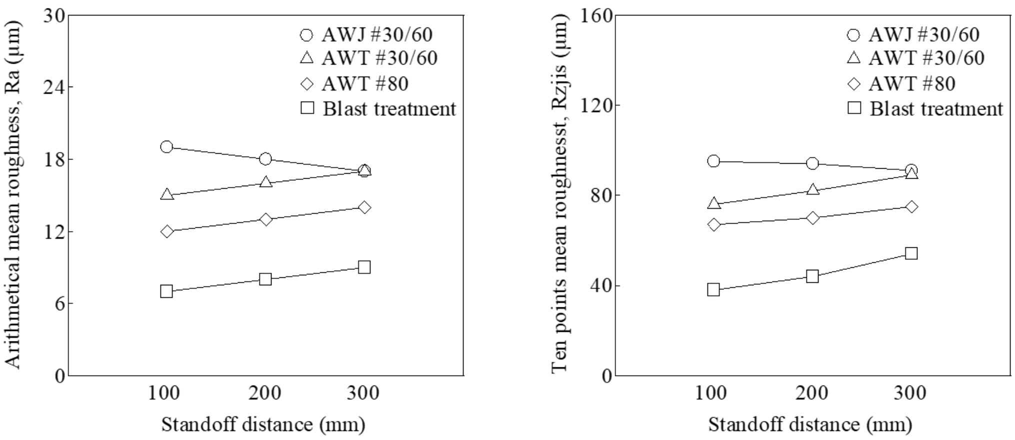

Figure 3-9 Surface roughness of the treated specimens.: Ra and Rzjis.

Interestingly, in the comparison of surface roughness, a trend of increasing roughness with the increase in standoff distance was observed, excluding specimens processed with the AWJ nozzle. This phenomenon is due to the existence of a critical roughness threshold, which represents the minimum roughness initiating the collapse of the initial roughness, forming new surface deformations characterized by grooves and ridges upon impact with the target material [19]. Before reaching this threshold, the concentrated impact energy on the target surface results in the deformation of the substrate, thereby increasing roughness with the increasing impact energy. Thus, prior to reaching the critical threshold, a decrease in standoff distance leads to an increase in the surface roughness of the target. However, once exceeding the critical threshold, the lack of sufficient force and impact density prevents the formation of new grooves or roughness, leading to irregular deformations confined to the existing roughness peaks. Consequently, roughness increased with the increase in standoff distance. According to this study, the roughness created by specimens treated with the AWJ nozzle remained below the critical threshold. As the standoff distance decreased, substrate-panel deformation amplified, leading to increased roughness. In contrast, for specimens treated with the AWT nozzle or by blasting, the generated roughness exceeded the critical threshold, thus limiting the concentrated deformation effect of the substrate across all standoff distance conditions compared to the AWJ nozzle. Therefore, the increase in roughness with increasing standoff distance is attributed not to extreme deformation of the substrate but to irregular transformations of the existing roughness. Consequently, it can be inferred that using the AWJ nozzle in the AWT process under the same experimental conditions exerts greater force on the substrate than using the AWT nozzle. According to the recommendations of the Japan Society of Civil Engineers (JSCE) for repainting steel bridges, the appropriate surface roughness value (Rzjis) before repainting falls within the range of 30~75μm. Based on the Rzjis values obtained in this study, the most suitable AWT condition for pre-coating was found to be the AWT nozzle combined with 80 mesh garnet.

3.3.2 Surface topography deformation

Figure 3-10 introduces a three-step methodology for analyzing surface topography deformation ratio: (1) measuring the cross-sectional image morphology of the treated specimen using SEM microscopy; (2) binarizing the deformed substrate shape using the

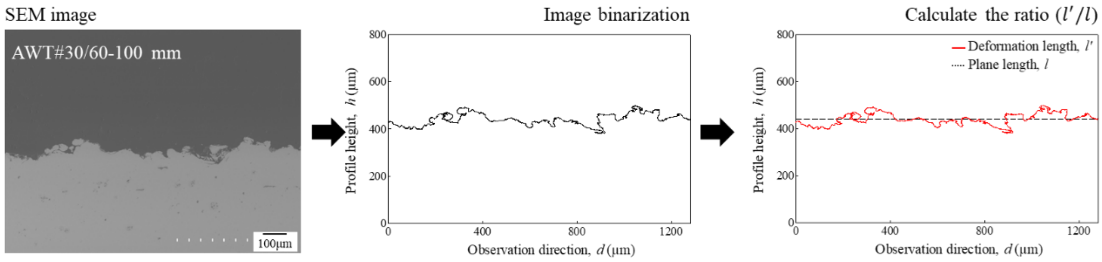

Figure 3-10 Measuring the surface deformation ratio of the treated specimens.

Image-J software; and (3) extracting the X,Y coordinates of the binary surface deformation area, then calculating the length of the altered area using the arc length method of a function graph, based on Taylor's formula [55]. This process allows for the definition of the interface area ratio (Surface Deformation Ratio, DR), which quantifies the degree of the interface area in comparison to an equivalent plane [56]. To provide statistically reliable data and high-confidence estimates, five rounds of image analysis were performed on samples treated under each condition. Additionally, the analysis encompassed not only the deformation length ratio but also the deformation range, which includes the degree of deformation. The deformation range is defined as the maximum and minimum peak-to-valley extents of the deformed area of each specimen, represented by the average of five measurements. For AWT specimens, the analysis only evaluated specimens treated with the AWT nozzle that produce roughness satisfying the JSCE's recommendations for repainting steel bridges.

Table 3-6 offers quantitative values of the altered surface topography after AWT and blasting treatment. The deformation ratio (DR) of the surface topography for the AWT-processed specimen was found to be 1.5 to 3 times larger than that of the blasted specimen. This indicates that the impact force of AWT on the substrate is greater than that of blasting, mirroring the trend observed in roughness parameter outcomes. Additionally, the DR and deformation range varies with the size of the abrasive particles; the specimen treated with AWT#30/60 showed up to 1.5 times greater values compared to AWT#80. This phenomenon can be attributed to higher collision energy produced by larger particles upon contact with the substrate, leading to terrain deformation or rougher surface formation. However, it is noted that while the AWT #30/60 (300) and AWT #80 (100) specimens exhibit nearly identical DR values of 3.5 and 3.4, respectively, the deformation zone of AWT #80 (100) is

Table 3-6 Surface deformation of the treated specimens.

Specimens	Standoff distance (mm)	Deformation ratio (DR)	Deformation range (μm)
AWT #30/60	100	4.2	134
	200	3.7	137
	300	3.5	120
AWT #80	100	3.4	88
	200	3.0	84
	300	2.9	97
Blast treatment	100	1.6	58
	200	1.4	52
	300	1.3	57

1.4 times larger. This underscores the importance of assessing both DR and deformation range when evaluating changes in surface topography. It is noteworthy that for both AWT and blasted specimens, an increase in the standoff distance led to increased roughness. However, the surface deformation parameters exhibited an opposite trend, decreasing with increased standoff distance. This is correlated with the formation of a minimum roughness threshold for surface deformation, as mentioned in the analysis of the surface roughness. In other words, for specimens treated with the AWT nozzle or blasting, the altered surface topography exceeded the threshold, thus limiting the concentrated deformation effect of the substrate under all increasing Standoff distance conditions. Consequently, the extent of surface deformation decreased with increasing the standoff distance, not due to severe deformation of the substrate but due to irregular transformations of existing roughness. Under the same experimental conditions, the DR values for the AWT #30/60 specimen, AWT #80 specimen, and blasted specimen were respectively found to be 3.5~4.5, 3~3.5, and 1~2. This implies that AWT processing, especially with larger abrasive particles, results in greater deformation of the substrate surface, ultimately exerting more significant force on the substrate compared to blasting.

3.3.3 Assessment of the quantity of residual abrasives.

Figure 3-11 presents a SEM-EDX image illustrating the distribution of Si on the centrally treated surface. The quantity of residual abrasives on the surface of AWT-processed specimens was significantly lower compared to the blasted specimen. Regardless of the nozzle type and particle size used in AWT processing, there was minimal variation in the amount of residual abrasive materials. However, the SEM-EDX image results, based on atomic percentage, were measured at the micro-scale. To overcome this limitation, a method based on area ratio was devised, enabling a quantitative comparison and assessment of the distribution of residual abrasives over a wider range. A composite EDX mapping image of Al, Si, and O, the primary chemical elements of garnet, was synthesized to extract an image of 3×4 mm size. The area ratio was calculated using Image J software. For comparing the amount of residual abrasives according to the surface treatment method, the area ratio of Si, which represents the highest proportion among the chemical components of the garnet, was utilized. Figure 3-12 depicts the area ratio of the residual abrasives remaining on the central surface of the treated area. AWT-processed samples exhibited an area ratio of 3-4%, irrespective of nozzle type and abrasive particle size, whereas blasted samples showed a significantly higher area ratio of 12-15%. The AWT-processed specimens consistently demonstrated a markedly lower amount of residual abrasive across all conditions compared to the blasted specimens. Additionally, there was no significant difference in the amount of

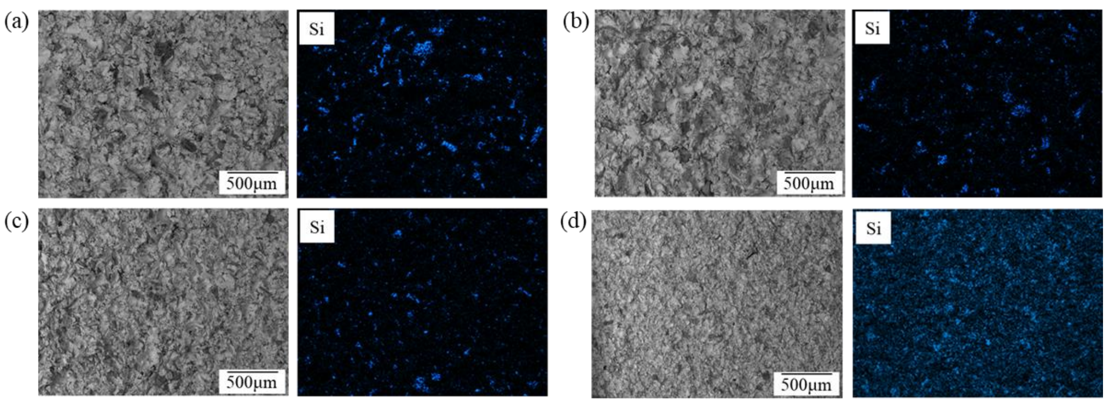

Figure 3-11 Elemental composition investigation illustrating the distribution of remaining abrasives on the processed surface: (a) AWJ#30/60, (b) AWT#30/60, (c) AWT#80, and (d) Blasted samples.

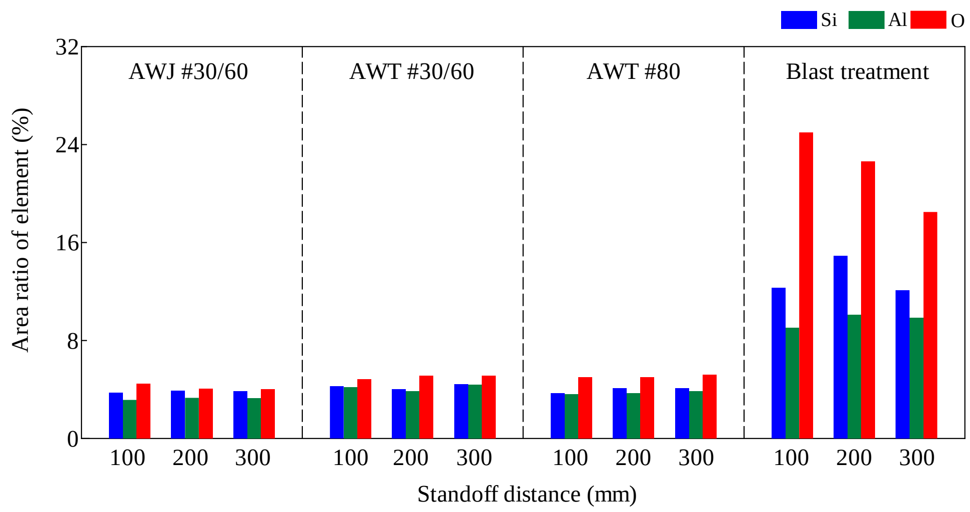

Figure 3-12 Proportion of residual abrasives on the processed surfaces.

residual abrasives based on the standoff distance.

Figure 3-13 illustrates the cross-sectional observations of the central part of the treated steel surface. Under all treatment conditions, the AWT-processed specimens showed that abrasives penetrated below the steel surface, partially embedding the abrasive particles, whereas blasting led to the formation of a significant layer of residual abrasives on top of the steel surface. Furthermore, the cross-section of AWT-processed specimens exhibited a more complex and rougher morphology compared to the blasted specimen. The reduced amount of residual abrasives following AWT can be attributed to the washing effect. The presence of significant residual abrasives on the target surface after blasting is undesirable, as it can create a barrier between the surface and coating, reducing adhesion and efficiency [51]. Excessive residual abrasive on the surface post-blasting can lead to the formation of microcracks, which in turn may cause fatigue cracks in the treated area [57], and the presence of contaminants and fine particles in the abrasive can reduce the corrosion resistance due to cracks [58]. Therefore, minimizing the amount of residual abrasives on the treated surface is crucial. Consequently, the AWT processing is expected to minimize damage and contamination of the steel surface compared to the blast treatment. This advantage makes AWT a preferable option for surface treatment in applications where the integrity and longevity of the material are critical.

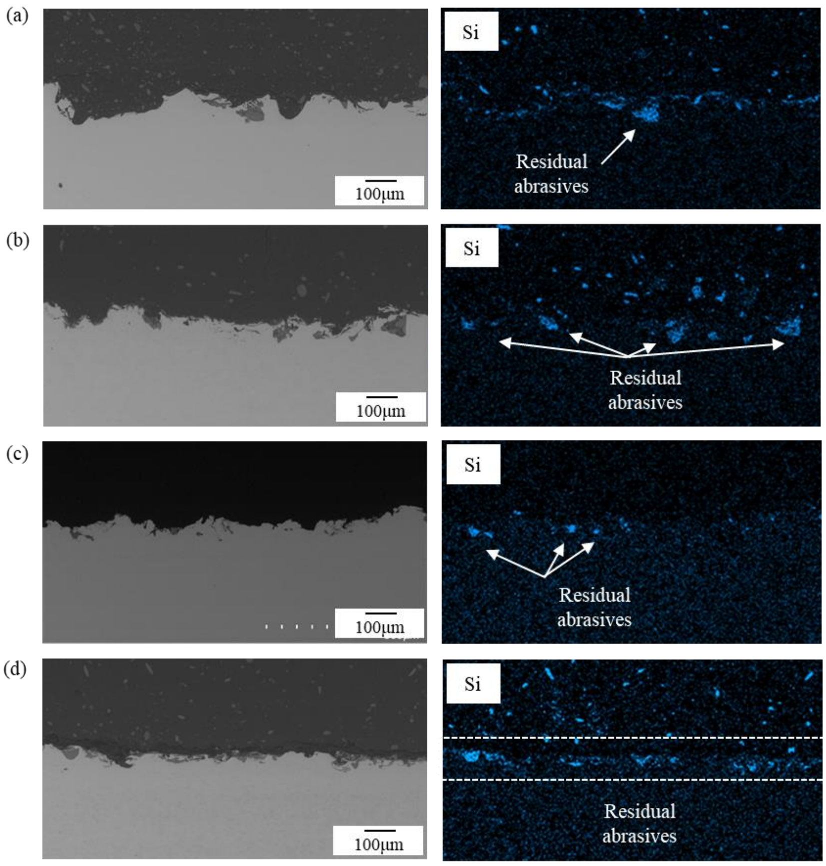

Figure 3-13 Cross-sectional images of the processed samples: (a) AWJ#30/60, (b) AWT#30/60, (c) AWT#80, and (d) Blasted samples.

3.4 Pull-off test

Table 3-7 shows the failure states of epoxy adhesive following pull-off tests on steel surfaces treated with AWT and blasting. After the pull-off tests, the residual epoxy adhesive on treated steel surfaces was retained below 30% only at a standoff distance of 300mm, indicating an interface failure between the steel surface and the epoxy adhesive. On the other hand, when the standoff distance is 200 mm or below, there is a retention of approximately 70-80% of the adhesive on the treated substrate, which correlates with a stronger adhesive bond compared to that observed on steel plates treated at a standoff distance of 300 mm. Figure 3-14 displays the relationship between load (P) and displacement (δ) during the pull-off test. In all treatment conditions, the force exerted on the substrates was approximately 4

Table 3-7 Destruction state of epoxy adhesive after pull-off test.

		Standoff distance (mm)		
		100	200	300
AWT #30/60	Substrate side		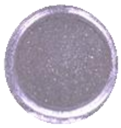	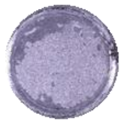
	Dolly side			
AWT #80	Substrate side			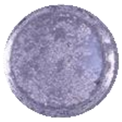
	Dolly side	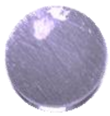		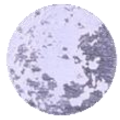
Blast treatment	Substrate side			
	Dolly side			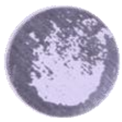

to 8 kN. Furthermore, no evidence of bending or other deformities caused by load reapplication was observed on the fracture faces in any treatment condition. Therefore, the test results indicate a high reliability of the P and δ relationship during load reapplication. Figure 3-15 shows the tensile bond strength (σ) of the epoxy adhesive to steel surfaces treated with various surface treatment methods. For blasted surfaces, the bond strength ranged from 8.3 to 10.8 MPa, decreasing with an increase in standoff distance. In the case of AWT, the adhesion strength varied depending on the type of garnet used. Specifically, specimens treated with AWT #30/60 and AWT #80 exhibited bonding strength values in the ranges of 7.5 to 8.8 MPa and 9 to 12 MPa, respectively. Additionally, a similar trend of decreasing adhesion strength with increasing treatment distance was observed in specimens treated with AWT. According to the results presented in sections 3.3.1 and 3.3.2, in both AWT processing using the divergent nozzle and blast treatment, as standoff distance

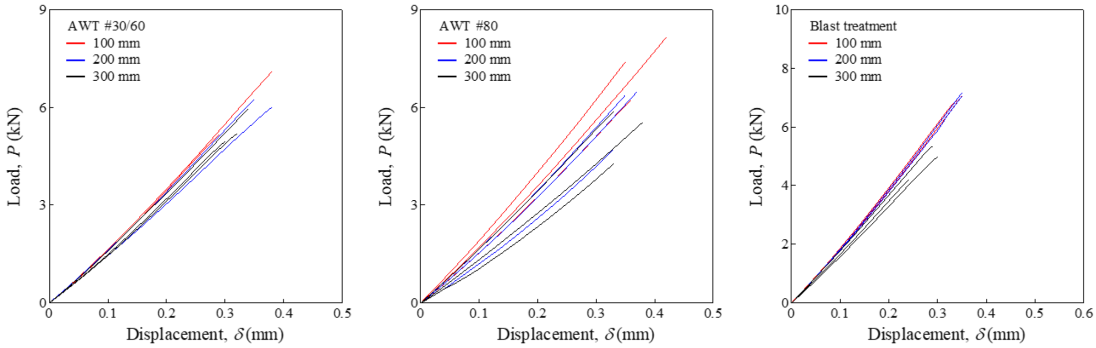

Figure 3-14 Relationship between load P and displacement δ after pull-off test.

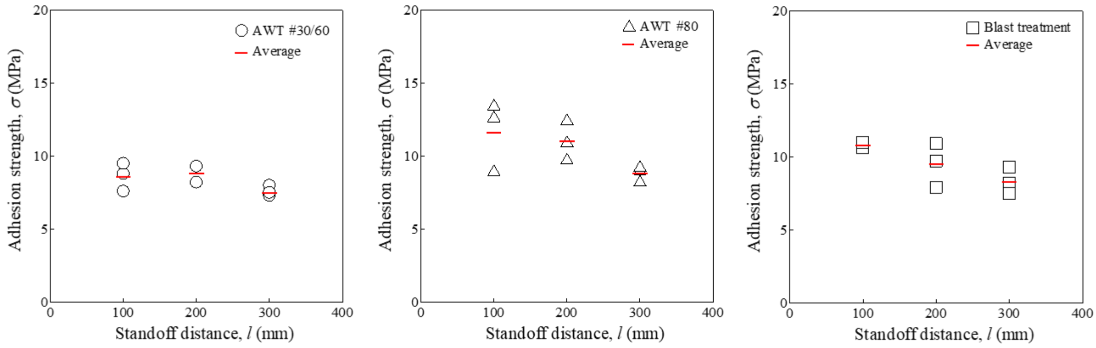

Figure 3-15 Adhesion strength of the treated steel plates according to standoff distances.

increased, surface roughness (Ra, Rzjis) increased, and the rate of change in surface topography decreased. Hence, under similar conditions, surface roughness and changes in surface morphology are inversely related. In terms of surface topography, a smaller standoff distance increased the force impacting the substrate, leading to greater substrate deformation. Conversely, in terms of roughness, an increase in standoff distance reduced the impact force on the substrate, resulting in increased surface roughness instead of substrate deformation. For adhesion strength, an increase in surface roughness led to decreased bond strength, while an increase in the rate of change in surface topography increased adhesion strength in this study. Notably, for AWT-processed specimens, especially AWT #30/60, there was a significant decrease in bond strength compared to AWT #80 specimens. This strongly suggests that changes in surface morphology, rather than roughness, have a more profound impact on the bonding strength with epoxy. Additionally, exceeding certain roughness levels and rates of topography change can result in a decrease in adhesion strength with epoxy.

3.4.1 Effect of surface topography alterations on bonding behavior with epoxy adhesive.

Until now, research on the mechanical interlocking between substrate surfaces and coatings has predominantly focused on surface roughness [59]. Generally, an increase in surface roughness tends to enhance the adhesion strength with coatings [48]. Conversely, excessive roughness can damage the coating due to sharp peaks [23], and overly deep valleys can hinder the penetration of paint, thereby reducing the adhesion strength between the substrate and coating [10]. Therefore, creating an appropriate level of surface roughness on the substrate before painting is a crucial step. Consequently, it has led existing research to focus primarily on roughness as a critical surface property affecting adhesion. However, it's increasingly recognized that morphological alterations like surface anchoring patterns could exert a more direct impact on adhesion strength than the microscale randomness of surface roughness [51]. Figure 3-16 demonstrates that changes in surface morphology after treatment

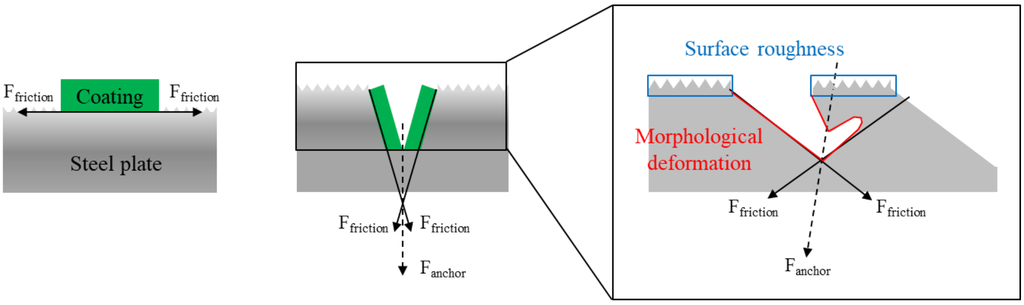

Figure 3-16 Impact of substrate surface morphology on the adhesion strength of the coating [59].

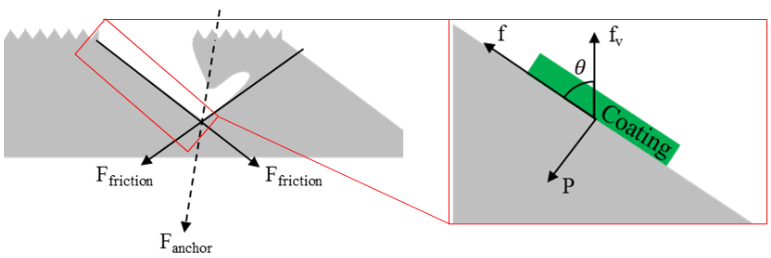

Figure 3-17 Adhesive forces acting on altered surface morphology during coating application [56], [59].

can exert a greater influence on the bonding strength with coatings during the coating application process.

During coating with an epoxy, the fluid flows over the surface of the substrate. Some of the coating gets trapped on the surface and adheres upon solidification when subjected to a certain level of pressure. The adhesion force depends on mechanical clamping and friction forces as a function of pressure. Figure 3-17 illustrates an image of a thin object placed on an inclined plane. When pressure P is applied at the interface between the object and the inclined plane, the friction force f is characterized as follows, according to Equation (3-1) through (3-7) [56].

$$f = \mu Ps \tag{3-1}$$

μ: Friction coefficient, s: Contact area,

$$f_v = f \cos\theta \tag{3-2}$$

f_v: Force needed to remove vertically the object

$$z = f(x, y) \tag{3-3}$$

Equation 3-2 demonstrates that the f_v is proportional to the projected area. After the sprayed coating fills the rough surface, represented by the function in orthogonal coordinates as per Equation 3-3, the f_v required to vertically remove the deposits over a minimal area ds of the surface is expressed as per Equation 3-4. where θ is the angle between tangent and normal of the differential area.

$$df_v = \mu P ds \cos\theta \tag{3-4}$$

The smallest force required to separate the deposits vertically from the rough surface area D is as described by Equation 3-5:

$$\int_D df_v = \int_S \mu P \cos\theta ds = \bar{\mu}\bar{P} \int_S \cos\theta ds \tag{3-5}$$

Replacing μ and P with their respective mean values over each area, the equation for the adhesion strength F can be expressed as follows, as per Equation 3-6:

$$F = \frac{\bar{\mu}\bar{P}\int_S \cos\theta ds}{D} \quad (3\text{-}6)$$

Therefore, the adhesion strength can be theoretically predicted through Equation 3-7, calculated using image analysis presented in Section 3.3.2, and the mechanical adhesion is directly linked to the factor DR, as identified through image analysis.

$$F = \bar{\mu}\bar{P}R, \quad R = \frac{\text{Adhesion Area}}{\text{Plane Area}} \quad (3\text{-}7)$$

Consequently, it is anticipated that steel treated with AWT, having a larger adhesive area, will exhibit higher adhesion values. The adhesion values appeared to be linearly dependent on the surface contact ratio indicated by DR.

3.4.2 Behavior of adhesion between the treated substrates and epoxy adhesive.

Figures 3-18 and 3-19 illustrate the correlation between roughness, deformation ratio (DR), and adhesion strength in the results of pull-off tests for surfaces treated with blasting and AWT processing. Figure 3-18 shows the adhesion strength of coatings on blasted surfaces, categorized by roughness and surface strain. As roughness (Ra, Rzjis) increases, adhesion strength decreases, exhibiting a negative correlation. Conversely, for DR, an increase in strain shows a positive linear correlation with increasing adhesion strength, exhibiting the highest correlation coefficient (0.796). Similarly, Figure 3-19 demonstrates the adhesion strength of coatings on steel surfaces treated with AWT using garnet 30/60 and 80, based on surface characteristics. Similar to blasted specimens, an increase in roughness (Ra, Rzjis) for AWT-processed specimens tends to decrease adhesion strength. However, for surface strain, an increase in strain tends to linearly increase adhesion strength. Thus, surface deformation ratio rather than roughness shows a positive correlation with the adhesion strength of coatings. Additionally, the correlation between surface characteristics and adhesion strength post-AWT treatment for all conditions showed a high correlation coefficient above 0.7 for both Rzjis and DR. Interestingly, for AWT specimens, a significant

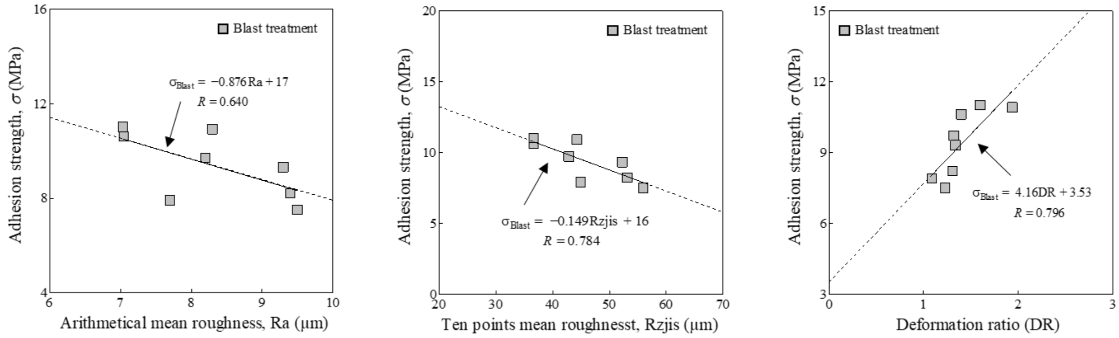

Figure 3-18 Correlation between roughness and DR and adhesion strength for pull-off test results of the blasted steel plate.

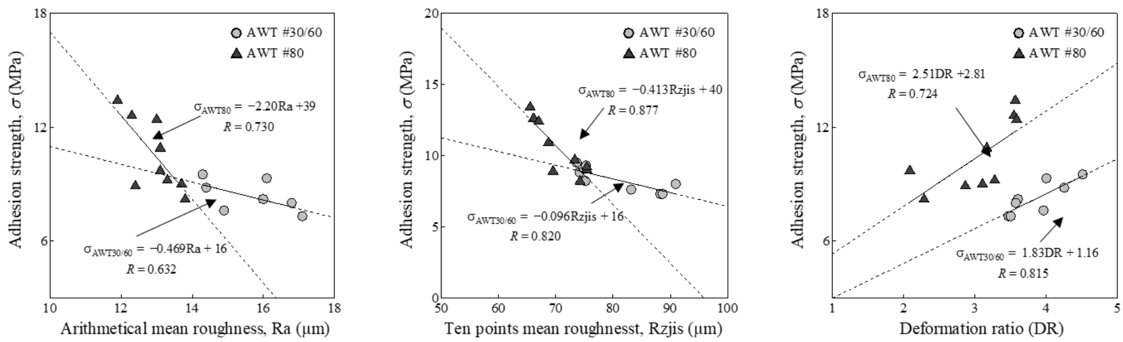

Figure 3-19 Correlation between roughness and DR and adhesion strength for pull-off test results of the AWT-processed steel plate.

decrease in adhesion strength is observed where Rzjis exceeds 75 μm and DR is above 3.5. According to the guidelines for bridge repainting in Japan, the optimal surface roughness value before repainting falls within the range of 30-75 μm for Rzjis, which can be inferred as the threshold for maximum adhesive strength with coatings. However, AWT#30/60 (100) and (200) specimens, with Rzjis values of 76 μm and 82 μm respectively, exceeding 75 μm, achieved adhesion strengths around 9 MPa. This indicates that there is a critical topography deformation ratio value, in addition to a specific surface roughness value, for achieving maximum adhesion strength.

Table 3-8 presents the quantitative values of average roughness, DR, Deformation range, and average adhesion strength from pull-off tests after various types of surface treatments.

In terms of adhesion strength with coatings, the trend was observed in the order of AWT #80, Blast, and AWT #30/60, with respective ranges of 9-12, 8-11, and 7-9 MPa. Furthermore, comparisons between AWT #80(200 and 300) and AWT #30/60(100) specimens, which had similar roughness values (Ra: 13-15 and Rzjis: 70-76 μm), revealed a significant difference in their surface deformation ratios of 2.9 to 4.2. Notably, even with higher DR, the adhesion strength was found to decrease. On the other hand, AWT #80(100) and AWT #30/60(300) specimens, with similar DR values of 3.4 and 3.5, respectively, showed a significant difference in adhesion strength, at 12 and 7.5 MPa. This suggests the existence of certain surface deformation ratios and extents that reduce adhesion strength.

For AWT #80 specimens with varying standoff distances, the surface deformation extent ranged within 80-100 μm, and DR values were between 3-3.5. In contrast, AWT #30/60 specimens had a surface deformation extent of 120-140 μm, with DR values of 3.5-4.5. Therefore, it can be inferred that even if the substrate's DR is below 3.5, exceeding a deformation extent of 120 μm will reduce the adhesion strength with the coating. From these results, it can be concluded that the surface characteristics most impacting the adhesion strength with coatings are the surface deformation ratio and range. Additionally, the optimal conditions for maximum adhesion strength between the substrate and coating are estimated to be using AWT #80, with a surface deformation extent of 80-100 μm and a DR of 3-3.5.

Table 3-8 Altered surface properties.

Specimens	Standoff distance (mm)	Ra (μm)	Rzjis (μm)	Deformation ratio (DR)	Deformation range (μm)	Adhesion Strength (MPa)
Blast treatment	100	7	38	1.6	58	10.8
	200	8	44	1.4	52	9.5
	300	9	54	1.3	57	8
AWT #80	100	12	67	3.4	88	12
	200	13	70	3.0	84	11
	300	14	75	2.9	97	9
AWT #30/60	100	15	76	4.2	134	8.6
	200	16	82	3.7	137	8.8
	300	17	89	3.5	120	7.5

3.5 Summary

Chapter 3 investigates the impact of nozzle type, abrasive particle size, and standoff distance in AWT processing on the surface characteristics of carbon steel plate. This included comparative evaluations of the treatment area, maximum erosion depth, surface roughness, and the amount of residual abrasive materials. Notably, for surface morphology, the study went beyond roughness to quantitatively analyze the extent of altered surface topography. Furthermore, pull-off tests were conducted to examine the tensile adhesion behavior between AWT-processed steel plate and epoxy adhesive. The chapter also delved into the adhesion mechanisms between steel surfaces and epoxy adhesive by analyzing not only the roughness but also the surface deformation ratio and extent following various surface treatments.

The principal outcomes of this chapter are summarized as follows:

1) The newly developed AWT process utilizing a divergent nozzle and smaller abrasive particles demonstrated a similar treatment range to abrasive blasting but resulted in higher surface roughness. Additionally, an increase in standoff distance led to an increase in both the treatment range and surface roughness.
2) The advanced AWT process employing a divergent nozzle with larger abrasive particles exhibited greater surface topography deformation compared to abrasive blasting. Moreover, as the standoff distance increased, the degree of surface topography deformation tended to decrease.
3) AWT results in significantly less residual abrasive remaining on the target material after processing compared to blasting. Whereas there was no notable difference in the amount of residual abrasive across various AWT processing conditions. The maximum erosion depth of the AWT-processed specimens exceeded that of the blasted specimens. During AWT, the depth of treatment using a divergent nozzle was about half that of specimens treated with a convergent nozzle. Additionally, smaller abrasive particle sizes resulted in reduced maximum erosion depth.
4) In conclusion, the use of the divergent nozzle and smaller abrasive particles in AWT processing is expected to prevent the narrow treatment range, significant roughness formation, and markedly deep treatment depths that occur with the convergent nozzle on steel plates.

5) After each surface treatment, the tensile adhesion strength between the steel's surface deformation ratio and the epoxy adhesive shows a positive linear correlation, while it has a negative linear correlation with surface roughness. Among the surface characteristics of treated steel, the surface deformation ratio has the highest correlation with the tensile adhesion strength of the epoxy adhesive. Consequently, there exists an optimal surface characteristic for maximum adhesion between the substrate and epoxy, where the surface deformation ratio is within a deformation range of 80-100 μm with a DR of 3-3.5, and roughness is estimated to be below 75 μm Rzjis.

CHAPTER 4 MECHANICAL AND ELECTROCHEMICAL PROPERTIES OF TREATED SURFACE

4.1 Introduction

For the prolonged durability of steel structures, ensuring the integrity of materials and components against fatigue and corrosion is essential. Typically, material failure due to fatigue, wear, and corrosion often initiates at the surface. The fatigue strength of materials and components is mainly influenced by factors such as residual stresses, stress concentrations, and microstructural characteristics [60]. Consequently, many recent researchers have focused considerable attention on mechanical properties like surface hardening and changes in the microstructure of particles. These mechanical characteristics, resulting from the introduction of compressive stresses, alter the surface properties of the base material and thereby impact its durability and corrosion resistance [61]. In particular, changes in the surface structure of steel and other metals not only affect their mechanical properties but can also alter their corrosion behavior [62]. Corrosion resistance in steel is vitally important for the long-term stability and endurance of structures. Steels with enhanced corrosion resistance can provide significant economic advantages by reducing the frequency of maintenance and lowering early replacement costs [63].

Common methods used to introduce compressive stress on surfaces include shot peening and laser shock peening among others [60]. Shot peening is a process where small spherical media, called shots, impact the target surface to create a layer of compressive residual stress and modify the mechanical properties of metals. It is typically applied to metal materials requiring high surface hardness and resistance to fatigue failure during use [64]. While shot peening is widely used as a mechanical surface treatment process in the automotive and aerospace industries, its application in civil engineering structures has not been extensively mentioned [65]. Laser shock peening, a cutting-edge peening technology first introduced in the aerospace industry, has garnered attention but still requires further research and development due to the need to consider heat-induced damage to the base material and various processing conditions like output power [66]. In civil engineering sites, a process similar to shot peening, known as shot blasting, is employed. However, the primary purpose of its use is not to enhance the mechanical properties of the material's surface but rather to remove surface rust, contaminants, and other impurities [67]. Therefore, there is a growing need for new surface technologies in civil engineering steel structures that can simultaneously remove surface contaminants and enhance the material's durability and corrosion resistance. Additionally, there is a necessity to elucidate the impact of surface properties and mechanical characteristics of carbon steel after surface treatment on its corrosion resistance. While some research has been conducted on the effects of traditional surface treatment methods like sandblasting on the corrosion resistance of carbon steel, comprehensive studies on the impact of surface and mechanical properties after various surface treatments remain still lacking.

Existing research indicates that the substantial energy produced by abrasive waterjet results in surface hardening and alterations in the microstructure, consequently modifying the surface and mechanical characteristics of the base material [68]. Therefore, Chapter 4 of this dissertation analyzes the impact of AWT under various conditions on the hardness and microstructural changes of steel, delving into their relationship with the corrosion behavior of the material. Additionally, this study also investigates the relationship between surface roughness, as mentioned in Chapter 3, and corrosion resistance aiming to elucidate the factors impacting corrosion resistance among both surface and mechanical properties.

4.2 Experimental method

4.2.1 Experimental process

The specimen was made using a steel plate of JIS G3106 SM490A with dimensions of 150×70×6mm. As described in Chapter 3, the surface of the steel plate (hereafter referred to as the milling steel plate) was processed. The AWT and Blast treatments were performed under the same conditions as shown in Tables 3-1 and 3-4, respectively.

4.2.2 Analysis methods for hardness and structural examinations

The microhardness values of the cross-sections in the treated steel specimens along the thickness direction were measured using a Vickers hardness test (HMV-G30S, Shimadzu Co.). To examine the microstructural alterations in the treated specimens, analyses were conducted on changes in crystallite size and micrographs of the specimens' cross-sections.

X-ray diffraction (XRD, SmartLab, Rigaku Co., Ltd.), utilizing a Cu-Kα radiation X-ray source at a generator setting of 40 kV and 30 mV, was employed for phase analysis and crystallite size determination. The scanning angle (2θ) ranged from 40° to 90°, utilizing a wavelength of 1.54. The crystallite sizes were calculated from the XRD data, and two separate measurements were taken at distinct points on the specimen surfaces. For microscopic observation, the specimens' cross-sections were prepared, polished, and etched with 2% nital, and then examined under a microscope (HR-2500E, Hirox Co., Ltd.).

4.2.3 Analysis methods for electrochemical tests

Prior to conducting electrochemical tests, the samples were meticulously cleaned and degreased using acetone, followed by washing with deionized water. The electrochemical evaluations were carried out using a potentiostat (Versa-STAT 4, Princeton Applied Research). The schematic representation of the electrochemical test is depicted in Figure 4-1. The setup for these experiments included a reference electrode (Ag/AgCl), a counter electrode (platinum foil), and a defined testing area of 100 mm². The tests, comprising open circuit potential (OCP), potentiodynamic polarization, and electrochemical impedance spectroscopy (EIS), were performed on each specimen immersed in a 3.5 wt% NaCl solution at standard room temperature. The open circuit potential (E_{ocp}) of each sample was monitored for 24 hours until it stabilized. Potentiodynamic polarization tests were then carried out at a

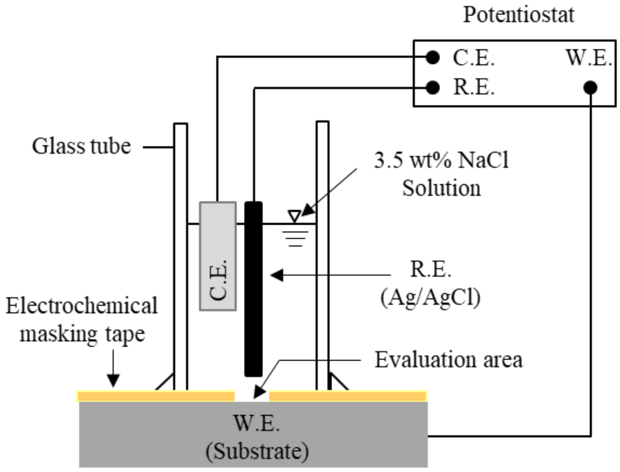

Figure 4-1 Schematic of electrochemical test.

scan rate of 10 mV/min within ±250 mV of the E_{ocp}. The Tafel extrapolation method was used to ascertain the corrosion current (i_{corr}) and corrosion potential (E_{corr}). EIS tests were conducted over a frequency range from 10 mHz to 100 kHz at a 10 mV signal amplitude relative to E_{ocp}. The EIS data were analyzed using ZSimpWin software (AMETEK) for simulation purposes.

4.3 Test results

4.3.1 Micro hardness

Figure 4-2 presents the microhardness-to-depth graph for specimens treated with AWT and blasting. Hardness was measured from the top of the treated surface down to a depth of 1500 μm. The AWT collision mechanism involves the immense energy effect of ultra-high-pressure water containing abrasive particles. Therefore, to understand the energy absorbed

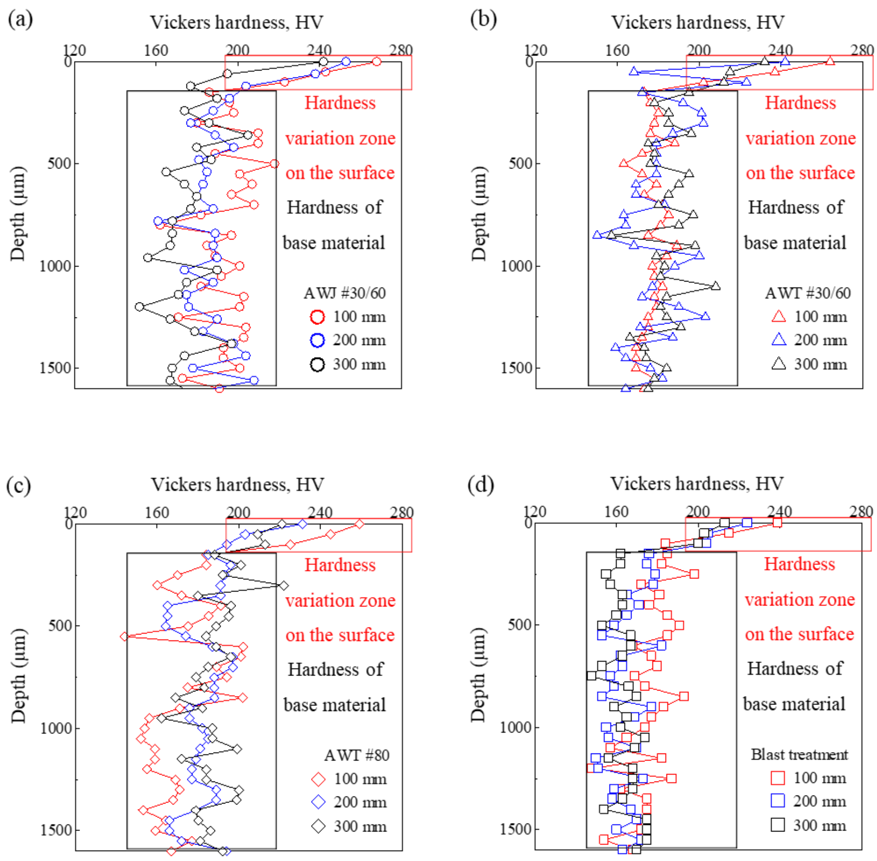

Figure 4-2 Microhardness values of the treated surface: (a) AWJ#30/60 specimen, (b) AWT#30/60 specimen, (c) AWT#80 specimen, and (d) Blasted specimen.

by the steel plate during treatment, changes in hardness beneath the specimen's surface were measured. The hardness values were recorded across the cross-section of the treated area, varying with the depth of the specimen. In this graph, the average hardness value for the untreated specimens is between 160 and 200 HV. Both AWT and blasted specimens exhibited an increase in hardness, reaching their maximum values at the treated surface. The surface hardness peaks at the surface and gradually decreases towards the end of the plastic deformation zone. The depth at which the hardness value reaches over 200 HV after surface treatment varies depending on the type of treatment, reaching depths of approximately 100-150 µm for blasting and 150-200 µm for AWT processing.

Table 4-1 provides a quantitative depiction of the maximum hardness values for each treated test specimen. All AWT specimens exhibited greater hardness values than those treated with blasting, with a maximum increase of up to 1.3 times. It was observed that under identical conditions, the use of the AWJ nozzle and larger abrasive particles in AWT processing achieved higher maximum hardness values. Additionally, in all types of treatments, a smaller standoff distance increased the energy reaching the substrate, resulting in higher surface hardness values. Notably, the maximum hardness values were reached

Table 4-1 The quantitative value of the microhardness.

Specimens	Standoff distance (mm)	Vickers hardness (HV)
AWJ #30/60	100	268
	200	253
	300	242
AWT #30/60	100	264
	200	242
	300	232
AWT #80	100	259
	200	231
	300	221
Blast treatment	100	239
	200	224
	300	213

under the condition of a 100mm standoff distance for each treatment. The increase in microhardness values can be attributed to the surface-hardening effect on the material. It is inferred that all types of surface treatments led to the formation of a plastically deformed surface layer, with an increase in hardness due to the reduction of pores, cracks, and grain boundaries [22], [69]. The altered microstructure could also be influenced by plastic deformation, which will be further elaborated in the following section.

4.3.2 Evaluation of the microstructure

Figure 4-3 depicts microscopic images of the actual plastically deformed cross-sections of specimens treated with AWT and blasting under various conditions. The differences in the plastic deformation layers were assessed through the degree of density change in the etched cross-section layers after each treatment. The depths of the plastic deformation layers formed due to changes in the standoff distance during surface treatment were observed to be 25-90μm for AWJ #30/60 specimens, 20-50 μm for AWT #30/60 specimens, 20-40 μm for AWT #80 specimens, and around 20μm for blasted specimens. It was confirmed that as the standoff distance decreased during surface treatment, the energy intensity on the treated surface increased, resulting in the formation of a maximum plastic deformation layer. Additionally, AWT processing was found to produce a larger plastic deformation layer than the blast treatment, with blasting showing the smallest deformation section. This suggests that the energy intensity of AWT impacting the steel surface is higher than that of blasting. Interestingly, while in blasted specimens, plastic deformation was observed only where the abrasive particles impacted the steel plate, in AWT-processed specimens, plastic deformation occurred even in areas without abrasive particles, indicating that the high-pressure waterjet alone can exert significant energy on the steel. Particularly, the cross-sectional morphology of the AWJ #30/60 (300) specimen suggests that the high-pressure waterjet directly penetrates the steel surface, eroding it via a water wedge effect. Furthermore, the plastic deformation layer and the increased hardness zone were almost identical, providing evidence of hardening due to plastic deformation of the steel plate. The density of the plastic deformation layer was highest in the AWJ #30/60 specimens, followed by AWT #30/60 and then AWT #80 specimens. Therefore, under similar conditions, the use of converging nozzles and larger abrasive particles in AWT processing can be seen to produce greater plastic deformation.

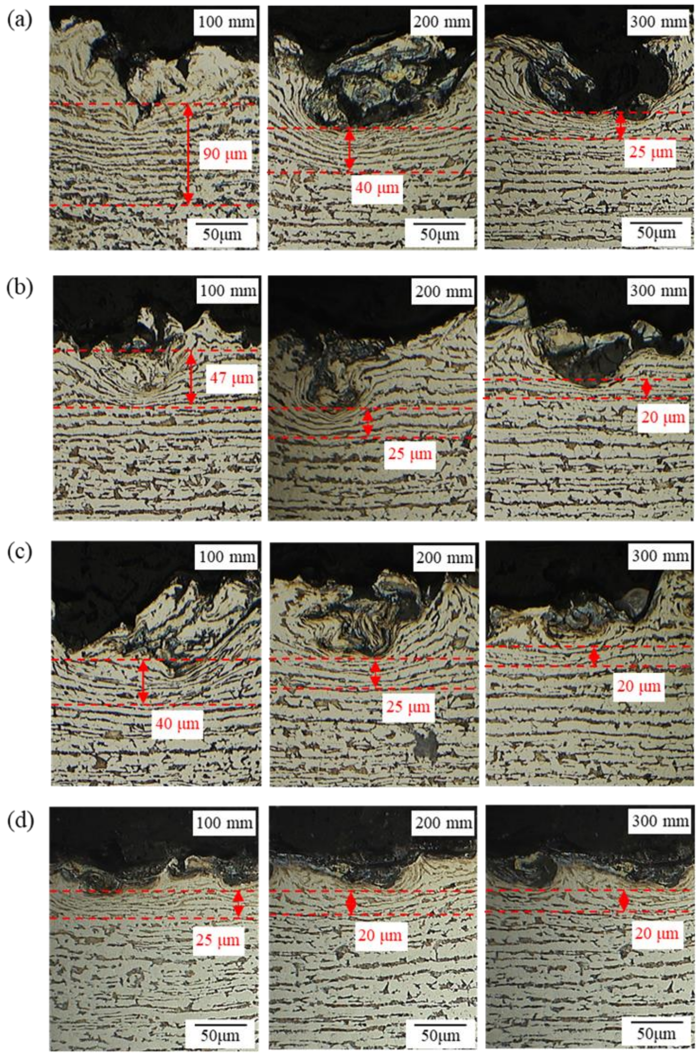

Figure 4-3 Microscopic images of microstructure on cross-section of the treated specimens under the different standoff distance: (a) AWJ #30/60 specimens, (b) AWT #30/60 specimens, (c) AWT #80 specimens, and (d) Blasted specimens.

Figure 4-4 presents the X-ray diffraction (XRD) patterns of specimens treated with AWT, blasting, and untreated samples. The experimental carbon steel is primarily composed of α-ferrite (α-Fe), as indicated by the patterns. Each sample, as analyzed, exhibited three strong peaks corresponding to the (110), (200), and (211) planes. The results demonstrate that α-Fe peaks shifted to lower diffraction angles from their original positions due to AWT, blasting, and milling processes. Typically, when compressive residual stresses are induced in a material, the characteristic peaks of the material shift to lower angles from their original

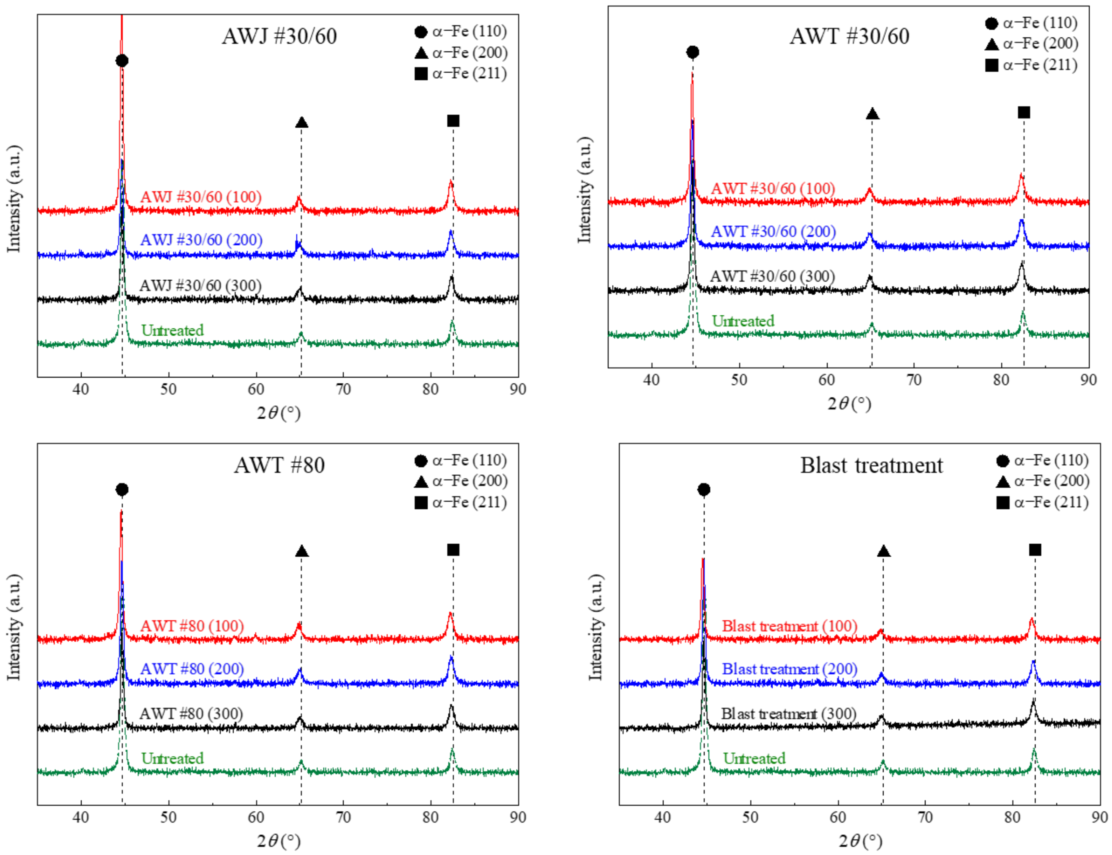

Figure 4-4 XRD diffraction patterns of the AWT, blasted, and untreated specimens.

positions [70]. Furthermore, as seen in this figure, with an increase in compressive residual stress values, plastic deformation increases, leading to the maximum peak shift in the AWJ #30/60 (100) specimen [71], [72]. Thus, the AWJ #30/60 (100) specimen exhibited the highest compressive residual stress. In contrast, the peak intensities of the blasted specimens were visually less than those of the AWT-processed specimens. Consequently, AWT induces greater compressive residual stresses on the steel surface compared to blasting. Additionally, it was noted that the use of the convergent nozzle and a smaller standoff distance during AWT processing further pronounced these characteristics.

Table 4-2 presents the values for the width of the diffraction peak at half the maximum value of diffraction (FWHM) and crystallite sizes for specimens treated with AWT and blasting. Compared to the untreated samples, both treated samples exhibited higher FWHM

Table 4-2 Crystallite size of the treated specimens.

Specimens	Standoff distance (mm)	Maximum peak position (2θ)	FWHM β (º)	Crystallite size (nm)
AWJ #30/60	100	44.55	0.355	25.2
	200	44.50	0.330	27.2
	300	44.60	0.298	30.1
AWT #30/60	100	44.57	0.338	26.5
	200	44.59	0.309	29.1
	300	44.62	0.297	30.2
AWT #80	100	44.46	0.333	27.0
	200	44.60	0.308	29.2
	300	44.62	0.298	30.0
Blast treatment	100	44.60	0.327	27.4
	200	44.57	0.306	29.3
	300	44.61	0.294	30.5
Untreated		44.70	0.287	31.3

values and smaller crystallite sizes. The broadening of peaks (increase in FWHM values) serves as an indicator of a decrease in crystallite size. Crystallite size is a measure that quantitatively represents the microstructural changes in the surface layer of treated specimens. Smaller crystallite sizes suggest greater energy reaching the surface, indicating a reduction in particle size and boundary at the surface. Additionally, FWHM is associated with grain size and distortion and is considered an indicator of the material's hardening index [73]. That is, a larger FWHM implies greater hardening of the measured surface [74]. The crystallite size (D) of the treated specimens was calculated using the Scherrer equation 4-1 [75].

$$D = \frac{K\lambda}{\beta \cos \theta} \tag{4-1}$$

Where K represents the Scherrer constant (0.89), λ is the wavelength of Cu (0.154 nm), β is the FWHM value, and θ is half the diffraction angle. Under identical standoff distance conditions, a trend of decreasing crystallite size was observed in the order of AWJ #30/60 specimens, AWT #30/60 specimens, AWT #80 specimens, and lastly, those treated with blasting. Furthermore, the crystallite size diminished with a decrease in standoff distance under all treatment conditions. However, it was noted that for all treated specimens, except for the AWJ #30/60 specimens, the crystallite sizes were almost similar under standoff distances other than the distance of 100 mm. As the energy reaching the steel surface increases, it reduces the size and boundaries of the surface particles. Consequently, it is inferred that AWT imparts greater energy to the steel surface compared to blasting, and a reduction in standoff distance during surface treatment tends to increase the force exerted on the steel plate. However, the use of the convergent nozzle in AWT processing showed a clear difference in the aforementioned characteristics, while the use of the divergent nozzle and different abrasive particle sizes did not show a distinct difference in crystallite size changes compared to blasted surfaces. Notably, the AWJ #30/60 (100) specimen exhibited the smallest grain size, suggesting it received the highest energy at the surface.

4.3.3 Potentiodynamic polarization cures of AWT treated specimens.

Figure 4-5 exhibits the potentiodynamic polarization measurement results for all treated specimens. The corrosion current density (i_{corr}) was evaluated from the polarization curves using the Tafel extrapolation method, employing the linear parts of the anodic and cathodic curves at the corrosion potential (E_{corr}) [76]. As depicted in this figure, the polarization curves for all treatment conditions exhibited a similar shape. In the anodic curves, the current density (i) increases with the rise in potential (E). On the other hand, in the cathodic curves, irrespective of the treatment condition, the current density appears to maintain a constant value of around 10μA/cm², suggesting no significant variation. This constancy of i in the cathodic curves, regardless of E, indicates it results from the diffusion-limited current due to oxygen and hydrogen evolution in the reduction reaction [77]. Therefore, it is presumed that the variety of surface characteristics produced on steel under different treatment conditions could influence the diffusion-limited current density in the cathodic curves. Table 4-3 quantitatively provides the corrosion potential (E_{corr}) and corrosion current density (i_{corr}) values derived from the polarization curves using the Tafel extrapolation method, and also includes the corrosion rate (CR) calculated from the i_{corr} values. The CR for each treated surface were determined using equations 4-2 and 4-3, based on the corrosion current density.

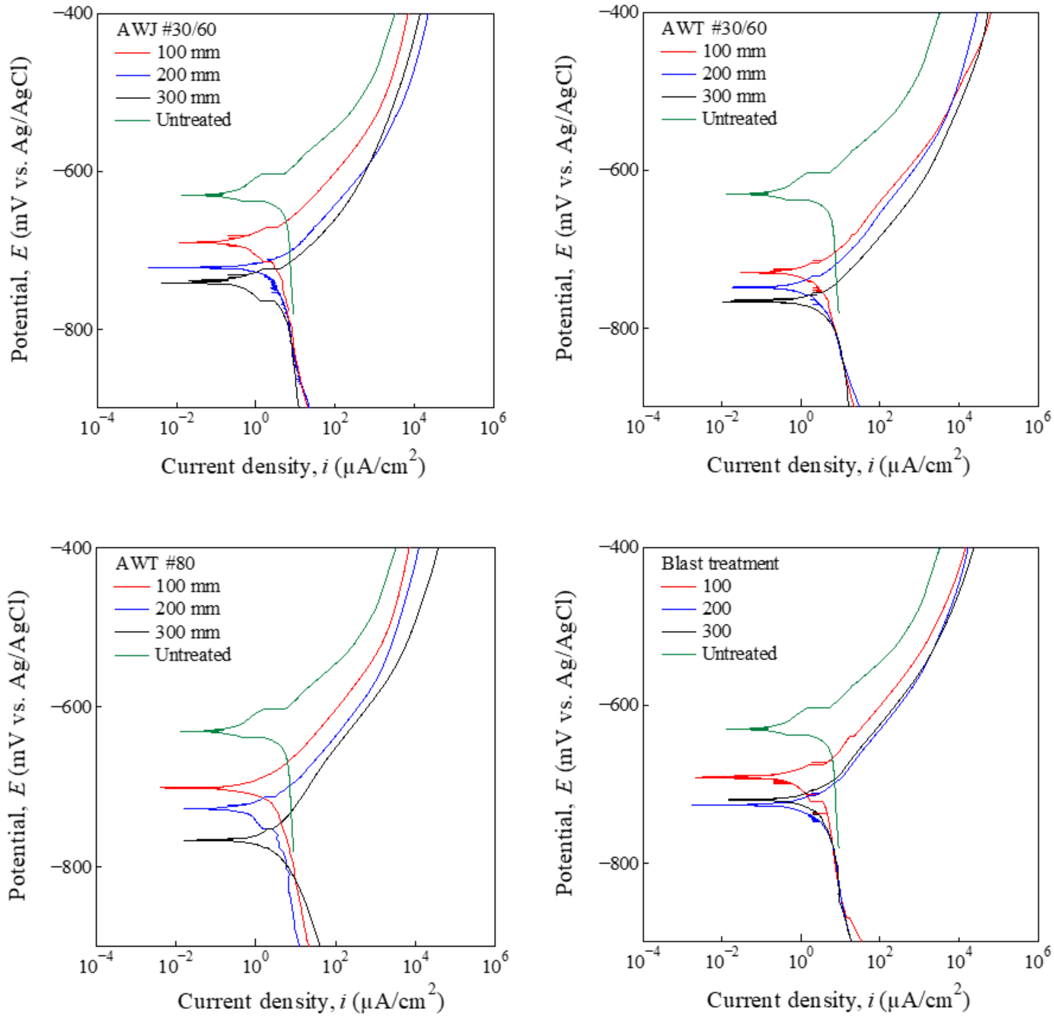

Figure 4-5 Potentiodynamic polarization curves of all specimens in 3.5 wt% NaCl solution.

Regarding the E_{corr} values, all treatments exhibited values approximately between -700 and -750mV$_{Ag/AgCl}$, with more positive potentials at smaller standoff distances. Conversely, the i_{corr} value was the lowest in the AWJ #30/60 specimen among all treated specimens, excluding those subjected to milling, with other specimens treated under different conditions exhibiting current density values ranging between 2 and 5μA/cm². Under all treatments, smaller standoff distances resulted in lower corrosion current densities.

$$m = \frac{M \cdot i_{corr}}{F \cdot z} \tag{4-2}$$

m: Mass of the substance, M: Molar mass of Fe, i_{corr}: Current density (μA /cm^2)

F: Faraday constant, z: Valency of the ion

Table 4-3 Fitted electrochemical parameters of the treated specimens in NaCl solution.

Specimens	Standoff distance (mm)	E_{corr} ($mV_{Ag/AgCl}$)	i_{corr} (μA /cm^2)	Corrosion rate CR (mm/yr)
Untreated	-	-633	0.42	0.005
AWJ #30/60	100	-711	0.64	0.007
	200	-729	0.90	0.010
	300	-740	1.44	0.017
AWT #30/60	100	-727	2.29	0.027
	200	-729	3.48	0.040
	300	-749	5.88	0.068
AWT #80	100	-701	1.76	0.020
	200	-727	3.10	0.036
	300	-767	3.69	0.043
Blast treatment	100	-702	2.21	0.026
	200	-727	3.32	0.039
	300	-726	4.68	0.054

$$CR = \frac{m \cdot t}{\rho_m \cdot A} \tag{4-3}$$

CR: Corrosion rate (mm/yr), m: Mass of the substance, t: Predicted corrosion period (1 year), ρm : Density of iron (g/cm^3), A: Area (cm^2)

Regarding the CR, they display a pattern similar to that of i_{corr}, irrespective of the surface treatment applied. Among the surface-treated specimens, except for the AWJ #30/60 specimens, which showed the CR less than 0.02 mm/yr, the others exhibited similar the CR ranging from 0.02 to 0.05 mm/yr. From a quantitative comparative perspective, considering only the numerical results, it can be seen that under identical standoff distance conditions, the AWJ #30/60 specimens exhibit up to four times slower CR than the other specimens. However, from a macroscopic viewpoint considering long-term use and durability, the CR post all treatments are generally very low, typically less than 0.1 mm per year.

Generally, i_{corr} is one of the most critical parameters for assessing corrosion performance, with lower i_{corr} indicating better corrosion resistance. Hence, the corrosion resistance of the AWJ #30/60 specimens was higher compared to other treated specimens, and it was observed that using the convergent nozzle and smaller standoff distances in AWT treatments led to enhanced corrosion resistance. This correlation is related to the surface characteristics of the material. Among the metal surface properties, roughness is a key factor affecting corrosion resistance. Typically, as the roughness of a metal surface increases, its corrosion resistance decreases [22], [78-81]. This is because a rougher surface increases the area of contact with the corrosive environment. In other words, increased surface roughness enlarges the interface between the electrolyte and the steel surface, thereby accelerating corrosion progression. In Chapter 3 of this paper, Table 3-8 showed that the surface roughness of AWT-processed specimens was more than twice that of blasted specimens, with the roughness of the AWJ #30/60 specimens increasing as the standoff distance decreased. However, the corrosion resistance was found to be better in the AWJ #30/60 specimens with higher roughness, following the order AWJ #30/60 (100), AWJ #30/60 (200), and AWJ #30/60 (300) specimens. This result is contrary to existing literature, implying that factors other than roughness significantly influence the corrosion resistance of treated specimens. Changes in corrosion resistance can be attributed to the plastically deformed surface layer formed after surface treatment. Thus, as the cross-sectional area of the plastic deformation layer increases, so does the compressive residual stress, leading to improved corrosion resistance following AWT processing with the convergent nozzle. This finding aligned with the study conducted by T. Wang et al. [61]. Additionally, the AWJ #30/60 specimens formed more grain refinement and sub-grains on the specimen surface compared to other AWT and blasted specimens. During AWT, smaller standoff distances increased the energy impacting the substrate, enhancing sub-grain formation. Consequently, AWT processing reduce grain size, forming new grains and sub-grains in the hardened surface layer. These formations ultimately remove parameters negatively affecting corrosion, thereby enhancing corrosion resistance. However, in AWT processing using the divergent nozzle, both AWT #30/60 and AWT #80 specimens exhibited similar or lower corrosion resistance compared to blasting under conditions other than a 100 mm standoff distance. This is corroborated by Tables 4-1 and 4-2 of this chapter, showing that under 100 mm standoff distance, specimens treated with the divergent nozzle reached a maximum hardness of over 260 HV and crystallite sizes under 27 nm, indicating increased corrosion resistance due to surface particle refinement and hardened layers.

4.3.4 EIS analysis on the AWT-processed specimens

Figure 4-6 presents the Nyquist plots results of AWT and blast specimens. The Nyquist plots indicate an increase in corrosion resistance as the capacitive loop expands [82]. Among the tested specimens, the milling specimen exhibited the largest Nyquist loop diameter, while among the surface-treated specimens, the AWJ #30/60 specimen had a larger loop diameter than the other surface-treated specimens. This implies that AWT using a convergent nozzle had a beneficial effect on corrosion resistance compared to AWT with the divergent nozzle and blast treatment. In particular, the AWJ #30/60 (100) specimen had the largest capacitive loop diameter among the treated specimens, signifying the highest corrosion resistance. Additionally, the Nyquist loop diameters of all specimens after treatment tended to increase with decreasing standoff distance.

The EIS data were analyzed using an equivalent circuit, as shown in Figure 4-7, to further investigate the surface improvement effects after treatment. The Randles circuit is suitable for indicating the situation of a film-free steel surface [83], [84]. The equivalent circuit consists of solution resistance (R_s), a constant phase element of the double electrical layer (CPE_{dl}), and charge transfer resistance (R_{ct}). A higher R_{ct} value indicates better corrosion resistance. Additionally, for the calculation of the CR, the Stern-Geary constant [16] was used to derive i_{corr} from R_{ct}, and CR was then calculated using Equations 4-3 and 4-4. Where the integer K is determined based on the type of metal or environmental conditions. In this study, a commonly used value of 0.0209V, as generally applied in engineering assessments, was employed.

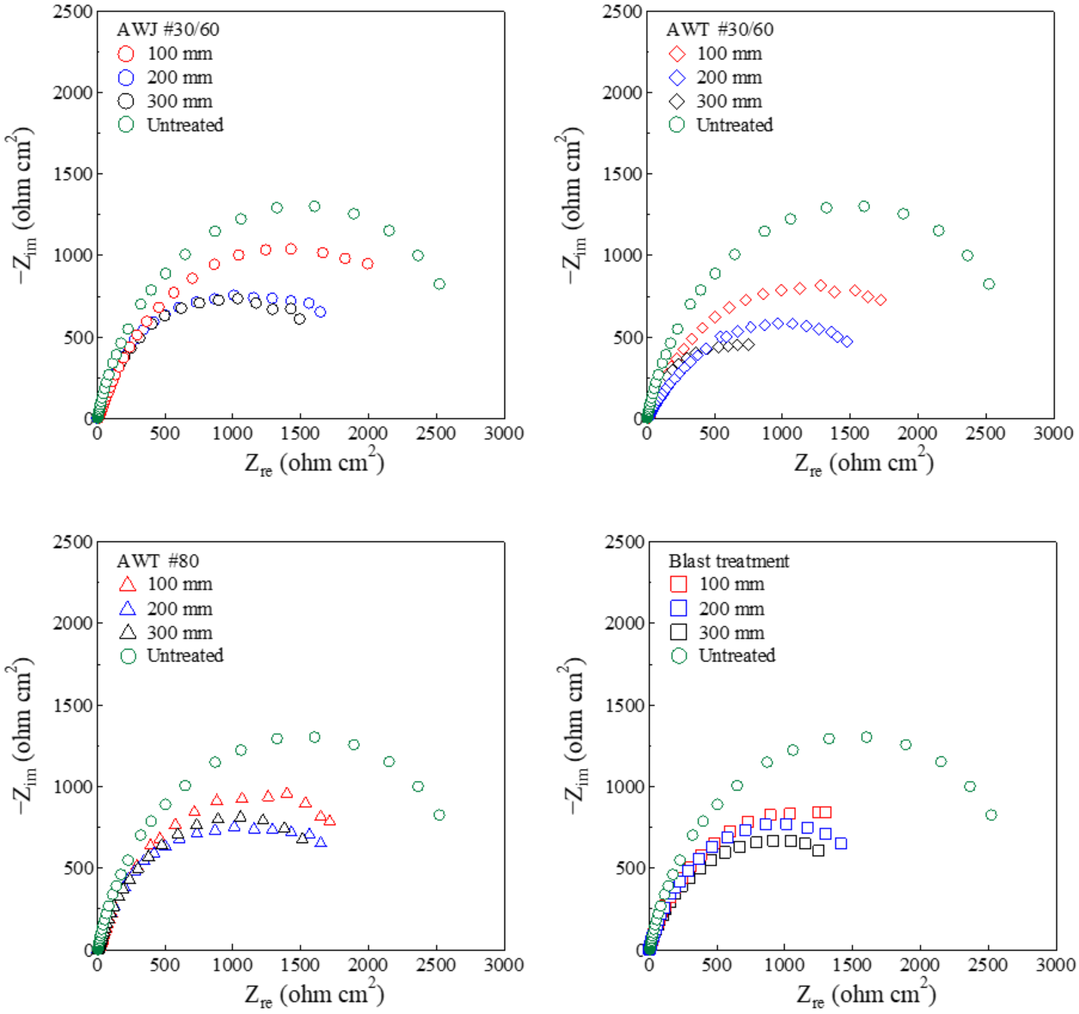

Figure 4-6 EIS results of all specimens in 3.5 wt% NaCl solution.

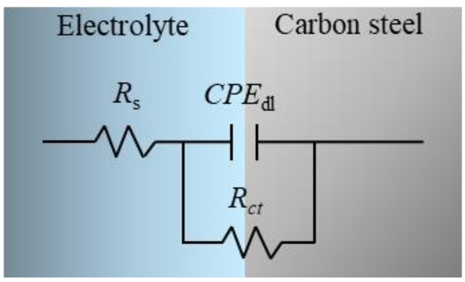

Figure 4-7 Equivalent circuit used to fit EIS data of all specimens.

$$i_{corr} = \frac{K}{R_{ct}} \qquad (4\text{-}4)$$

i_{corr}: Current density (μA /cm^2), K: Stern-Geary constant (0.0209 V),

R_{ct} : Charge transfer resistance

Table 4-4 Fitted impedance parameters from EIS of the treated and untreated specimens.

Specimens	Standoff distance (mm)	R_s (Ω cm^2)	CPE_{dl} (×10^{-3}) (Ω^{-1} s^n cm^{-2})	n	R_{ct} (Ω cm^2)	i_{corr} (μA/cm^2)	Corrosion rate, CR (mm/yr)
Untreated	-	7.16	0.37	0.874	2,860	7.31	0.085
AWJ #30/60	100	8.05	1.62	0.750	2,640	7.92	0.092
	200	10.0	1.58	0.770	2,600	8.04	0.093
	300	7.16	1.40	0.743	2,090	10.0	0.116
AWT #30/60	100	1.23	1.82	0.773	2,300	9.09	0.105
	200	8.26	3.75	0.797	1,760	11.9	0.138
	300	2.58	4.75	0.728	1,650	12.6	0.147
AWT #80	100	13.7	1.58	0.750	2,470	8.46	0.098
	200	1.26	3.17	0.722	2,120	9.84	0.114
	300	5.21	4.29	0.743	2,050	10.2	0.118
Blasting	100	3.69	2.82	0.786	2,300	9.09	0.105
	200	8.04	2.37	0.844	1,880	11.1	0.129
	300	7.14	4.39	0.765	1,820	11.5	0.133

The R_{ct} values and CR of AWT-processed and blasted specimens are presented in Table 4-4. As shown in the table, the R_{ct} value of the milling plate is the highest among all surface-treated specimens. Additionally, for all treated specimens, the R_{ct} values exhibited a similar trend as the semicircular diameter of the Nyquist loop under the same conditions. R_{ct} values increased with the use of a convergent nozzle in AWT processing, particularly with smaller standoff distances. R_{ct} values were influenced by surface modifications. Therefore, it was observed that the R_{ct} values of AWJ #30/60 specimens were larger than those of specimens treated with divergent nozzle and blast treatment, likely due to elevated energy intensity affecting the formation of subgrains and crystallite size reduction on the treated surface. It was also noted that under the same treatment conditions, smaller standoff distances and smaller abrasive particle sizes resulted in larger R_{ct} values.

In terms of CR, the AWJ #30/60 specimen exhibited CR similar to the milling specimen at standoff distances of less than 200 mm, with an error range of less than 10%. However, for specimens processed under different conditions, they exhibited CR 1.4 to 1.7 times higher. Additionally, under all processing conditions, CR decreased as the standoff distance decreased, and increased with larger abrasive particle sizes. Nevertheless, from a macroscopic perspective considering long-term usage and durability, the CR observed after all treatments remained consistently below 0.15 mm per year, indicating an overall very low CR. Consequently, it became evident that the use of the convergent nozzle and shorter standoff distance during AWT processing further accentuated these characteristics.

Based on all the structural and electrochemical test results mentioned above, it can be concluded that the surface of steel subjected to AWT treatment exhibits superior corrosion resistance compared to steel treated with the blast method. Additionally, it is evident that the hardened subsurface layer, characterized by subgrain formation and reduced grain size, is more extensive in AWT-processed steel plates than in blasted steel plates. Particularly, when AWT processing is conducted using the convergent nozzle with a standoff distance of 200 mm or less, similar R_{ct} values and CR within a 10% margin of error were achieved compared to the milling specimen. Therefore, it can be inferred that the formation of the subsurface layer has a more significant beneficial effect on corrosion resistance than surface roughness.

4.4 Summary

Chapter 4 investigates the impact of various treatment conditions during the AWT process on the surface hardness and microstructure changes of steel plates. The study elucidates the impact of these mechanical characteristics of the surfaces on the electrochemical properties of the steel surface. Additionally, we investigate the correlation between the influence of surface roughness, as discussed in Chapter 3, and the electrochemical characteristics.

The findings of this study can be summarized as follows:

1) AWT-processed steel plates exhibited greater surface roughness, hardness, and microstructural changes in surface particles compared to blasted ones. Furthermore, these characteristics increased as the use of the convergent nozzle and a reduction in standoff distance were implemented during the AWT processing. Therefore, the maximum values for surface roughness, hardness, and microstructural changes were obtained for AWJ #30/60 specimens treated with the convergent nozzle and a standoff distance of 100mm.
2) AWT-processed steel plates with the convergent nozzle showed a greater tendency for plastic deformation compared to other surface-treated steel plates. Additionally, an increase in hardness was observed as plastic deformation occurred. Under all types of treatment, a decrease in standoff distance led to an increase in hardness and surface plastic deformation. However, except for the conditions using a standoff distance of 100mm, AWT processing with the divergent nozzle exhibited hardness and plastic deformation similar to the blast treatment.
3) The AWT processing with the convergent nozzle improved corrosion resistance compared to blast treatment. This enhancement in corrosion resistance is primarily attributed to the increase in energy imparted to the steel surface, resulting in surface hardening and plastic deformation, which in turn modified the microstructure.
4) In the case of AWT using the divergent nozzle, it exhibited a corrosion behavior similar to the blasted steel plate. Furthermore, under the same conditions during AWT, smaller abrasive particle sizes were associated with higher corrosion resistance, although the difference was not significant.

CHAPTER 5 CORROSION REMOVAL EFFICIENCY BY AWT PROCESSING

5.1 Introduction

Due to the increasing factors of corrosion such as the construction of structures in marine environments and the use of anti-freezing agents, the importance of maintaining and repairing steel structures has been emphasized. In particular, the attachment of a large amount of chloride is a direct cause of severe corrosion in weathering steel structures. In the case of weathering steel, it is designed to form a stable and protective rust layer when exposed to less aggressive environments with low chloride content [85]. This rust layer is dense and tightly adhered, delaying additional corrosion. However, in highly saline, high-temperature, and humid environments, weathering steel experiences significantly increased CR as it cannot form a dense oxide layer. Furthermore, another significant factor affecting the durability of structures in aggressive environments influenced by seawater or coastal areas is pitting corrosion. Pitting corrosion is a localized form of corrosion where the protective oxide layer within the metal substrate is destroyed by halogen elements such as chlorine [86]. This allows chloride ions to penetrate deep into the steel surface, leading to the formation of small pits or crevices. Figure 5-1 illustrates the areas of extensive pitting corrosion on structural components of weathering steel bridges. While pitting corrosion may be less extensive, it can cause more rapid and severe damage to the metal than general corrosion. Therefore, detecting the symptoms of pitting corrosion early and addressing them promptly is crucial. On the other hand, chlorides can also cause severe damage to regular

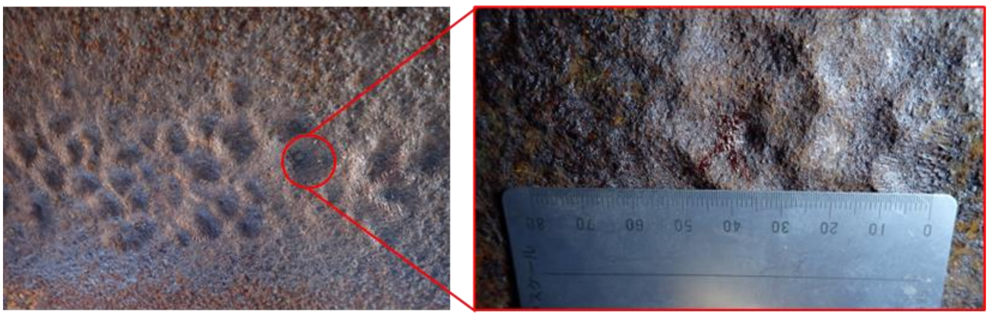

Figure 5-1 Extensive pitting corrosion on a weathering steel bridge member.

steel structures. If chlorides and corrosion products are not adequately removed, moisture can infiltrate from the coating to the boundary between the coating and the steel due to differences in chloride concentration. Once moisture and chloride have penetrated, a new corrosion reaction occurs beneath the coating, leading to blistering and delamination of the coating [11]. Thus, proper surface preparation is crucial for both weather-resistant and regular steel to ensure the structural integrity and longevity of the structure.

The depth of corrosion in weathering steel structures can reach several millimeters. Even when conventional abrasive blasting methods are used to treat heavily corroded steel, achieving a visually clean surface with no impurities at Sa 2.5 level or higher may not prevent flash rusting within a few hours at room temperature. Research findings indicate that significant instances of flash rusting were observed on the treated surface within 24 hours after abrasive blasting, primarily due to the presence of residual corrosion products and chlorides [17]. In Japan, regulations stipulate a time frame of 4-24 hours between abrasive blasting and coating application to prevent flash rusting and surface contamination [87]. Therefore, if flash rusting occurs within 24 hours after abrasive blasting, repeated cleaning becomes necessary, leading to increased construction cycles and costs. However, the challenge of addressing corrosion in deep areas, such as pitting corrosion, remains unresolved despite repetitive blasting procedures [15].

To investigate the effectiveness of chloride and corrosion product removal and the feasibility of AWT conditioning, Chapter 5 uses two types of test specimens with varying degrees of corrosion: weathering steel and carbon steel plates. For weathering steel, severely corroded handhole components from bridges exposed to sea breezes were utilized. For standard carbon steel, specimens were exposed to chloride and subjected to accelerated corrosion to create corroded test specimens. The efficiency of corrosion products and chloride removal during AWT processing under different conditions is assessed using weathering steel plates with substantial corrosion thickness. Lastly, to evaluate the presence of flash rusting in corroded carbon steel plates after AWT processing, a quantitative assessment method known as the "turning time" method is introduced, considering cleaning efficiency and the elapsed time following treatment.

5.2 Experimental method

5.2.1 Preparation of specimens

For the corrosion removal efficiency test, a handhole plate from a heavily corroded bridge was used as the sample (Material: weathering steel SMA400AW, Construction year: 1998). A piece measuring 120 × 60 × 9 mm was cut from the original handhole plate (dimensions: 1260 × 120 × 9 mm) for testing purposes. This bridge located approximately 5 km from the coastline in Kagoshima, Japan (Lat. 31°37'04" N, Long. 130°23'20" E), is subject to sea breezes and consequently faces severe corrosion issues as shown in Figure 5-2(a). These issues are exacerbated by a moist environment (17°C, 75% RH), airborne sea salt, and anti-freezing salt exposure (0.35 mdd), as depicted in Figure 5-2(b). Weathering steel is typically designed to form a protective rust layer that prevents further corrosion. However, in this case, an atypical rust formation led to delamination, with the delaminated corrosion products reaching a thickness of approximately 10 mm. Following the removal of the plate-like rust layers, the average and maximum corrosion depths of the dense rust layer were determined using a laser-focus measuring system and weight loss data measurements [88]. These depths were found to be 0.2 mm and 0.5 mm, respectively. The AWT process was carried out to identify the corrosion removal efficiency of the bridge samples. For the specific operating conditions of AWT to evaluate conditioning efficiency, a standoff distance of 300 mm was chosen, while the remaining conditions are as detailed in Table 3-1, already

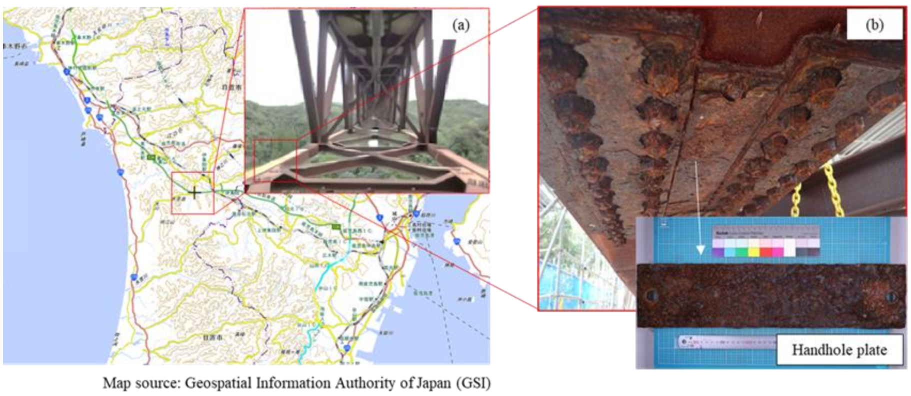

Figure 5-2 Heavily corroded weathering steel member.

[Map source: Geospatial Information Authority of Japan (GSI)] described in Chapter 3 of this paper. The efficiency of removing corrosion products and chlorides was examined and compared based on the type of nozzle and abrasive particle size during AWT processing. To serve as a control group, a standoff distance of 300 mm was maintained for assessing the efficiency of corrosion removal through blasting. The other variables are also detailed in Table 3-4, already described in Chapter 3 of this paper.

In the turning test, a specimen was prepared from a common steel plate conforming to JISG 3106 SM490A standards The dimensions of the specimen were set to 150×70×6 mm. To uniformly apply salt to the specimen, an ultrasonic spray method [89], a precision quantitative salt attachment technique, was utilized. It has been reported [90,91] that the amount of salt adhered to bridge parts in a marine environment exceeds 1000~10,000 mg/m². Following this method, a quantity of salt equivalent to 1000 mg/m² was applied to the surface of the specimen. Subsequently, the specimen was subjected to corrosion for approximately one month in a constant temperature and humidity chamber, replicating atmospheric conditions through a cyclic electrostatic dew point [92,93]. This cycle was designed to simulate the high-corrosion environment of Ryukyu University (2015/01-2019/09) during the summer. The temperature and humidity of the cyclic electrostatic dew point are presented in Figure 5-3.

Figure 5-4 shows the appearance of the corroded steel plate. The surface and inherent salt content of the corroded steel plate were 1,850 mg/m^2 and 118 mg/m^2, respectively. Additionally, the average and maximum corrosion depths were 0.1 mm and 0.3 mm, respectively. For the turning test, the formation of flash rust on the steel surface over time

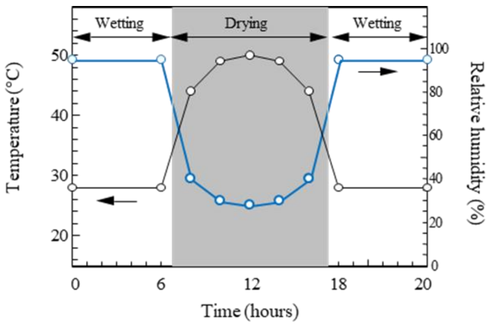

Figure 5-3 Wet and dry cycle used accelerated corrosion.

Figure 5-4 Appearance of corroded carbon steel plate.

was examined following AWT and blast treatment. The AWT conditions for the turning test were a standoff distance of 300 mm and garnet #80, with a processing time of 30 seconds to reach ISO 8501-1 Sa 3. For blasting, a standoff distance of 300 mm and garnet #80 were selected, and the spray time was 90 seconds to reach ISO 8501-1 Sa 3. Following this, the turning test was conducted in a constant temperature and humidity environment, based on the average summer daytime conditions at Ryukyu University (2015/01-2019/09), at 30°C, 90% RH (measured values: 29°C, 82% RH). The time intervals for the turning test were set at 0, 4, 12, 24, 36, 48, and 72 hours, resulting in seven different time points.

5.2.2 Analysis methods for corrosion removal efficiency

The efficiency of chloride and corrosion product removal after AWT processing on a severely corroded weathering steel bridge sample was analyzed through observation of the surface and cross-section of the treated specimens. To assess the occurrence of flash rust on the steel surface over time post-surface treatment, the appearance was monitored using a digital camera. For the turning tests, the surface images of the specimens were binarized, enabling the extraction of data on the recurrence rate of corrosion and the number of affected points. Additionally, the surface morphology of all samples was examined and analyzed using a 3D digital optical microscope (VHX-1000, Keyence Co., Ltd.). The elemental chemical composition of the treated surfaces was measured using the SEM-EDX method introduced in Section 2.2.2 of this paper.

5.3 Test results

5.3.1 Removal efficiency of corrosion products and chlorides in AWT processing

Prior to commencing this study, preliminary tests were conducted to assess the effectiveness and feasibility of removing corrosion products from corroded specimens using both conventional convergent nozzle and newly developed divergent nozzle in AWT processing. Figures 5-5 and 5-6 display the surface morphology and SEM-EDX images of the corroded specimens treated with the AWJ (convergent) and AWT (divergent) nozzles, respectively, under the conditions of a 300mm standoff distance and garnet #80. Independently of the nozzle type, surfaces treated with AWT satisfied the Sa 3 level with no residual corrosion products. Moreover, the removal efficiency of corrosion products and chlorides was investigated by sequentially measuring SEM-EDX images from untreated areas at point 1 to the central areas of treated sections at point 5. The treated areas were approximately 60 mm and 90 mm for the AWJ and AWT nozzles, respectively, with the majority of corrosion products and chlorides being removed from the treatment areas. Notably, Cl clusters present prior to the processing were completely eliminated after AWT

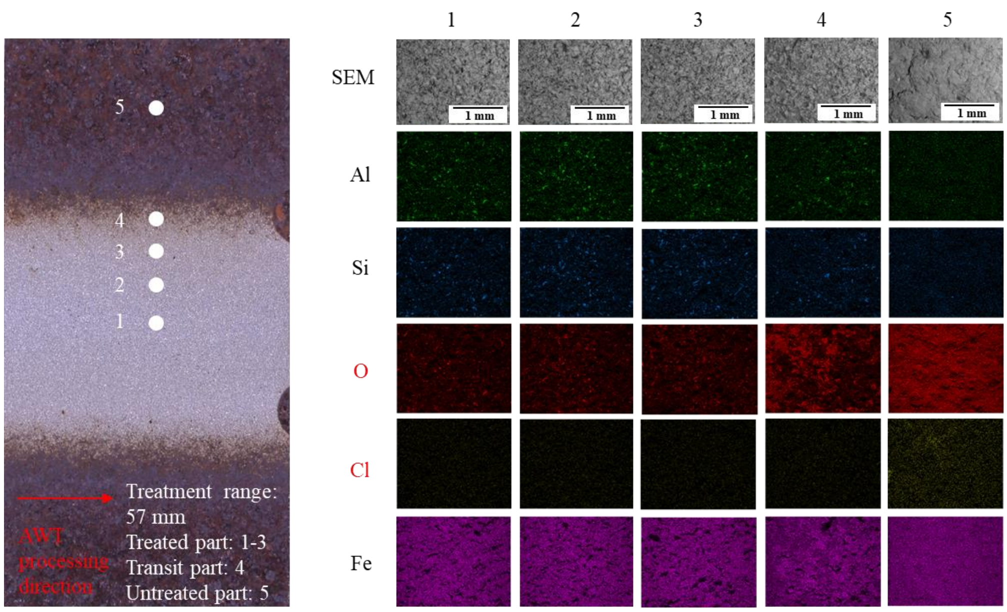

Figure 5-5 Elemental composition investigation from the unprocessed part to the midpoint of the AWJ #80 specimen.

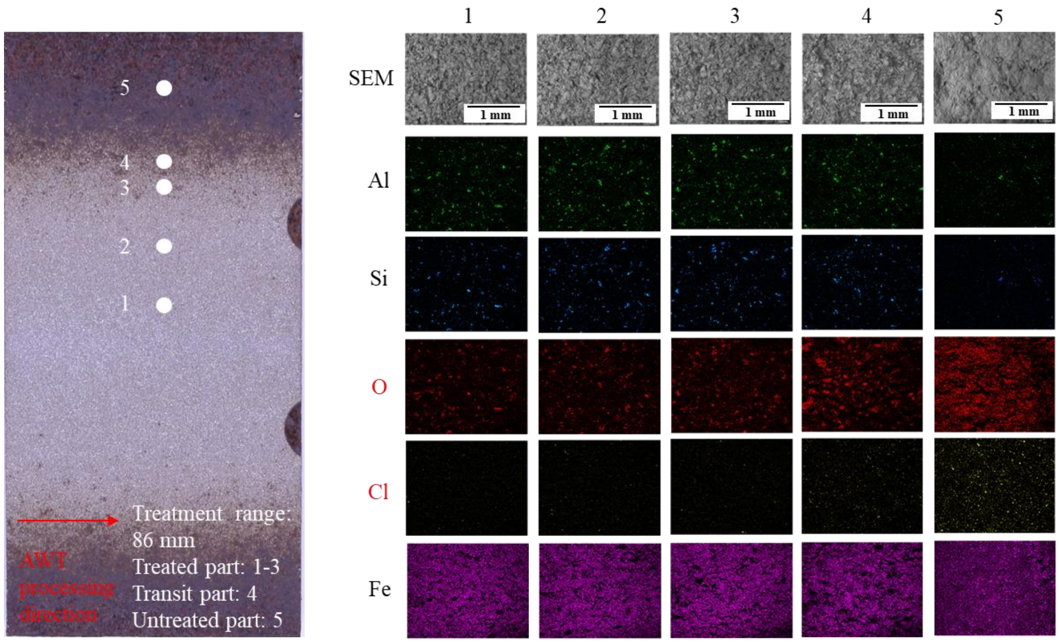

Figure 5-6 Elemental composition investigation from the unprocessed part to the midpoint of the AWT #80 specimen.

processing with all types of nozzles. This was particularly evident in the treated and boundary areas at point 2, where a significant portion of the corrosion products was removed, demonstrating the excellent rust removal efficiency of AWT. Consequently, at the same standoff distance, AWT nozzle formed a treatment area 1.5 times larger than that of AWJ nozzle and demonstrated superior effectiveness in removing both corrosion products and salts within these areas. Therefore, when applying AWT to corroded components, the use of divergent nozzle is considered to be more efficient.

In this study, the SEM-EDX images of the surfaces treated with AWT and blasting are presented in Figure 5-7. As shown in Figure 5-7(a, b), before surface treatment, a substantial amount of corrosion products and Cl clusters were observed, which significantly decreased after blasting. However, some corrosion products and Cl clusters still remained on the blasted surface. In contrast, as seen in Figure 5-7(c-e), most contaminants and chlorides were completely removed after AWT processing under all conditions. Furthermore, the amount of residual abrasive materials remaining on the surface was considerably lower in the case of AWT-processed specimens. Figure 5-8 presents the cross-sectional SEM-EDX images of

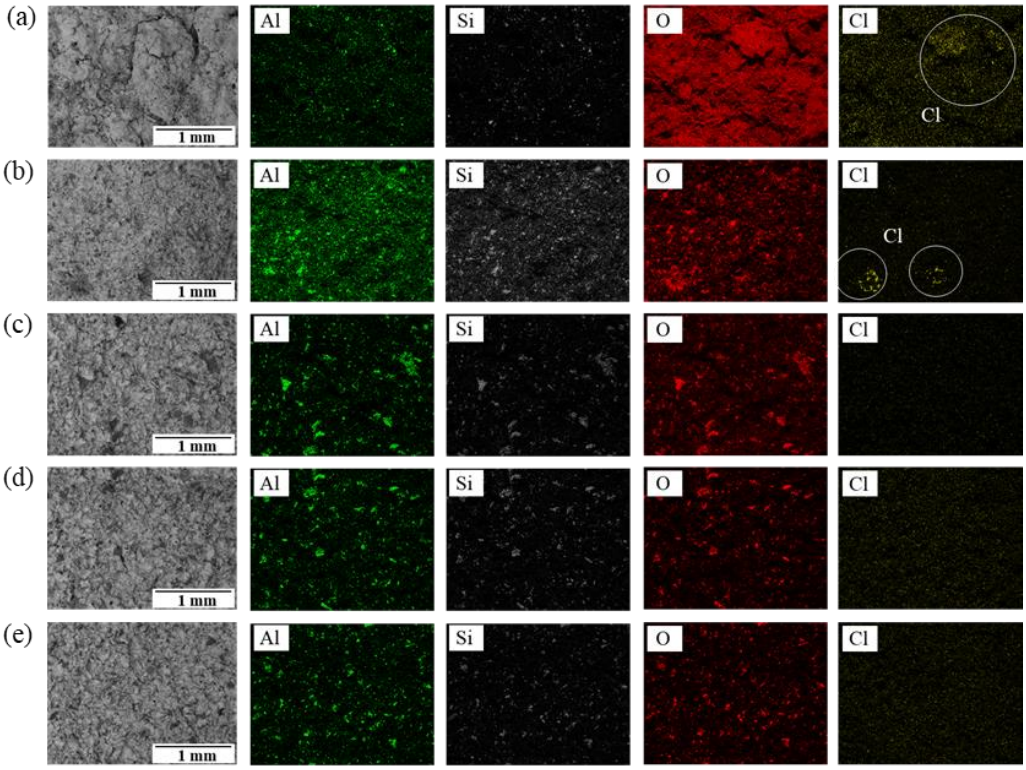

Figure 5-7 Elemental composition investigation illustrates the remaining chlorides and corrosion residues across untreated and treated surfaces: (a) Significantly corroded state, (b) Blasted, (c) AWJ #30/60, (d) AWT #30/60, and (e) AWT #80 samples.

various surface treatments. Figure 5-8(a) shows the presence of corrosion products, including internal chlorides, before surface treatment. These corrosion products included secondary pitting corrosion, with the depth of the secondary pits reaching several hundred micrometers. Figure 5-8(b) illustrates that, after blasting, corrosion products remained under the steel plate, and a significant amount of residual abrasives was detected. This suggests that blasting has limitations in removing thick or deeply embedded corrosion products. Moreover, the abundant residual abrasive material on the steel surface after blasting could act as a protective layer for corrosion products and chlorides [15], potentially causing early onset of corrosion underneath the coating. In contrast, as indicated in Figure 5-8(c-e), almost all corrosion products and chlorides were removed after AWT processing under all conditions. Compared to blasting, AWT leaves significantly less residual abrasive materials

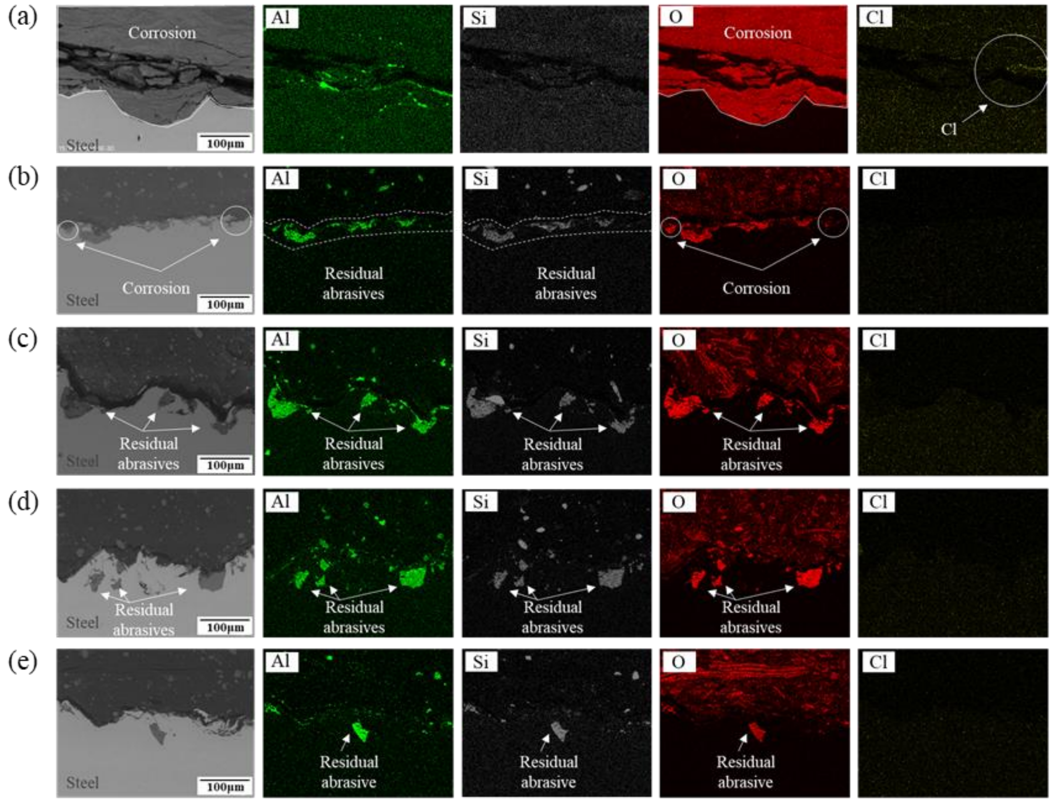

Figure 5-8 Cross-sectional electron microscopy images depicting unprocessed and processed specimens: (a) Significantly corroded state, (b) Blasted, (c) AWJ #30/60, (d) AWT #30/60, and (e) AWT #80 samples.

and is also expected to create complex surface profiles, enhancing coating adhesion [94]. When performing surface treatment on corroded structures, it is essential to remove all contaminants within the official corrosion. Failure to do so can lead to the formation of bubbles, cracks, or eventual delamination of the coating [11].

5.3.2 Turning time test

Figure 5-9 presents the appearance, surface morphology, and microscopic photographs of corroded steel plates immediately after AWT and blast treatments This figure illustrates the results of surface treatments that achieved the ISO 8501-1 Sa3 standard for each processing technique. As depicted, no rust was observable to the naked eye on any of the treated surfaces post-treatment, all displaying a uniform metallic color. Additionally, it was challenging to detect any rust even under high magnification using a microscope. The surface

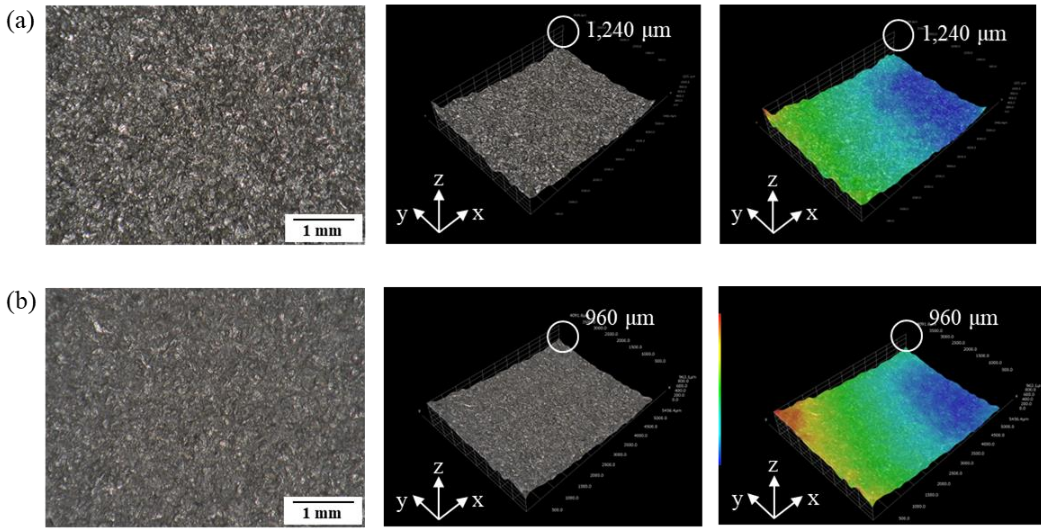

Figure 5-9 Microscope images of the processed surfaces: (a) AWT #80 and (b) Blasted samples.

of the steel plates treated with AWT exhibited a higher gloss compared to those treated with blasting, with the roughness profile peak values being about 1.3 times higher.

Figure 5-10 shows the surface conditions over time, from immediately after AWT and blast treatment up to 72 hours. The turning test was conducted at different time intervals following each surface treatment, under the average summer daytime conditions at Ryukyu University (30°C, 90% RH), showing the treated surface states at 0, 4, 12, 24, 36, 48, and 72 hours. Figure 5-10(a) depicts the surface condition of steel over time following AWT processing, showing no occurrence of flash rust for up to 72 hours and maintaining surface conditions exceeding the Sa 3 level. In contrast, the specimens treated with blasting exhibited extensive corrosion and flash rust formation as early as 4 hours after treatment, with the severity increasing over time, as illustrated in Figure 5-10(b).

Figure 5-11 presents the SEM-EDX mapping results of the surface before and after AWT processing, as well as over time. The substantial amount of corrosion products and chlorides present on the corroded steel plate before treatment were completely removed immediately afterwards, and no corrosion products or chlorides were detected on the treated surface even after 72 hours. However, the SEM-EDX images, which are based on atomic percentage, were measured on a micro-scale. Therefore, using the area ratio method

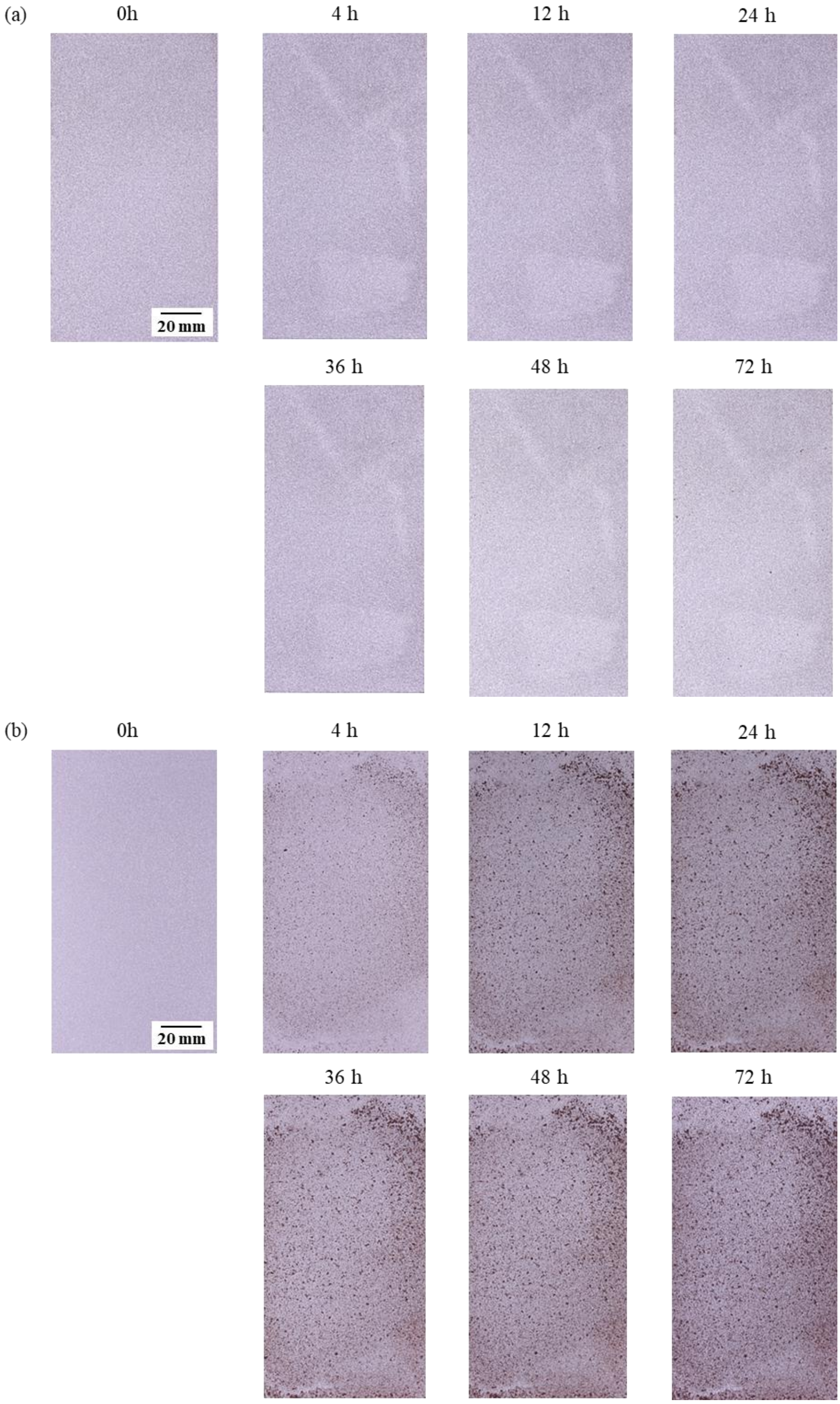

Figure 5-10 Turning time test of severely corroded specimens after surface treatment: (a) AWT #80 and (b) blasted specimens.

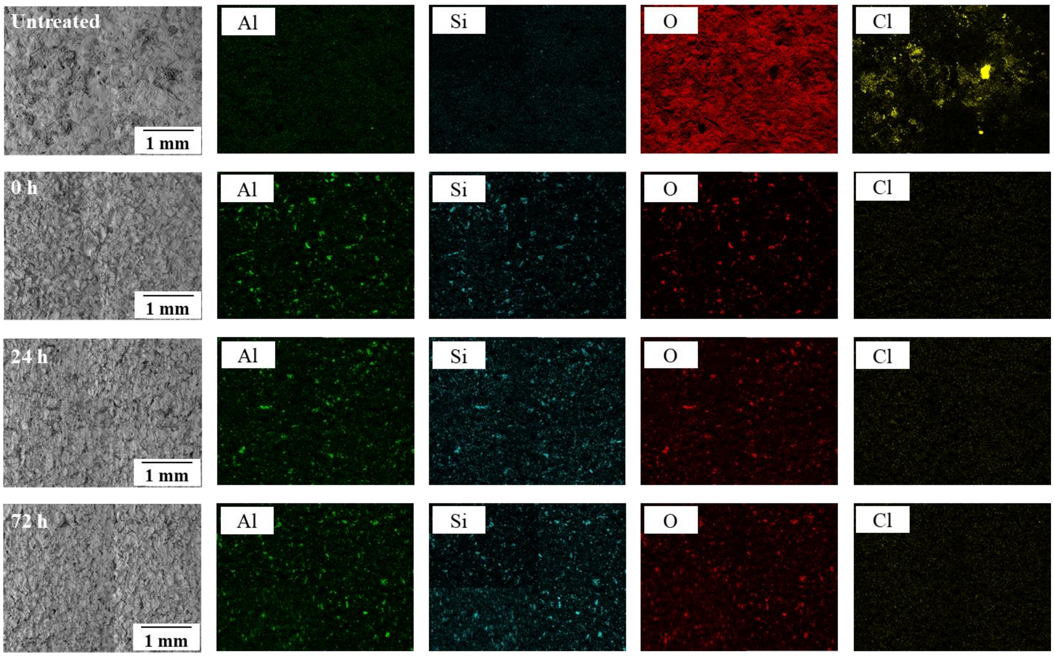

Figure 5-11 Elemental composition investigation illustrating the AWT-processed samples after the turning test (0, 24, and 72hrs).

introduced in Chapter 2 of this paper, a more comprehensive quantitative comparison and evaluation of the residual elements' distribution over a broader range were possible. The elements measured were Al, Si, and Cl, with Al and Si being the main components of garnet, and Cl representing the chloride content.

Figure 5-12 presents the area ratio results of residual elements for each treated specimen over time after turning. For the AWT-processed samples, irrespective of time elapsed, Cl showed less than 1% (considered as noise), Si was around 4-5%, and Al was about 4% in terms of area ratio. In the case of the blasted specimens, Cl was at 2%, Si ranged between 9-10%, and Al was at 8%. Although there was no significant variation in the elemental area ratios over time, the blast-treated specimens exhibited a Cl area ratio twice as high as that of the AWT-processed ones, likely due to the influence of clustered Cl. Furthermore, the area ratios of Si and Al in the blast-treated samples were approximately double those in the AWT-processed samples, indicating that the residual surface area of these elements was significantly greater in the blasted specimens compared to the AWT-processed ones.

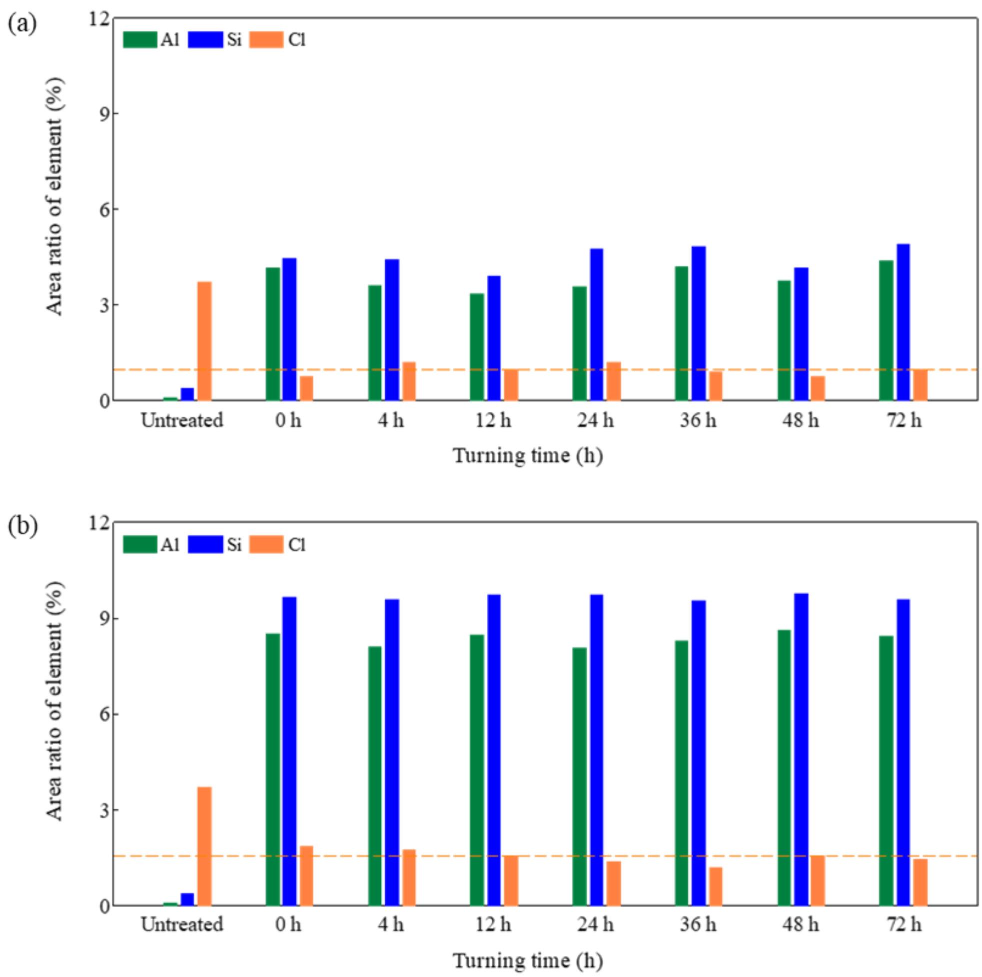

Figure 5-12 Area ratio of elements on the AWT-processed specimens after the turning test: (a) AWT and (b) Blasted specimens.

Figure 5-13 illustrates the relationship between the re-corrosion ratio (α) and the number of corrosion points (N) over time, following immediate treatment with AWT and blasting. The analysis and evaluation were conducted for the target area of the specimen surface (120×70mm). The dotted lines in each graph of the figure represent the regression lines for the re-corrosion rate and number of corrosion points over time for the blasted specimens, showing that both α and N increase linearly with time, with correlation coefficients above 0.8. Notably, for the blasted specimens, the most significant increase in α and N occurred between 4-12 hours, with a relatively constant rate maintained from 12-24 hours. This observation supports the standards currently adopted in Japan [87], which stipulate the

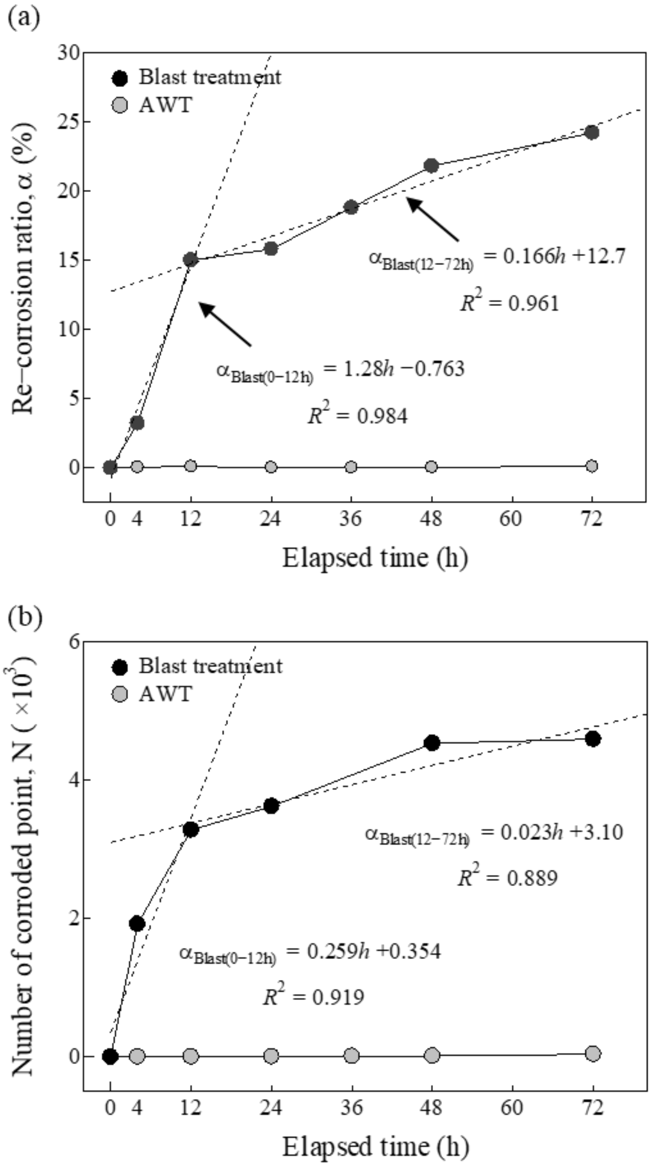

Figure 5-13 Turning test results over time from immediately after surface treatment: (a) Corrosion ratio and (b) Number of corroded points.

recommend a time frame of 4-24 hours between blasting and coating application to avert flash rust and surface impurities, underscoring the criticality of achieving the right surface conditions for coating within the first 12 hours. In the case of AWT processing, there was no occurrence of re-corrosion or flash rust over time, leading to α and N values converging close to zero across all time conditions, indicating no significant difference. Therefore, the quantitative evaluation of surface cleanliness over time following AWT treatment revealed that flash rust and re-corrosion do not occur for up to 72 hours. Moreover, AWT processing has been proven to completely remove residual corrosion products and chlorides from the surface in a processing time reduced by one-third compared to blasting.

To examine the tensile adhesion behavior between the surfaces of steel specimens treated in various ways after the turning test and an epoxy adhesive, the method introduced in section 3.2.3 of this paper was employed. Figure 5-14 illustrates the relationship between the load (P) and displacement (δ) during the pull-off test between the specimens in the turning time test and the epoxy adhesive. Under all treatment conditions, the force exerted on the substrate was found to be approximately 6-8 kN for AWT-processed samples and 5-7 kN for blasted samples, indicating that AWT consistently exerted a higher force than blasting. Additionally, no signs of bending due to irregularities such as warping were observed on the fracture surfaces under any surface treatment condition. Therefore, the test results indicate that the relationship between P and δ during load application provides reliable adhesion results for all treated surfaces. Table 5-1 presents the observations of the fracture states of the steel surfaces and dollies using a digital microscope after the completion of the pull-off test. The failure mode of the epoxy adhesive after the tensile adhesion test was predominantly interfacial failure between the steel surface and the epoxy adhesive under

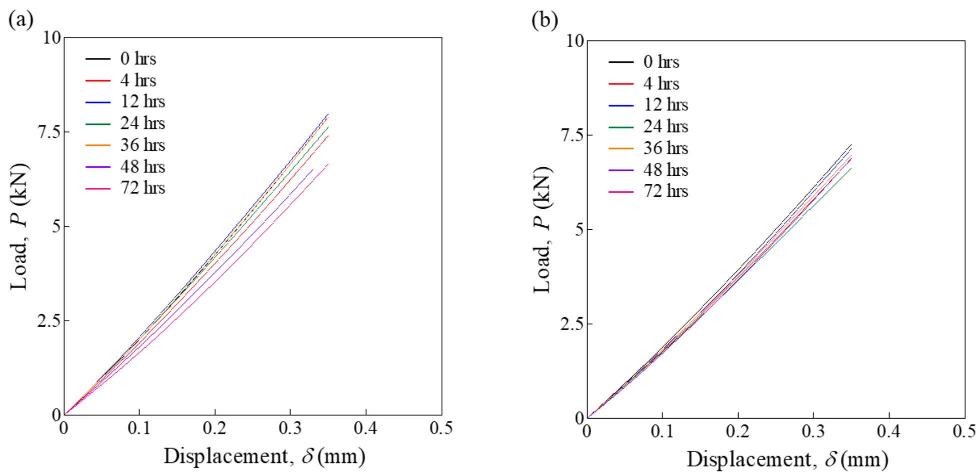

Figure 5-14 Relationship between load P and displacement δ after pull-off test: (a) AWT and (b) Blast treatment.

Table 5-1 Destruction state of epoxy adhesive after pull-off test.

(a) AWT processing

Turning time (hrs)	0	4	12	24	36	48	72
Substrate side							
Dolly side							

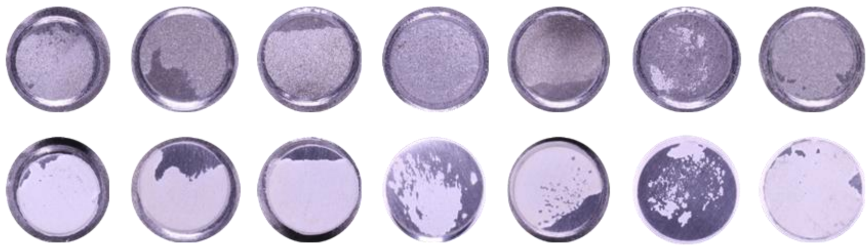

(b) Blast treatment

Turning time (hrs)	0	4	12	24	36	48	72
Substrate side							
Dolly side							

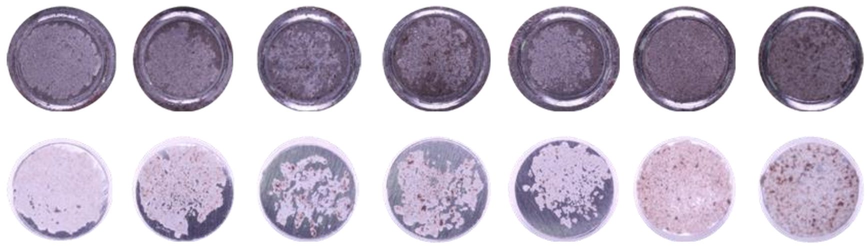

most treatment conditions. Notably, for the blasted specimens, corrosion products visibly remained on the surfaces of the steel plate and dollies after more than 4 hours of the turning test. In contrast, for AWT-processed specimens, no corrosion products were observed on the surfaces of the steel and dolly after the pull-off test, up to a maximum of 72 hours post-treatment.

Figure 5-15 shows the tensile adhesion strength (σ) between the steel surfaces treated under various conditions after the turning test and the epoxy adhesive. The tensile adhesion strength is represented by the results of three tests conducted per condition and their average values. The dotted lines in the graph represent the adhesion strength between the epoxy adhesive and the carbon steel plates (milling) treated under identical conditions, as explained in Chapter 3. Regardless of the presence of flash rust, it was observed that the adhesion strength of the corroded steel plates treated with AWT and blasting was higher than that of the carbon steel plates. This increase in adhesion strength is attributed to the surface

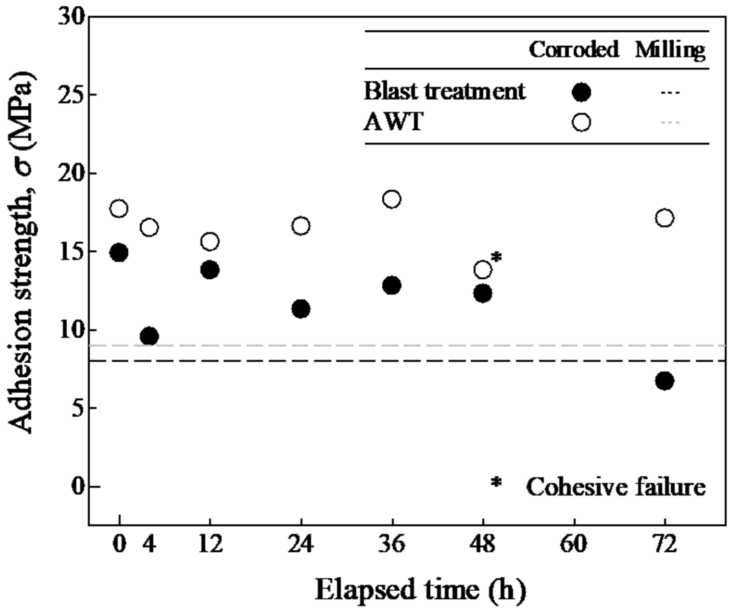

Figure 5-15 Effect of surface properties on adhesion strength to epoxy adhesive after turning test over time.

deformation of the steel during corrosion, supporting the conclusion in Chapter 3 of this paper that surface deformation ratio has the highest correlation with adhesion strength of the epoxy adhesive. For AWT-processed samples, the adhesion strength remained nearly constant from immediately after treatment up to 72 hours, indicating that no flash rust developed during this period. A noticeable decrease in adhesion strength was observed in the 48-hour turning test specimens. This could be attributed not to surface corrosion but to a variation in the deformation of the corroded steel plate compared to other specimens under the same conditions. On the other hand, for the blasted surfaces, a trend of decreasing adhesion strength over time was noted. Specifically, after 4 hours, the adhesion strength decreased by 36% compared to uncorroded surfaces. This decrease could be attributed to initial corrosion increasing surface roughness while simultaneously damaging the chemical structure of the surface, thereby reducing adhesion [95]. From 12 to 48 hours of the turning test, the adhesion strength fluctuated, initially increasing and then decreasing. This could be due to the formation of fine defects on the surface from ongoing corrosion, creating an effective roughness [95] and allowing the adhesive to better penetrate and form mechanical interlocks. However, continued corrosion would likely weaken the surface integrity over time, leading to a decrease in adhesion strength. The adhesion strength of specimens after 72 hours of turning time decreased by up to 55% compared to immediately post-treatment. This suggests severe damage to the steel surface due to prolonged corrosion, significantly reducing structural integrity and adhesion. In conclusion, corrosion has a complex impact on adhesion strength, varying with the extent and duration of corrosion. While initial corrosion might temporarily enhance adhesion, prolonged corrosion tends to have a detrimental effect, suggesting the need for further research.

5.4 Summary

Chapter 5 examines the efficiency of removing corrosion products and chlorides from severely corroded weathering steel bridge components treated with AWT under various conditions. Additionally, this chapter also investigates the cleaning efficiency of AWT on the corroded carbon steel plates, examining the occurrence of flash rust over time post-treatment, and elucidates the adhesion behavior between the treated steel surface and epoxy adhesive.

The main outcomes of this chapter are as follows:

1) Under all conditions, AWT processing demonstrated superior corrosion product and chloride removal efficiency compared to blast treatment. Notably, it was capable of completely removing deeply and densely corroded areas, such as pitting corrosion.
2) The application of AWT on corroded steel plates reached the cleanliness level specified by ISO 8501-1 Sa 3 in a processing time that was one-third shorter than that required for blasting. Additionally, the removal of most pollutants and chlorides was confirmed not only through visual examination but also through quantitative SEM-EDX analysis of the remaining elemental quantities.
3) The results of the turning time test revealed that, unlike blast treatment where significant amounts of rust developed comprehensively within just 4 hours, AWT processing showed no occurrence of flash rust for up to 72 hours.
4) In conclusion, AWT processing completely removed residual chlorides and contaminants from the surface in a shorter processing time compared to blasting, thereby preventing re-corrosion and the development of flash rust. This result supports the standards adopted in Japanese civil bridge construction, which stipulate

the recommended time frame of 4-24 hours between blasting and coating application. Furthermore, AWT offers economic advantages as it eliminates the need for repeated treatments.

CHAPTER 6 ENGINEERING APPLICATION OF AWT

6.1 Introduction

AWT is an innovative approach for cleaning severely corroded steel structures and materials, with potential applications across various fields. However, the practical applications and research concerning the effectiveness of AWT cleaning remain limited. Consequently, it is essential to verify how AWT can be applied and utilized in real-world conditions. Especially in the case of structures like bridges at high altitudes, conventional blasting methods experience a significant reduction in efficiency due to pressure losses at such altitudes, often not achieving the standard site requirement of 0.8 MPa [96]. Moreover, the extensive dust produced during blasting not only makes complete recovery challenging but also leads to environmental contamination and poses health risks to workers. For bridges' interiors or enclosed spaces, the usage of blasting methods is restricted due to the risk of fire.

To overcome the limitations of the previously mentioned blast cleaning process has developed specialized equipment for the application of AWT processing in the field and its engineering applications. The equipment for on-site AWT application is designed to maintain a pressure above 230 MPa, regardless of the altitude, and includes technology to collect and purify both the waste abrasive materials and the treated water after the operation. Most importantly, the equipment and machinery are customized according to the shape and height of the components to maximize processing efficiency. Additionally, to address potential safety issues during AWT processing, the company has independently developed an AWT processing safety guide.

In order to verify the practical applicability of AWT for cleaning, Chapter 6 examines the effectiveness of corrosion removal on severely corroded bridge components by applying AWT under the treatment conditions selected based on the content presented in the preceding chapters. To accurately assess the efficacy of AWT in removing corrosion products and chlorides, core samples from the components were taken before and after treatment. These samples were then examined using SEM-EDX to observe the cross-sections. Additionally, the surface condition of the components treated on-site was monitored over 24 hours to check for the occurrence of flash rust. The findings of this chapter provide a substantial basis for the use of AWT cleaning technology in the maintenance of severely corroded structures and will serve as an important reference in the field of surface cleaning engineering.

This study presents a novel approach to surface treatment technologies. Moving beyond the traditional focus on the effectiveness of corrosion product removal, it systematically analyzes and evaluates the surface characteristics of steel from a multidisciplinary perspective, including material science, surface science, electrochemistry, and mechanics. This study focuses on revealing the characteristics and limitations of steel surfaces treated with blasting on corroded plates, a topic that has remained unresolved for the past 150 years. Based on these findings, a new surface treatment technology, AWT, has been developed. AWT offers a novel approach for accurately establishing the necessary roughness and anchor patterns according to the conditions of corrosion and construction requirements. This method adopts the selection of optimal construction parameters, including the grain size of abrasive materials and the distance of treatment. This technology emphasizes not only the effectiveness of removing corrosion but also the capability to reproduce specific surface characteristics values as a surface treatment method. Particularly in cases like the repainting of steel bridges, it is essential to meet various roughness standards and surface cleanliness conditions. This study explores the reproducibility of surface characteristics under specific surface treatment conditions, which previous methods have not explicitly defined. Furthermore, AWT enables accurate determination of the suitable surface roughness before painting with minimal measurements, thereby expecting to reduce construction periods and costs for materials and labor.

6.2 Experimental method

6.2.1 Application of AWT to the actual field

The efficiency of corrosion removal by directly applying AWT processing to a corroded bridge was evaluated, and the feasibility of its engineering application was investigated. To ascertain the corrosion removal efficiency of the AWT process, the divergent nozzle and Garnet 80 mesh size were selected, with a standoff distance of 300 mm, and other conditions were set in accordance with Table 3-3 in chapter 3. Specialized equipment developed was

Field photograph of the bridge where AWT processing will be directly applied.

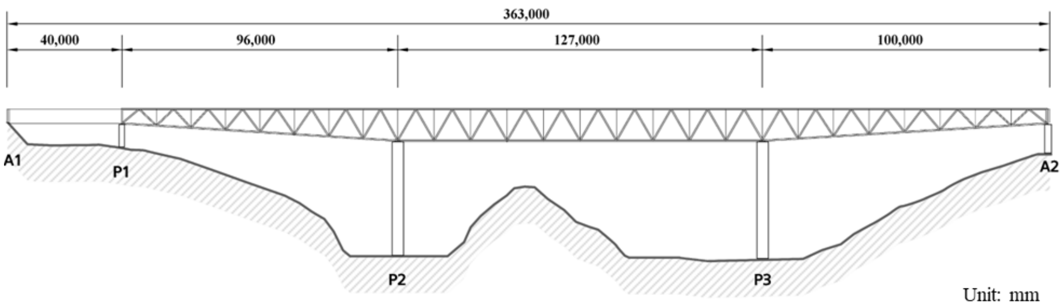

Lateral view of the bridge [97].

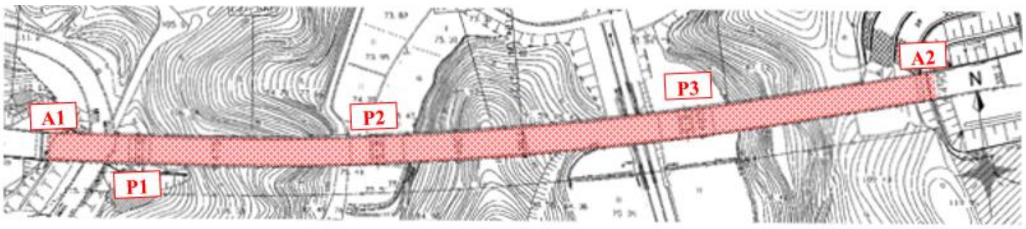

Plan view of the bridge [97].

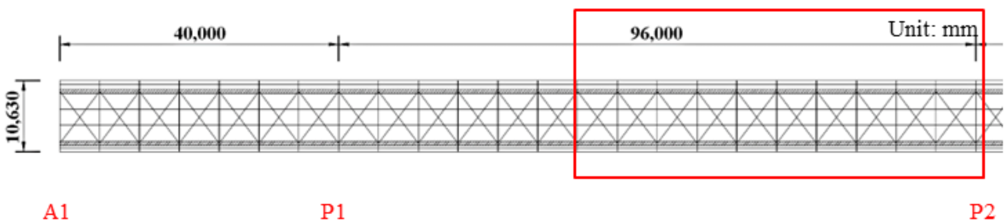

Processing location in bridge.

Figure 6-1 The exterior appearance and detailed design plans of the bridge [97].

utilized for the on-site application of AWT. Figure 6-1 presents the bridge design and the section under examination, which is located in Kagoshima, Japan (latitude 31° 37' 04" N, longitude 130° 23' 20" E). The section designated for AWT processing was the lower truss member between points P1 and P2, situated in a moist environment with minimal exposure to sea breeze and sunlight, where it was severely corroded.

6.2.2 Analysis methods for corrosion removal efficiency.

Figure 6-2 visually represents the actual implementation of AWT processing at the site. The ambient temperature and relative humidity at the location were maintained at 15°C and 65% RH, respectively. Widespread instances of pitting corrosion phenomena, with a diameter of 5mm, were observed on various parts of the structural member. Core samples of structural steel (20 mm in diameter) were cut and collected before and after the AWT processing. The cross-sections of these cut samples were analyzed for residual elements using SEM-EDX. Additionally, Figure 6-3 describes the method for measuring the chloride content on the treated surface. The surface soluble salts were measured twice using the

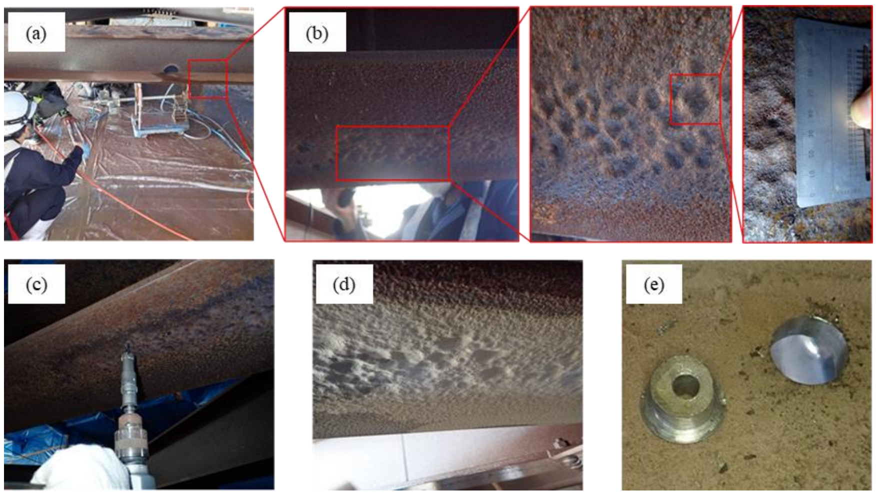

Figure 6-2 Implementation of AWT in severely corroded structures on-site: (a) Heavily corroded component, (b) Focused area of pitting corrosion, (c) Cutting with a hole saw pre-AWT, (d) Pitting corrosion area component post-AWT, and (e) Sample extracted using a hole saw.

Figure 6-3 Assessment of surface salinity levels following AWT processing using the Bresle patch method.

Bresle patch test, which was conducted on a square patch of 1,250 mm² area following the ISO 8502-6 testing method. The test involved injecting a solution onto the test area and leaving it immersed for one minute before measurement. To meticulously investigate the removal efficiency of corrosion products and chlorides, Ion chromatography was employed to record the chloride content in the water used in the AWT processing.

6.3 Test results

6.3.1 Efficiency of corrosion and chloride removal during AWT in the field

After the application of AWT processing, the surface chloride content of the structural steel member was measured at 12mg/m² and 14mg/m², respectively. These values meet the standard requirement of less than 50mg/m² stipulated in the Japanese manual for corrosion prevention in bridge coatings [98]. Such findings indicate the potential for meeting the surface salt standards required for pre-coating of steel and various materials in a range of applications, from naval vessels to structures and equipment used in NASA space missions. In particular, structures like naval submarine tanks and bilges require chloride levels below 30mg/m² [99], while structures used in NASA space missions demand chloride levels less than 50mg/m² [100]. These results highlight the capability of AWT processing to meet surface preparation requirements in diverse fields. For a more accurate measurement of surface chloride content, water extracted during the Bresle patch test was analyzed using Ion chromatography. According to the results of Ion chromatography, the salinity of the treated steel surface after AWT processing was measured at 3.67 and 3.98 mg/m², demonstrating excellent chloride removal efficiency. Subsequently, Ion chromatography analysis determined the salinity of the water used in AWT processing to be 13.4 mg/m², confirming the absence of cross-contamination with the water used in the treatment [101].

As depicted in Figure 6-4, the efficiency of chloride and corrosion product removal by AWT processing was investigated by examining images of core samples extracted from pitting corrosion areas, using microscopy and SEM-EDX. As shown in Figure 6-4(a), pitting corrosion of up to 500 µm depth was observed, with chloride residues found inside the pits. In contrast, Figure 6-4(b) displays the state of the area post-AWT processing. After the treatment, only abrasive residues remained, with chlorides and corrosion products being completely removed. These results clearly demonstrate the superior efficiency of AWT in removing chlorides and corrosion products.

Figure 6-5 visually represents the presence or absence of flash rust overtime on a structural steel member severely affected by pitting corrosion after AWT application. In Japan, the time between the blast treatment and coating application is typically limited to 4-24 hours to prevent flash rust and surface contamination [87]. No occurrence of flash rust

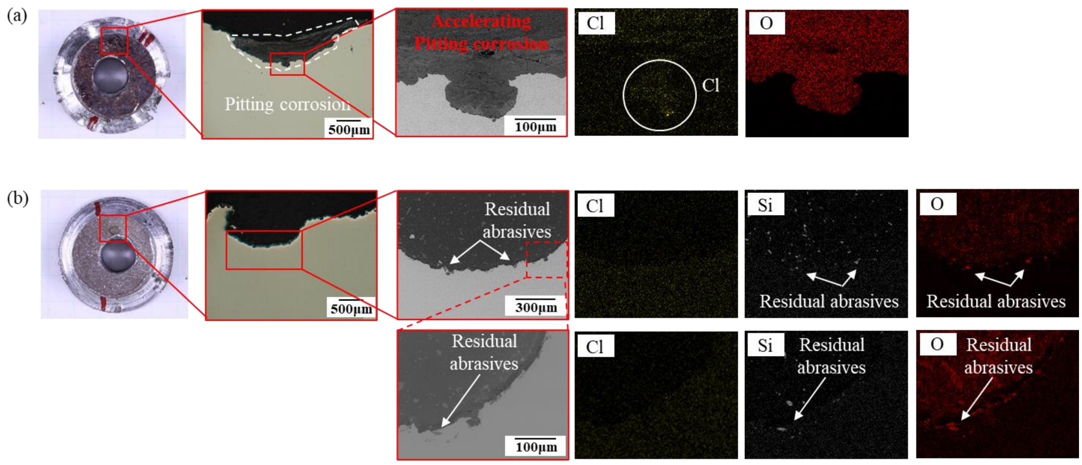

Figure 6-4 Microscopic analysis and SEM-EDX images of core specimens extracted from an area of pitting corrosion: (a) Section before treatment and (b) Section after AWT processing.

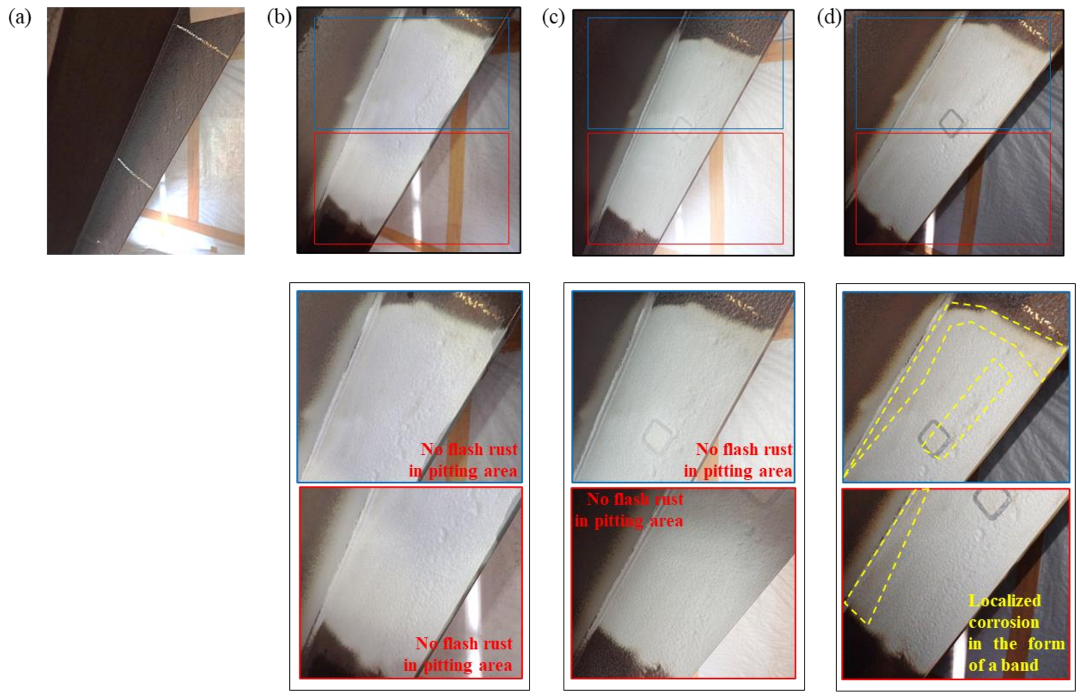

Figure 6-5 Changes in surface state through time: (a) Beginning state of the corroded steel member, (b) Directly following AWT application, (c) 12 hours later, and (d) 24 hours later.

was observed up to 24 hours after AWT, and the surface condition met the optimal Sa 3 level for surface quality before coating or painting [102]. Notably, the absence of flash rust in the pit area indicates that contaminants and chlorides were completely removed, even in the deeply corroded sections. During blast cleaning, even when no visible corrosion products are observed on the treated surface, flash rust can occur within a few hours at room temperature. According to related research, within 24 hours of blast cleaning, considerable localized rust was observed on the surface due to the residual corrosion products and chlorides [17]. However, in this study, localized corrosion was observed around the treated area 24 hours after AWT processing. This corrosion is presumed to be caused by aqueous contaminants, including corrosion products that came into contact with the treated area during the rinsing process after AWT processing. This type of corrosion appears in a band-like formation near the treated area and differs from corrosion caused by chlorides or corrosion products [17]. Therefore, this suggests the need to consider measures such as masking in future on-site applications of AWT processing on corroded structures to prevent the effects of corrosion in the target areas.

6.3.2 Comparison of mechanisms of surface treatment effects

Considering the surface characteristics and the effectiveness in removing corrosion products and chlorides, it can be summarized that using the divergent nozzle with garnet mesh size 80 as the abrasive is the ideal condition for achieving optimal AWT process results. Furthermore, this technology has been applied to actual corroded steel structures, demonstrating its effectiveness in removing corroded parts of steel and chlorides. The AWT processing, utilizing ultra-high-pressure water, successfully removed thick layers of rust and corrosion products from pitting areas hundreds of micrometers deep in a single treatment. The cleaning mechanism of AWT significantly differs from that of blasting. Figure 6-6(a) illustrates a schematic of the blasting mechanism, which, unlike AWT, removes target materials by sweeping or scraping the surface. As a result, as seen in Figure 6-6(b), a considerable amount of residual abrasive remains on the surface after blasting, and the removal of corrosion products beneath the steel surface is limited.

In contrast, AWT induces a water wedge effect due to the divergent flow of the jet, leading to the formation of small cracks on the surface and sides of the target material. This amplifies the crack surfaces, contributing to the removal of the material. Figure 6-7 displays

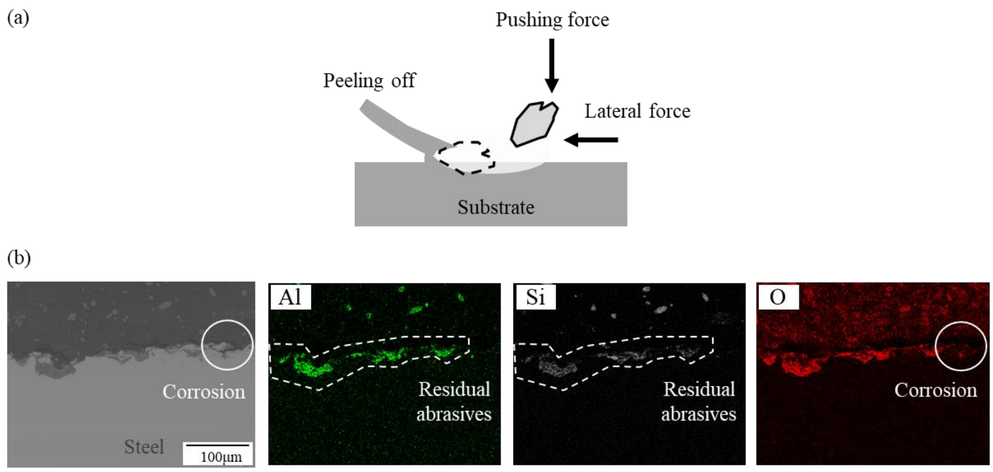

Figure 6-6 Impacts of blast treatment mechanisms: (a) Fundamentals of blasting and (b) After blasting the cross-sectional appearance of the steel plate.

the cross-section of a steel plate after AWT, showing the dense layers of corrosion formed in various directions. The high-pressure water jet, infused with abrasive particles during AWT, penetrates the rust layers directly, breaking them apart through the water wedge effect and completely removing the thick layers of rust remaining on the steel surface. Additionally, the abrasive particles, working in conjunction with the high-pressure water, penetrate beneath the steel surface, effectively removing corrosion products through erosion and cracking. As a result, there is no occurrence of flash rust due to residual corrosion productsand chlorides for 24 hours after treatment, maintaining a cleanliness level of Sa 3 or higher. Furthermore, as mentioned in Chapter 3 of this paper, it creates the most favorable surface characteristics for subsequent coating and demonstrates high efficiency in the removal of corrosion products.

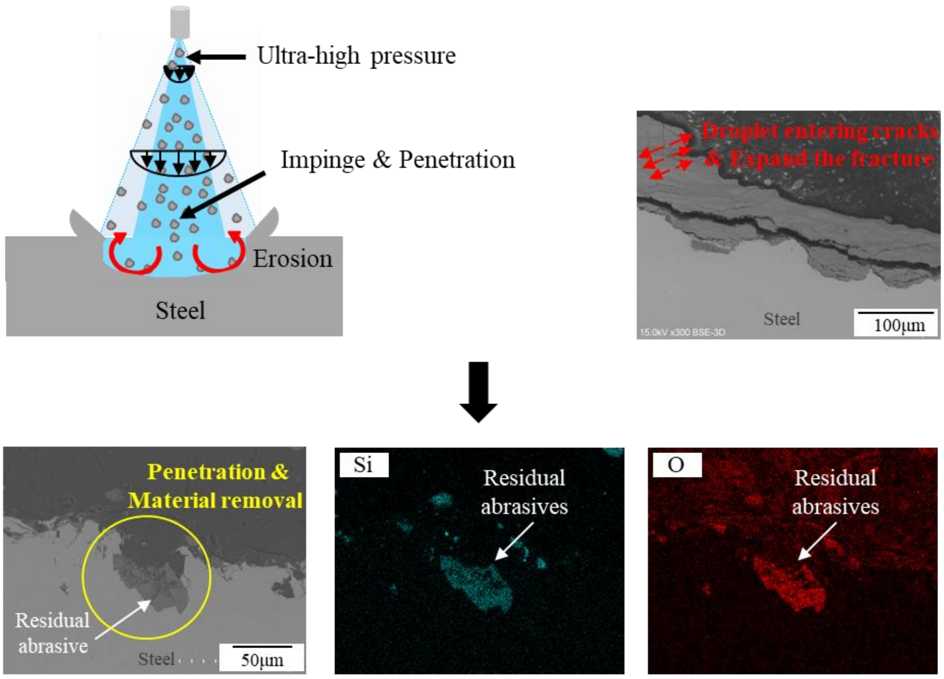

Figure 6-7 Principle of AWT polishing impact.

6.3.3 Quantitative assessment of steel surface quality under AWT conditions

Table 6-1 illustrates the impact of the treatment pressures on diverse surface properties and their effectiveness in removing corrosion and chloride. While most surface characteristics showed similar results regardless of different pressures, a notable difference was observed in the maximum erosion depth. Specifically, at the same standoff distance, a pressure of 230 MPa resulted in approximately 1.3 times deeper erosion than 180 MPa. This outcome is expected to enhance corrosion removal efficiency while maintaining erosion depths below 200 μm, thereby preventing stress concentration in epoxy adhesives and improving adhesive efficiency. In contrast, at 180 MPa, residual corrosion products and chlorides were still observed after AWT processing, indicating lower efficacy.

Table 6-2 presents the effects of varying abrasive supplies on surface characteristics and the efficacy of removing corrosion products and chlorides. With an abrasive supply of 600 g/min, the abrasive achieved up to 1.3 times wider treatment range compared to other conditions and demonstrated superior contaminant removal efficiency. While the maximum erosion depth and the amount of residual abrasives were consistent in most conditions, the surface roughness was approximately 1.3 times lower compared to other settings, resulting in a smoother surface.

Table 6-1 Various surface property values according to processing pressure.

Parameters	Pressure (MPa)*	
	180	230
Treatment range (mm)	44	45
Maximum erosion depth (μm)	97	158
Surface roughness, Ra (μm)	22	23
Residual abrasives, Area ratio of Si (%)	3.3	3.9
Observed residual corrosion product and chloride	Present	Absent

*(Constant conditions: Abrasive supply: 200 g/min, Standoff distance: 300 mm, Number of processing: one time)

Table 6-2 Various surface property values according to abrasive supply.

Parameters	Abrasive supply (g/min) *		
	200	400	600
Treatment range (mm)	45	50	60
Maximum erosion depth (μm)	197	176	193
Surface roughness, Ra (μm)	23	22	17
Residual abrasives, Area ratio of Si (%)	3.7	3.9	3.9
Observed residual corrosion product and chloride	Present		Absent

*(Constant conditions: Pressure: 230 MPa, Standoff distance: 300 mm, Number of processing: one time)

Table 6-3 Various surface property values according to processing counts.

Parameters	Processing counts (N)*	
	1	2
Treatment range (mm)	42	46
Maximum erosion depth (μm)	158	197
Surface roughness, Ra (μm)	22	23
Residual abrasives, Area ratio of Si (%)	3.3	3.9
Observed residual corrosion product and chloride	Absent	Absent

*(Constant conditions: Pressure: 230 MPa, Abrasive supply: 200 g/min, Standoff distance: 300 mm)

Table 6-3 shows the impact of treatment frequency on surface properties and the removal of corrosion products and chlorides. Reciprocating treatments led to about 1.3 times deeper erosion depths than single treatments, with this trend expected to become more marked with shorter treatment distances. Nevertheless, apart from the maximum erosion depth, other surface characteristics showed comparable outcomes to those from single treatments. Optimal surface characteristics for coating application include a wide treatment area and the prevention of excessive erosion depth and roughness. Additionally, the removal of corrosion products and chlorides is considered the most crucial element of surface treatment. From this perspective, within the scope of this study, the most effective AWT processing conditions were identified as a pressure of 230 MPa, an abrasive supply of 600 g/min, and a single treatment application.

Tables 6-4 to 6-11 extensively detail the range of surface characteristics formed under various AWT processing conditions, including nozzle type, standoff distance, and garnet variety. Table 6-4 displays the results of the treatment range based on these conditions. The range of treatment areas formed by a single AWT processing from 20 mm to 90 mm under different processing conditions, showcases the adaptability of the treatment across a broad spectrum. This indicates that AWT processing is capable of efficiently addressing corrosion products on structures of various scales, ranging from tight spaces to broad areas of steel bridges, in practical field applications.

Table 6-4 Treatment range by AWT processing conditions.

Treatment range (mm)	20~ 40	40~ 60	60~70	70~80	80~ 90
Nozzle types (Divergent/Convergent)	Convergent	Divergent/Convergent		Divergent	
Standoff distance (mm)	100	100/ 200/ 300		200/ 300	300
Garnet (#)			30-60/ 80		80

Table 6-5 Maximum erosion depth by AWT processing conditions.

Maximum erosion depth (μm)	100~ 200	200~ 300	300~ 400	500~
Nozzle types (Divergent/Convergent)		Divergent/ Convergent		Convergent
Standoff distance (mm)	300	200	100/ 200	100
Garnet (#)		30-60/ 80		

Table 6-5 presents the results of maximum erosion depths achieved under various conditions during AWT processing. The data indicate that maximum erosion depths of up to 400 μm can be attained by adjusting various nozzle types, standoff distances, and garnet varieties. in contrast, erosion depths exceeding 500 μm were only achieved using the convergent nozzle at a standoff distance of 100 mm. These findings suggest that AWT can effectively remove the majority of corrosion products and chlorides under all conditions.

The practical application of AWT is expected to be versatile enough to cater to structures located in high positions or varying terrains and settings. Furthermore, the utilization of the convergent nozzle is anticipated to be effective in efficiently removing thick layers of rust, extending to several tens of millimeters.

Table 6-6 provides the results of surface roughness, Rzjis, achieved under various AWT processing conditions. The surface roughness values, ranging from 60 to 100μm for the single treatment under various conditions, are expected to meet the quality standards required in various industrial sectors. For instance, while Japanese steel bridge repainting works necessitate an Rzjis value below 75μm, heavy industries, and machinery manufacturing that require increased friction or enhanced mechanical properties may demand higher levels of roughness. Additionally, fields requiring strengthened mechanical bonding, such as specialized coatings or the emerging area of composite materials like fiber-reinforced polymer (FRP), may also find higher roughness levels advantageous. Hence, these research outcomes are not limited to specific industrial sectors but can be applicable across various industries that require a range of roughness levels. By further refining and

Table 6-6 Surface roughness by AWT processing conditions.

Surface roughness, Rzjis (μm)	60~ 75	75~ 90	90~100
Garnet (#)	80	30-60	
Nozzle types (Divergent/Convergent)	Divergent		Convergent
Standoff distance (mm)	100/ 200/ 300		

Table 6-7 Surface deformation ratio by AWT processing conditions.

Deformation ratio (DR)	1~ 2	2~ 3	3~ 3.5	3.5~ 4.5
Garnet (#)	-	-	80	30-60
*Nozzle types (Divergent/Convergent)	-	-	Divergent	
Standoff distance (mm)	100/ 200 /300			

*Measurements for the convergent nozzle are excluded since Rzjis significantly exceeds 75μm.

diversifying the processing conditions and integrating them into robotic automation and AI systems, it is expected that a consistent range of surface roughness values can be obtained.

Table 6-7 displays the results of surface deformation ratio (DR) under various conditions. This study focused on surface conditions prior to repainting steel bridges, and therefore, surfaces treated with the convergent nozzle exceeding an Rzjis of 75μm were excluded from DR and adhesion analysis. During AWT processing at varying standoff distances, the DR exhibited a consistent range depending on the type of garnet used. Notably, larger particle sizes showed a tendency to increase DR values. While most material surface quality management relies on evaluating micro-scale roughness values, DR extends beyond mere roughness, enabling an interpretation of macroscopic changes in surface morphology. Consequently, DR will be a critical determinant in establishing the appropriateness of surface preparation before painting.

Table 6-8 shows the adhesion strength results between steel surfaces treated under various conditions and epoxy adhesives, also indicating the ranges of roughness and DR that yield optimal adhesion. Under identical treatment conditions, a garnet mesh size of 80 displayed about 1.3 times higher adhesion compared to 30/60 during AWT processing. The ranges for maximum adhesion in terms of roughness and DR, as presented in Tables 6-6 and 6-7, were 60-75μm and 3-3.5, respectively, with a noted decrease in adhesive strength for values exceeding these ranges. This indicates that beyond certain levels of roughness and surface morphology changes, the adhesion to the adhesive diminishes. Furthermore, according to this study, under all AWT conditions, the adhesive strength between steel plates and epoxy adhesive was over 7MPa, satisfying the minimum requirement of 5MPa for the adhesive strength between paint and steel surfaces in coated steel structures as per ISO 12944. This suggests effective protection against corrosion and environmental factors due to the

Table 6-8 Adhesion strength by AWT processing conditions.

Adhesion strength (MPa)	7~ 9	9~ 12
Garnet (#)	30-60	80
*Nozzle types (Divergent/Convergent)	Divergent	
Standoff distance (mm)	100/ 200/ 300	

*Measurements for the convergent nozzle are excluded since Rzjis significantly exceeds 75μm.

Table 6-9 Residual abrasive quantities by AWT processing conditions.

Area ratio of Si (%)	< 4
Nozzle types (Divergent/Convergent)	All types
Garnet (#)	All types
Standoff distance (mm)	100/ 200/ 300

strong bonding of the coating to the steel surface. However, as the adhesion strengths reported in this study are between adhesives and steel surfaces, not coatings, future research will analyze actual coating application results to ascertain a more accurate relationship between surface properties and paint adhesion.

Table 6-9 provides the distribution levels of residual abrasive material on steel surfaces under various AWT processing conditions. The analysis, focusing on the area ratio of silicon (Si), a primary component of garnet, revealed that all AWT processing conditions resulted in less than 4% area ratio of residual abrasives. This indicates that AWT technology can reduce the quantity of residual abrasives to less than one-third compared to traditional blasting techniques, thereby minimizing potential damage and impact on the steel surface from the abrasive materials themselves. Additionally, the consistency in the amount of residual abrasive material enables a more precise analysis of its correlation with surface roughness, topography, and the adhesion properties of epoxy adhesives.

Table 6-10 details the corrosion rates of steel plates subjected to various AWT processing conditions. The corrosion rates observed across all treatment conditions were less than 0.15mm per year, indicating an exceptionally low rate in terms of long-term use and durability of steel plates. However, as noted in Section 4.3.4, a micro-scale analysis revealed that under conditions with a standoff distance of less than 200mm and the use of the convergent nozzle, the corrosion rate was up to 1.7 times lower compared to other conditions. This reduction in corrosion rate is attributed to the formation of a hardened surface layer with plastic deformation and residual compressive stress from the AWT processing, enhancing the material's resistance to corrosion. Such outcomes suggest that the application of this treatment on areas of bridges under tension, such as cables and bolt connections, can extend the material's fatigue life and enhance its corrosion resistance through effective

Table 6-10 Corrosion rate by AWT processing conditions.

Corrosion rate (mm/yr)	< 0.15
Nozzle types (Divergent/Convergent)	All types
Garnet (#)	All types
Standoff distance (mm)	100/ 200/ 300

Table 6-11 Corrosion removal efficiency by AWT processing conditions.

Surface salinity (mg/m^2)	< 15
Nozzle types (Divergent/Convergent)	All types
Garnet (#)	All types
Standoff distance (mm)	100/ 200/ 300

corrosion removal and the peening effect. Therefore, this technology is also projected to extend its application to various industries beyond civil engineering, including aerospace, automotive, marine oceanic, and rail industries, where durability and high strength are essential requirements.

Table 6-11 illustrates the levels of chloride on steel surfaces after AWT processing under various conditions, with chloride concentrations remaining below 15mg/m^2 in all scenarios. This result meets the surface chloride standards required in diverse fields such as Japanese road bridges, the U.S. Navy [99], and NASA [100] underscoring the capability of AWT processing to fulfill a range of surface treatment specifications. This study confirms the potential of AWT processing to enhance various surface characteristics of steel plates, effectively removing corrosion and chloride, thus making it applicable in numerous industrial sectors. However, the current research did not extensively evaluate the effects of surface treatment on the tensile and yield strength, fatigue, and other durability aspects of steel plates. Particularly, the impact of the maximum erosion depth resulting from AWT processing on the durability of steel plates is a critical consideration. Future research will focus on quantitatively assessing the influence of surface characteristics on the mechanical and physical properties of steel treated with AWT.

6.4 Summary

Chapter 6 reveals that AWT processing under various operational conditions consistently manifests reproducible surface properties and provides broad-scope values of treatment range, maximum erosion depth, and surface roughness. Moreover, it significantly reduces the chloride content on the surfaces of structural steel components. This meets the criteria set by the Japanese anti-corrosion painting manual and other international standards, proving its effectiveness in surface preparation for diverse industrial applications ranging from naval vessels to NASA space missions. The superior efficiency of AWT in removing chlorides and corrosion products is further substantiated through the analysis of pitting corrosion areas or deepest corroded parts. Maintaining a cleanliness level above Sa 3 without flash rust even after 24 hours post-treatment emphasizes its potential applicability in various industries, including bridge construction, maritime, and aerospace sectors.

The key findings of this chapter are as follows:

1) AWT processing can be flexibly adjusted to meet specific treatment requirements, allowing its application even in challenging conditions such as elevated or confined spaces. Furthermore, when applied to corroded steel plate, it was able to maintain surface chloride levels below 20 mg/m^2, while simultaneously achieving surface treatment conditions of Sa 3 or higher as per ISO 8501-1.
2) AWT processing effectively eliminated corrosion products and chlorides to a depth of several hundred micrometers, while preserving a surface condition of Sa3 or higher for a continuous 24-hour period following treatment, with no incidence of flash rust, consistent with the condition immediately after treatment.
3) AWT processing exhibits reproducibility in achieving specific consistent surface properties under varying conditions, offering wide scope values of the treatment range, maximum erosion depth, and surface roughness. This demonstrates its applicability in diverse industrial sectors such as bridge construction, maritime, and aerospace industries.

CHAPTER 7 CONCLUSIONS AND FUTURE WORK

7.1 Summary and conclusions

Corrosion is an inevitable phenomenon in steel structures, with the degree of corrosion varying depending on the atmospheric conditions, material of the structure, and corrosion prevention methods employed. Consequently, effective corrosion cleaning is a crucial procedure for maintaining steel structures. Although various surface treatment methods have been proposed and used, the diversity of standards and specifications, along with the reliance on the experience and subjective judgment of field engineers, leads to the incompleteness of surface treatment. This can result in incomplete rust removal and subsequent corrosion after painting, especially in cases of severe corrosion. This paper highlights the limitations of traditional blast cleaning methods and discusses the effectiveness of a new surface treatment method, AWT processing.

Chapter 2 of this dissertation presents the potential of surface treatment using AWT and discusses its effectiveness under appropriate conditions. Chapter 3 delves into a thorough analysis of the relationship between the surface properties of AWT-processed steel plates and the adhesive strength of epoxy adhesives. In Chapter 4, the changes in mechanical properties and the impact on corrosion resistance of AWT-processed steel are examined. Chapter 5 evaluates the efficiency of removing corrosion products and chlorides when applying AWT to severely corroded steel members. Finally, Chapter 6 verifies the cleaning effect of applying a portable AWT device to an actual corroded bridge member and investigates the reproducibility of achieving consistent surface properties under various conditions during treatment.

In conclusion, AWT has demonstrated its potential as an effective method for corrosion cleaning, especially showing outstanding performance in treating severely corroded structures. This study has drawn the following conclusions to propose a new methodology for the maintenance and long-term durability enhancement of corroded steel structures.

1) AWT processing achieved a surface state of Sa3 or higher with a single treatment, effectively removing most corrosion contaminants and chlorides. Considering the surface properties of steel such as treatment range, maximum erosion depth, surface

roughness, and residual abrasive quantity, this study proposes AWT processing conditions of 230 MPa pressure, 600 g/min abrasive supply, and single treatment as an effective surface treatment method.

2) Using AWT processing with the divergent nozzle and smaller abrasive particles can mitigate the issues of limited treatment range, excessive roughness, and deep erosion depth seen with the convergent nozzle. AWT processing leaves much less residual abrasive on the steel surface compared to blast processing. The difference in the amount of residual abrasive under various AWT processing conditions is minimal. Among the surface properties of the treated steel, the surface deformation ratio has the highest correlation with the tensile adhesion strength of the epoxy adhesive. Additionally, there exists an optimal surface property for maximum adhesion between the substrate and the epoxy, where the surface deformation ratio and roughness are within the deformation range of 80-100 μm, DR is 3-3.5, and roughness (Rzjis) is estimated to be less than 75 μm.
3) Steel plates treated with AWT showed increased surface roughness, hardness, and microstructural changes compared to those treated with blasting, particularly when the convergent nozzle was used and the stand-off distance was reduced, enhancing these properties and resulting in heightened plastic deformation and hardness. These changes contributed to improved corrosion resistance through surface hardening and microstructural alterations, and AWT processing with the convergent nozzle demonstrated better corrosion resistance compared to using the divergent nozzle and blast treatment.
4) AWT processing effectively removes corrosion products and chlorides compared to blast treatment, reducing the processing time required to achieve the cleanliness level of ISO 8501-1 Sa 3 by one-third. Additionally, it suppresses the occurrence of flash rust for up to 72 hours, preventing re-corrosion. These results align with Japan's civil bridge construction standards for painting and are expected to provide economic benefits by eliminating the need for repeated treatments.
5) AWT processing can reproduce consistent surface properties under various treatment conditions, providing a wide range of values for treatment range, maximum erosion

depth, and surface roughness to be expected to satisfy the surface conditions required in diverse industrial sectors. Additionally, this technology significantly reduces the corrosion products and chloride content in structural steel components. This meets the criteria of Japan's anti-corrosion painting manual and other international standards, proving its effectiveness in surface preparation for a variety of industries, from naval ships to NASA space missions. The surface state maintains a cleanliness level of Sa 3 or higher and prevents the occurrence of flash rust even 24 hours after treatment.

7.2 Recommendation for future work

This dissertation utilizes AWT as a surface treatment technology to generate various surface properties of steel and presents its application scope and efficacy. By applying this technology to severely corroded steel structures, its engineering applicability and practicality are verified. However, the current research still implies potential for development, suggesting the need for further studies in the future.

1) Future work should investigate the impact of surface characteristics of AWT-processed steel plates on the adhesion of coatings applied subsequently. While this study focused on the relationship between surface characteristics and the adhesion of epoxy adhesives following AWT processing under various conditions, it is crucial for practical application to examine the adhesion between treated surfaces and coatings after coating application, and to establish quantitative evaluation criteria for suitable surface conditions prior to painting.
2) Evaluating the durability and corrosion resistance of coatings applied to severely corroded steel structures treated with AWT is essential. This study demonstrated the effective removal of corrosion products and salts from corroded test specimens and components using AWT, particularly proving the absence of flash rust for up to 72 hours during the turning test. However, this research did not examine the deterioration of coatings after surface treatment and painting. Therefore, it is necessary to paint and coat AWT-processed surfaces and then assess the long-term degradation of the coatings through accelerated corrosion tests and atmospheric exposure tests. This will allow for a more detailed examination of corrosion beneath

the coating, as well as its durability and corrosion resistance.

3) In addition to evaluating the efficiency of removing corrosion product and chloride from corroded member surfaces through AWT processing, it is also necessary to assess whether sufficient quality can be ensured in narrow spaces and gaps between members, such as tight areas and areas adjacent to bolts, where surface treatment of structures is challenging.
4) The application of AWT on steel induces a multitude of surface characteristics. This study assessed the surface attributes post-AWT processing on the carbon steel, considering factors such as treatment range, maximum erosion depth, surface roughness, alterations in surface topography, and the distribution of residual abrasives. However, for broader industrial application of this technology, it is imperative to evaluate the surface characteristics that emerge when this technology is applied to a diverse array of materials, including aluminum alloy, in addition to conventional steel. Furthermore, there is a requirement for an expanded assessment of surface characteristics to ascertain the material's durability, extending beyond the surface properties addressed in this research.
5) Future research will focus on developing a capability to adjust the treatment distance between the laser tool and the target material during AWT processing. This will facilitate the application of the quality achieved in the laboratory of AWT to actual structures by establishing precise rules for controlling distance and angles.

REFERENCE

[1] G. Madhavan, C.E. Phelps, R.R. Colwell, R. Rappuoli, H. V. Fineberg, In plain view: A transparent systems approach for enhancing health policy decisions, Bridge. 46 (2016) 5–10.

[2] P. R. Roberge, and P. Eng, Corrosion engineering. Principles and practice, (2005) 1.

[3] Z. Ahmad, Principles of corrosion engineering and corrosion control. Elsevier, (2006).

[4] P.P. Deshpande, N.G. Jadhav, V.J. Gelling, D. Sazou, Conducting polymers for corrosion protection: A review, J. Coatings Technol. Res. 11 (2014) 473–494. https://doi.org/10.1007/s11998-014-9586-7.

[5] M.F. Montemor, Functional and smart coatings for corrosion protection: A review ofrecent advances, Surf. Coatings Technol. 258 (2014) 17–37. https://doi.org/10.1016/j.surfcoat.2014.06.031.

[6] S. Guo, R. Si, Q. Dai, Z. You, Y. Ma, J. Wang, A critical review of corrosion development and rust removal techniques on the structural/environmental performance of corroded steel bridges, J. Clean. Prod. 233 (2019) 126–146. https://doi.org/10.1016/j.jclepro.2019.06.023.

[7] 藤原博, 田原芳雄, 鋼橋塗装の長期防食性能の評価に関する研究, 土木学会論文集. 570 (1997) 129–140.

[8] 日本道路協会. 鋼道路橋塗装・防食便覧 (2005).

[9] A.W. Momber, W.D. Greverath, Surface preparation standards for steel substrates - A critical review, J. Prot. Coatings Linings. 21 (2004) 48–52.

[10] A. Rudawska, I. Danczak, M. Müller, P. Valasek, The effect of sandblasting on surface properties for adhesion, Int. J. Adhes. Adhes. 70 (2016) 176–190. https://doi.org/10.1016/j.ijadhadh.2016.06.010.

[11] W. Funke, Blistering of paint films and filiform corrosion, Prog. Org. Coatings. 9 (1981) 29–46. https://doi.org/10.1016/0033-0655(81)80014-3.

[12] D. Hansel, Abrasive blasting systems, Met. Finish. 97 (1999) 29–55. https://doi.org/10.1016/s0026-0576(99)80758-2.

[13] M. Gadge, G. Lohar, S. Chinchanikar, A review on micro-blasting as surface treatment

technique for improved cutting tool performance, Mater. Today Proc. 64 (2022) 725–730. https://doi.org/10.1016/j.matpr.2022.05.196.

[14] N.L. Tshimanga, G.A. Combrink, M.W. Kalenga, Surface morphology characterization of grade 304L stainless steel after abrasive blasting, Mater. Today Proc. 38 (2021) 544–548. https://doi.org/10.1016/j.matpr.2020.02.397.

[15] A. Kim, S. Kainuma, M. Yang, Surface characteristics and corrosion behavior of carbon steel treated by abrasive blasting, Metals (Basel). 11 (2021). https://doi.org/10.3390/met11122065.

[16] Albrecht, P., & Simon, S. Fatigue notch factors for structural details. Journal of the Structural Division, 107(7), (1981) 1279-1296.

[17] S. KAINUMA, Steel Surface Preparation by Abrasive Blast Treatment in Existing Steel Road Bridges, J. Surf. Finish. Soc. Japan. 72 (2021) 12–16. https://doi.org/10.4139/sfj.72.12.

[18] Y. Natarajan, P.K. Murugesan, M. Mohan, S.A. Liyakath Ali Khan, Abrasive Water Jet Machining process: A state of art of review, J. Manuf. Process. 49 (2020) 271–322. https://doi.org/10.1016/j.jmapro.2019.11.030.

[19] F. Li, Experimental and numerical investigation of abrasive waterjet polishing technology, Public Health. (2007) 125.

[20] H.T. Zhu, C.Z. Huang, J. Wang, Q.L. Li, C.L. Che, Experimental study on abrasive waterjet polishing for hard-brittle materials, Int. J. Mach. Tools Manuf. 49 (2009) 569–578. https://doi.org/10.1016/j.ijmachtools.2009.02.005.

[21] S. Park，S. Kainuma，T. Ikeda，T. Asano and Y. Morita, Characterizing Steel Surface Features Affected by Abrasive Waterjet Treatment, 鋼構造年次論文報告集. 29 (2021) 585-592.

[22] S.H. PARK, S. KAINUMA, T. IKEDA, Y. TOYOTA, Y. MORITA, Effect of Surface Characteristics of Abrasive Water-jet Treatment on Corrosion Behavior of Carbon Steel, Zairyo-to-Kankyo. 72 (2023) 169–178. https://doi.org/10.3323/jcorr.72.169.

[23] M. Morcillo, J.M. Bastidas, J. Simancas, J.C. Galvan, The effect of the abrasive work mix on paint performance over blasted steel, Anti-Corrosion Methods Mater. 36 (1989) 4–8. https://doi.org/10.1108/eb020755.

[24] A. Perec, Research into the disintegration of abrasive materials in the abrasive water jet machining process, Materials (Basel). 14 (2021). https://doi.org/10.3390/ma14143940.

[25] A. Perec, Disintegration and recycling possibility of selected abrasives for waterjet cutting, DYNA. 84 (2017) 249–256. https://doi.org/10.15446/dyna.v84n203.62592.

[26] V.B. Nguyen, Q.B. Nguyen, Y.W. Zhang, C.Y.H. Lim, B.C. Khoo, Effect of particle size on erosion characteristics, Wear. 348–349 (2016) 126–137. https://doi.org/10.1016/j.wear.2015.12.003.

[27] L. D. Vincent, Surface preparation standards, NACE CORROSION. (2001) NACE-01659.

[28] 上野和夫， 桑嶋孝幸，溶射産業規格の歴史と現状．日本溶射学会誌 溶射，60(1) (2023) 42-44.

[29] M. Shaw, M. Fairchild, Evaluating the 1931 CIE color-matching functions, Color Res. Appl. 27 (2002) 316–329. https://doi.org/10.1002/col.10077.

[30] FHW, A. Technology Team (1997).

[31] K. Kambham, S. Sangameswaran, S.R. Datar, B. Kura, Copper slag: optimization of productivity and consumption for cleaner production in dry abrasive blasting, J. Clean. Prod. 15 (2007) 465–473. https://doi.org/10.1016/j.jclepro.2005.11.024.

[32] S. Zhuang, S. Kainuma, M. Yang, M. Haraguchi, T. Asano, Investigation on the peak temperature and surface defects on the carbon steel treated by rotating CW laser, Opt. Laser Technol. 135 (2021) 106727. https://doi.org/10.1016/j.optlastec.2020.106727.

[33] S.J. Kim, M. Okido, K.M. Moon, An electrochemical study of cathodic protection of steel used for marine structures, Korean J. Chem. Eng. 20 (2003) 560–565. https://doi.org/10.1007/BF02705566.

[34] M. Regel-Rosocka, A review on methods of regeneration of spent pickling solutions from steel processing, J. Hazard. Mater. 177 (2010) 57–69. https://doi.org/10.1016/j.jhazmat.2009.12.043.

[35] S.A. Jafar, A.A. Aabid, J.I. Humadi, Corrosion behavior of carbon steel in 1 M, 2 M, and 3 M HCl solutions, Mater. Today Proc. 57 (2022) 412–417. https://doi.org/10.1016/j.matpr.2021.12.295.

[36] A. Raj Sharma, H.S. Arora, H.S. Grewal, Nano sponge like metal-based coating with self-regenerative superhydrophobicity using simple flame spraying, Mater. Lett. 334 (2023) 133709. https://doi.org/10.1016/j.matlet.2022.133709.

[37] H. Lais, P.S. Lowe, J. Kanfoud, T.H. Gan, Advancements in fouling removal using high power ultrasonics for industrial applications, 2017 IEEE Int. Conf. Ind. Inf. Syst. ICIIS 2017 - Proc. 2018-Janua (2017) 1–6. https://doi.org/10.1109/ICIINFS.2017.8300357.

[38] S. Wang, Z. Ye, G. Pu, J. Liu, L. Yang, W. Jing, M. Yu, F. Yang, Y. Peng, F. Gou, J. Wei, In-situ non-destructive removal of tin particles by low-energy plasma for imitation of EUV optical mirrors self-cleaning, Vacuum. 212 (2023) 111963. https://doi.org/10.1016/j.vacuum.2023.111963.

[39] A. Momber, Blast cleaning technology. Springer Science & Business Media (2007).

[40] M.B. Islam, M. Islam, S.U. Islam, Facile fabrication of abrasive materials for sandpaper from waste materials, Clean. Waste Syst. 4 (2023) 100066. https://doi.org/10.1016/j.clwas.2022.100066.

[41] D.K. Liu, G. Dissayanake, P.B. Manamperi, P.A. Brooks, G. Fang, G. Paul, S. Webb, N. Kirchner, P. Chotiprayanakul, N.M. Kwok, T.R. Ren, A robotic system for steel bridge maintenance: Research challenges and system design, Proc. 2008 Australas. Conf. Robot. Autom. ACRA 2008. (2008).

[42] K. Subramani, A. Vasudevan, K. Karthik, S. Kolappan, Insights of abrasive water jet polishing process characteristics and its advancements, Mater. Today Proc. (2021). https://doi.org/10.1016/j.matpr.2021.11.005.

[43] A. W. Momber, R. Kovacevic, Principles of abrasive water jet machining. Springer Science & Business Media (2012).

[44] S. Kainuma, Challenges and new techniques in surface preparation of existing steel structures, The 43rd corrosion and rust prevention technology presentation conference, Japan Association of Corrosion Control (2023).

[45] N.P. Singh, D.S. Srinivasu, N.R. Babu, Thermal Analysis of Abrasive Waterjet Machining Process, (n.d.) 31–34.

[46] B. Simon, Dissolution rates of NaCl and KCl in aqueous solution, J. Cryst. Growth. 52 (1981) 789–794. https://doi.org/10.1016/0022-0248(81)90377-8.

[47] W. Funke, Problems and progress in organic coatings science and technology, Prog. Org. Coatings. 31 (1997) 5–9. https://doi.org/10.1016/S0300-9440(97)00013-1.

[48] B.J. Griffiths, D.T. Gawne, G. Dong, A definition of the topography of grit-blasted surfaces for plasma sprayed alumina coatings, J. Manuf. Sci. Eng. Trans. ASME. 121 (1999) 49–53. https://doi.org/10.1115/1.2830574.

[49] G.D. Davis, Surface treatments of selected materials, 2018. https://doi.org/10.1007/978-3-319-55411-2_8.

[50] H. Wei, J. Xia, W. Zhou, L. Zhou, G. Hussain, Q. Li, K. (Ken) Ostrikov, Adhesion and cohesion of epoxy-based industrial composite coatings, Compos. Part B Eng. 193 (2020) 108035. https://doi.org/10.1016/j.compositesb.2020.108035.

[51] S. Amada, A. Satoh, Fractal analysis of surfaces roughened by grit blasting, J. Adhes. Sci. Technol. 14 (2000) 27–41. https://doi.org/10.1163/15685610074209

[52] （一財）日本工業規格：JIS K 5600「塗料一般試験方法−第 5 部：塗膜の機械的性質− 第 7 節：付着性（プルオフ法)」, (2014).

[53] K. Words, NaCl による高腐食性環境における Al-5Mg 合金 溶射皮膜の耐食 ・ 防食特性に関する基礎的研究, 72 (2016) 440–452.

[54] C.L. Che, C.Z. Huang, J. Wang, H.T. Zhu, Study of abrasive water jet polishing technology, Key Eng. Mater. 487 (2011) 327–331. https://doi.org/10.4028/www.scientific.net/KEM.487.327.

[55] P. Nystedt, Arc length of function graphs via Taylor’s formula, Int. J. Math. Educ. Sci. Technol. 52 (2021) 310–323. https://doi.org/10.1080/0020739X.2020.1751320.

[56] R. Kromer, S. Costil, J. Cormier, D. Courapied, L. Berthe, P. Peyre, M. Boustie, Laser surface patterning to enhance adhesion of plasma sprayed coatings, Surf. Coatings Technol. 278 (2015) 171–182. https://doi.org/10.1016/j.surfcoat.2015.07.022.

[57] A. Rivero, A. Alberdi, T. Artaza, L. Mendia, A. Lamikiz, Surface properties and fatigue failure analysis of alloy 718 surfaces milled by abrasive and plain waterjet, Int. J. Adv. Manuf. Technol. 94 (2018) 2929–2938. https://doi.org/10.1007/s00170-017-0979-5.

[58] A. Da Cunha Rocha, Á.V. Do Nascimento, I.C.P. Margarit-Mattos, K. Dos Santos Assis, O.R. Mattos, Abrasive blasting contamination in super duplex and carbon steels -A quantification approach by rietveld analysis, Mater. Res. 17 (2014) 1356–1366. https://doi.org/10.1590/1516-1439.313514.

[59] C.H.M. Hagen, The effect of surface roughness and topography on the organic coating/steel interface stability Doctoral thesis, (2020).

[60] M. Srivastava, R. Tripathi, S. Hloch, S. Chattopadhyaya, A.R. Dixit, Potential of using water jet peening as a surface treatment process for welded joints, Procedia Eng. 149 (2016) 472–480. https://doi.org/10.1016/j.proeng.2016.06.694.

[61] T. Wang, J. Yu, B. Dong, Surface nanocrystallization induced by shot peening and its effect on corrosion resistance of 1Cr18Ni9Ti stainless steel, Surf. Coatings Technol. 200 (2006) 4777–4781. https://doi.org/10.1016/j.surfcoat.2005.04.046.

[62] L. Ding, H. Torbati-Sarraf, A. Poursaee, The influence of the sandblasting as a surface mechanical attrition treatment on the electrochemical behavior of carbon steel in different pH solutions, Surf. Coatings Technol. 352 (2018) 112–119. https://doi.org/10.1016/j.surfcoat.2018.08.013.

[63] Davis, J. R. (Ed.), Corrosion: Understanding the basics. Asm International (2000).

[64] W.B. Lee, K.T. Cho, K.H. Kim, K.I. Moon, Y. Lee, The effect of the cementite phase on the surface hardening of carbon steels by shot peening, Mater. Sci. Eng. A. 527 (2010) 5852–5857. https://doi.org/10.1016/j.msea.2010.05.083.

[65] P. Sanjurjo, C. Rodrguez, I.F. Pariente, F.J. Belzunce, A.F. Canteli, The influence of shot peening on the fatigue behaviour of duplex stainless steels, Procedia Eng. 2 (2010) 1539–1546. https://doi.org/10.1016/j.proeng.2010.03.166.

[66] A. Azhari, S. Sulaiman, A.K.P. Rao, A review on the application of peening processes for surface treatment, IOP Conf. Ser. Mater. Sci. Eng. 114 (2016). https://doi.org/10.1088/1757-899X/114/1/012002.

[67] J. Zhang, X. Dong, Y. Zhou, J. Liu, Surface derusting of rust-covered metallic surface via shot blasting: A smoothed particle hydrodynamics simulation, Wear. 514–515 (2023) 204566. https://doi.org/10.1016/j.wear.2022.204566.

[68] M. Mieszala, P.L. Torrubia, D.A. Axinte, J.J. Schwiedrzik, Y. Guo, S. Mischler, J. Michler, L. Philippe, Erosion mechanisms during abrasive waterjet machining: Model microstructures and single particle experiments, J. Mater. Process. Technol. 247 (2017) 92–102. https://doi.org/10.1016/j.jmatprotec.2017.04.003.

[69] S.M. Hassani-Gangaraj, A. Moridi, M. Guagliano, A. Ghidini, Nitriding duration reduction without sacrificing mechanical characteristics and fatigue behavior: The beneficial effect of surface nano-crystallization by prior severe shot peening, Mater. Des. 55 (2014) 492–498. https://doi.org/10.1016/j.matdes.2013.10.015.

[70] H. Kovacı, Y.B. Bozkurt, A.F. Yetim, M. Aslan, A. Çelik, The effect of surface plastic deformation produced by shot peening on corrosion behavior of a low-alloy steel, Surf.

Coatings Technol. 360 (2019) 78–86. https://doi.org/10.1016/j.surfcoat.2019.01.003.

[71] M. Srivastava, S. Hloch, R. Tripathi, D. Kozak, S. Chattopadhyaya, A.R. Dixit, J. Foldyna, P. Hvizdos, M. Fides, P. Adamcik, Ultrasonically generated pulsed water jet peening of austenitic stainless-steel surfaces, J. Manuf. Process. 32 (2018) 455–468. https://doi.org/10.1016/j.jmapro.2018.03.016.

[72] J. Foldyna, L. Sitek, J. Ščučka, P. Martinec, J. Valíček, K. Páleníková, Effects of pulsating water jet impact on aluminium surface, J. Mater. Process. Technol. 209 (2009) 6174–6180. https://doi.org/10.1016/j.jmatprotec.2009.06.004.

[73] S.M. Hassani-Gangaraj, A. Moridi, M. Guagliano, A. Ghidini, M. Boniardi, The effect of nitriding, severe shot peening and their combination on the fatigue behavior and micro-structure of a low-alloy steel, Int. J. Fatigue. 62 (2014) 67–76. https://doi.org/10.1016/j.ijfatigue.2013.04.017.

[74] I. Fernández Pariente, M. Guagliano, About the role of residual stresses and surface work hardening on fatigue ΔKth of a nitrided and shot peened low-alloy steel, Surf. Coatings Technol. 202 (2008) 3072–3080. https://doi.org/10.1016/j.surfcoat.2007.11.015.

[75] T.R. Gupta, S.S. Sidhu, J.K. Katiyar, H.S. Payal, Measurements of lattice strain in cold-rolled CR4 steel sheets using X-ray diffraction, Mater. Sci. Eng. B Solid-State Mater. Adv. Technol. 264 (2021) 114930. https://doi.org/10.1016/j.mseb.2020.114930.

[76] C. Liu, H. Zheng, X. Gu, B. Jiang, J. Liang, Effect of severe shot peening on corrosion behavior of AZ31 and AZ91 magnesium alloys, J. Alloys Compd. 770 (2019) 500–506. https://doi.org/10.1016/j.jallcom.2018.08.141.

[77] X. Chen, C. Zhang, G.L. Song, D. Zheng, Y. Guo, X. Huang, Electrochemical activity and damage of single carbon fiber, Materials (Basel). 14 (2021) 1–20. https://doi.org/10.3390/ma14071758.

[78] L. Abosrra, A.F. Ashour, S.C. Mitchell, M. Youseffi, Corrosion of mild steel and 316L austenitic stainless steel with different surface roughness in sodium chloride saline solutions, WIT Trans. Eng. Sci. 65 (2009) 161–172. https://doi.org/10.2495/ECOR090161.

[79] L.R. Hilbert, D. Bagge-Ravn, J. Kold, L. Gram, Influence of surface roughness of stainless steel on microbial adhesion and corrosion resistance, Int. Biodeterior. Biodegrad. 52 (2003) 175–185. https://doi.org/10.1016/S0964-8305(03)00104-5.

[80] K. Sasaki, G.T. Burstein, The generation of surface roughness during slurry erosion-corrosion and its effect on the pitting potential, Corros. Sci. 38 (1996) 2111–2120. https://doi.org/10.1016/S0010-938X(96)00066-2.

[81] A. Toloei, V. Stoilov, D. Northwood, The relationship between surface roughness and corrosion, ASME Int. Mech. Eng. Congr. Expo. Proc. 2 B (2013). https://doi.org/10.1115/IMECE2013-65498.

[82] J. K. Saha, Corrosion of constructional steels in marine and industrial environment: frontier work in atmospheric corrosion. Springer Science & Business Media (2012).

[83] S. He, Z. Wang, J. Hu, J. Zhu, L. Wei, Z. Chen, Formation of superhydrophobic micro-nanostructured iron oxide for corrosion protection of N80 steel, Mater. Des. 160 (2018) 84–94. https://doi.org/10.1016/j.matdes.2018.09.002.

[84] X. Lu, Y. Li, P. Ju, Y. Chen, J. Yang, K. Qian, T. Zhang, F. Wang, Unveiling the inhibition mechanism of an effective inhibitor for AZ91 Mg alloy, Corros. Sci. 148 (2019) 264–271. https://doi.org/10.1016/j.corsci.2018.12.025.

[85] C. Han, Z. Li, X. Yang, J. Wang, Corrosion behavior and mechanical performance of weathering steel in industrial and rural atmospheric environments, Constr. Build. Mater. 411 (2024) 134284. https://doi.org/10.1016/j.conbuildmat.2023.134284.

[86] J. Bhandari, F. Khan, R. Abbassi, V. Garaniya, R. Ojeda, Modelling of pitting corrosion in marine and offshore steel structures - A technical review, J. Loss Prev. Process Ind. 37 (2015) 39–62. https://doi.org/10.1016/j.jlp.2015.06.008.

[87] Japan society of civil engineers (JSCE), Issues and Countermeasures for Recovering Anticorrosion Performance of Steel Structures in Atmospheric Environment, Maruzen, (2019).

[88] S. Kainuma, Y. Yamamoto, H. Hayashi, Y. Itoh, Practical method for estimating corrosion depth of uncoated carbon steel using thickness of the corrosion-product layer, Key Eng. Mater. 577–578 (2014) 201–204.

[89] 貝沼重信，キムアラン：超音波噴霧による定量塩付着方法の提案と塩付着性状に関する基礎的検討，防錆管理，64-.6 (2020) 201-211.

[90] 武邊勝道，松崎靖彦，大屋誠，安食正太，古川貴士，麻生稔彦：耐候性鋼橋梁の表面状態と付着塩類量の関係，土木学会論文集 F，63-.2 (2007) 172-180.

[91] 山元弘，石松豊，河北憲治：鋼橋塗替え塗装の高度化に関する研究（1）（施工管理/維持管理/安全管理/情報管理/その他），土木研究所成果報告書， (2005) 1137- 1144.

[92] T. Shimada, Y. Oya, Y. Honkawa, Y. Kojima, I. Muto, Effects of deposited salts on corrosion behavior for 1100 aluminum alloy during constant dew point test, Zair. to Kankyo/ Corros. Eng. 62 (2013) 56–60. https://doi.org/10.3323/jcorr.62.56.

[93] C. Kim, H. Son, N. Hwang, C. Kim, Rapid and automated determination of rusted surface areas of a steel bridge for robotic maintenance systems, Autom. Constr. 42 (2014) 13–24. https://doi.org/10.1016/j.autcon.2014.02.016.

[94] J.P.B. van Dam, S.T. Abrahami, A. Yilmaz, Y. Gonzalez-Garcia, H. Terryn, J.M.C. Mol, Effect of surface roughness and chemistry on the adhesion and durability of a steel-epoxy adhesive interface, Int. J. Adhes. Adhes. 96 (2020) 102450.

[95] Y. Park, W.J. Choi, B.C. Yoon, Analysis of effects of process factors on corrosion resistance of adhesive bonded joints for aluminum alloys, J. Mater. Process. Technol. 276 (2020) 116412.

[96] X. Yu, X. Wei, X. Huang, L. Zhang, Study on the Modeling Method and Influencing Parameters of Sandblasting Process for Blade Grinding, Adv. Mater. Sci. Eng. 2022 (2022). https://doi.org/10.1155/2022/7905927.

[97] 藤岡靖, 藁科彰, 高木真一郎, 仲健一, 貝沼重信, 道野正嗣, & 山本悠哉. 高腐食性環境における無塗装耐候性鋼上路トラス橋における腐食損傷の要因推定と腐食性評価 (その 1) 腐食損傷の調査. 防錆管理/日本防錆技術協会[編], 60(7) (2016) 264-272.

[98] Japanese Road Association, Steel Road Bridge Corrosion Prevention Handbook (2014).

[99] NSRP / ASE Surface Preparation and Coatings Panel (SP-3) Study to Determine the Level of Salt Mitigation as related to the Accuracy of the Measurement and Cost Benefits Final Report Prepared by Lydia M. Frenzel, Ph. D. Advanced Technology Institute 5300 International Blvd. North Charleston, SC 29418 Support Services Agreement No. 2010-385 NSRP Surface Preparation and Coatings Panel (SPC), (2011).

[100] W. B. Keegan Protective coating of carbon steel, stainless steel, and aluminum on launch structures, facilities, and ground support equipment, NASA technical standard,

(2016) 1–103.

[101] T. Fujii, T. Kodama, H. Baba, Influence of water quality and flow conditions on corrosion of carbon steel pipes in freshwater, Corrosion Prevention Technology. 31 (1982) 637–642 (In Japan).

[102] ISO 8501-1, Preparation of steel substrates before application of paints and related products — Visual assessment of surface cleanliness — Part 1: Rust grades and preparation grades of uncoated steel substrates and of steel substrates after overall removal of previous coatings. (2007).

ACKNOWLEDGMENTS

This dissertation, the culmination of three years of doctoral work, could not have been realized without the unwavering support of the executives and colleagues at the structural design laboratory of Kyushu University. I am particularly indebted to my supervisor, Prof. Shigenobu Kainuma. As a mentor and educator, he has imparted not just academic knowledge but also instilled in me the zeal and self-belief essential for a researcher. Thank you for your kindness and for accepting me to experience your extensive knowledge in steel bridge and maintenance management engineering. I would like to acknowledge Tatsuya Ikeda from Ikeda kogyo Company Limited, Yusuke Toyota from West Nippon Expressway Company Limited, and Takehiko Arakawa from Sugino Machine Limited for their wonderful collaboration. I would particularly like to single out research assistant professor Muye Yang, Secretary Ms. Reiko Kato and Ms. Kumi Kawano in structural design laboratory, for their patient support. I would like to extend my heartfelt gratitude to research assistant professor Aran Kim, my esteemed Korean colleague in the laboratory. Her friendship and guidance have been a cornerstone of my experience here. Thanks so much to my friend, Assistant Professor Shusen Zhuang, always helped me a lot when I had trouble and often discussed everything. My sincere thanks also goes to Cai Lianheng and another fellow labmates. I would also like to thank Professor Jin-hee Ahn in Korea for all his help. Nobody has been more important to me in my dissertation than the members of my family. I would like to thank my parents, whose love and guidance are with me. They are the ultimate role models. Most importantly, I wish to thank my loving and supportive wife, Jeong-hyeon Moon. With gratitude for her boundless trust and belief in me, this paper is dedicated to her dedication and hard work.

Thank you very much, everyone!

Sanghong PARK

Fukuoka, September, 2024.